Finanziato dall'Unione europea
NextGenerationEU

UNIVERSITÀ degli STUDI di CATANIA
SEDE AMMINISTRATIVA

MUR

SAPIENZA
UNIVERSITÀ DI ROMA

NONLINEAR HYSTERETIC TUNED MASS DAMPERS FOR SEISMIC PROTECTION: DESIGN, OPTIMIZATION, AND EXPERIMENTAL VALIDATION FOR STRUCTURAL RETROFITTING

Dottorato di Ricerca Nazionale

in

Difesa Dai Rischi Naturali e Transizione Ecologica Del Costruito

Ciclo XXXVIII

By

PRANATH KUMAR GOURISHETTY

University of Catania - Department of Civil Engineering and Architecture

Sapienza University of Rome - Department of Structural and Geotechnical Engineering

Principal Advisor

Prof. Walter Lacarbonara , Sapienza University of Rome

Co-Advisors

Prof. Satish Nagarajaiah, Rice University, USA

Prof. Biagio Carboni, Sapienza University of Rome

Prof. Giuseppe Quaranta, Sapienza University of Rome

Abstract

This dissertation provides a comprehensive study of the design, optimization and validation of nonlinear Hysteretic Tuned Mass Dampers (HTMDs) for the purpose of seismic protection of civil structures. This research investigates the basic shortcomings of traditional linear tuned mass dampers with unique hysteretic energy dissipation devices that provide better response control under seismic excitation.

The major advancement presented in this research is the development of a cost effective HTMD using conventional steel wire rope, and introducing the novel double sliding clamping mechanisms which produce the pinched hysteretic behaviour without the need for high cost shape memory alloys. The device has a modular frame to provide user flexibility in configuration and optimized design features with the ability to apply to any type of structure. Furthermore, the novel design avoids mechanical limitations of hybrid NiTiNOL-steel wire ropes while also providing nonlinear performance tolerated, which is essential for seismic mitigation.

Significant experimental testing was conducted on a 5-story prototype structure, using earthquake ground motions according to the Italian Building Code standard design methodology. The experimental testing involved full characterization of the HTMD device with frequency response and force-displacement tests, then complete shaking table testing for various earthquake loads. The testing demonstrated an improvement of structural response to seismic excitation, achieving increased overall structural performance, with average reductions of 69% in RMS acceleration and 75% in peak acceleration for seismic loading periods, which is better than linear TMD system unique to this study.

The research provides insights into practical applications, including a case study on protecting a reinforced concrete building. An advanced optimization process based on Differential Evolution algorithms is employed to optimize parameters for application-oriented goals. This process evaluates multiple, equally important performance measures, ensuring robust overall performance under varying seismic loading conditions.

A new phenomenological model based on a modifying Bouc-Wen relation was developed that captured all experimental results of pinched hysteretic behavior. The model was capturing stiffness to some degree using an exponential displacement dependence, and results yielded a good correlation to experimental data. The validated model aids in providing simple numerical modeling for design optimization and performance prediction without the need for extensive mechanical modeling at the device or component level.

Overall, the dissertation concludes with a generic methodology for the complete design life of a seismic mitigation device, including structural identification, numerical modeling, optimization, and experimental testing and protocols. In summary, the expansive creative field of passive vibration control is nurtured forward for active vibration control. The methodology offers a practical tool for engineers seeking to reduce potential seismic risk features of structural designs for new construction and retrofitting.

Keywords: Hysteretic Tuned Mass Damper, Seismic Protection, Nonlinear Vibration Control, Structural Retrofitting, Experimental Validation, Optimization, Pinched Hysteresis

Acknowledgments

I would like to sincerely thank my principal advisor, Prof. Walter Lacarbonara, for his support and intellectual guidance and determination for excellence at every point of this doctoral journey.

I wish also to thank my co-advisors: Prof. Satish Nagarajaiah at Rice University hospitality was essential for establishing an international research perspective and demonstrated advanced control strategies; Prof. Biagio Carboni for sharing his technical knowledge in experimental mechanics and device configuration; and Prof. Giuseppe Quaranta for sharing his implemented numerical modeling and optimization approaches.

I would also wish to thank my research colleague Vinay Yadav Janga, for his joint experimental investigations and numerical modeling that made this research possible. Our publication in the Journal of Sound and Vibration reflects our joint ventures of creative passion and development in advancing our research professional community.

I would like thank the technical staff and the Materials and Structures Laboratory of Sapienza University, especially in operating the experimental setup and data acquisition systems on the MOOG and Dongling shaking tables. They displayed the utmost professionalism and deserves recognition.

I thank for the doctoral program coordinators and administrative staff support for the doctoral program. And finally, I would like to sincerely thank my family and friends who supported my endeavors and for their patience and understanding during this arduous, but rewarding journey in academic pursuit.

Contents

List of Figures

List of Tables

Chapter 1

Introduction

The devastating effects of earthquakes is one of the greatest challenges that civil engineers and society face. While there has been progress in structural analysis, materials, and building codes, earthquakes in different parts of the world reveal serious weaknesses in the built environment. These weaknesses are not just the loss of life and immediate structural failure, but the economic devastation and long-term social displacement. The weakness problem is not just a structural stability problem, but the building is destroyed beyond the ability to repair making the building completely useless and triggering secondary catastrophes as a consequence of the lost utility of buildings. Old design philosophy of life-safety for a medium level event result in failure of the structure for extreme event, not as a collapse, but as damage such that the performances caused the occupants to evacuate and the structure rendered unrepairable.Thus the new goal would be to replace the design philosophy who don't collapse, but return to function and focus on resilience so structures could with stand the shaking with damage and occupants in the life-safety state be issued permits for occupancy to return back after an event.

In the means of mitigating structural vibration, Tuned Mass Dampers (TMDs) are a wonderful simple idea. This method is attaching a mass-spring-damper system to the structure, where the frequency of the TMD system is matched to a given structural frequency. While the structure vibrates the TMD is out of phase thereby developing inertial force which dampens the structural motion. TMD has seen remarkable success

in wind engineering and in addition to many tall structures such as Taipei 101. TMDs prove to decrease perceived accelerations improve occupant comfort.

However, the derivation of this success to seismic protection has faced some significant fundamental structural issues. As stated above linear TMDs face three main limitations for seismic applications. First high modal mass ratios are required for effective reductions in response under a wide-band transient earthquake load (generally 5-10%). This gives you large benefited tremors, and requires very large auxiliary systems that pose significant practical issues from an architecturally, structurally and cost-effective perspective. Second they suffer from limited detuning robustness because building dynamic properties have a drift over time dependent on errors in construction, aging of materials, influences of environment, limit states, and more importantly, the degradation of stiffness from a strong earthquake when the structure reached yield. Tuning the TMD on the initial elastic frequency of the system would not work, would become ineffective or even detrimental if the elastic frequency was to drift. Third, linear TMDs are narrow-band and not intended for consistent response; particularly with the time-varying complex rich frequency content nature of seismic ground motions.

Next-generation TMD research has evaluated the use of advanced materials, specifically Shape Memory Alloys (SMAs), as a way to overcome limitations on linear TMDs. Hysteretic TMDs that utilize SMAs have hysteresis loops with a flag shape hysteresis loop configuration that allowed for self-centering with reasonable energy dissipation capability and some detuning robustness. But cost inhibits commercial implementation and universal acceptance. High-performance NiTiNOL alloys can be 50 – 100 times more than a comparable steel. With the expense of the materials and processing complexity, SMA damping solutions limited to an elite high-budget projects, excluding almost all standard buildings and structures and therefore the vast majority of potentially seismic vulnerable building stock.

This dissertation approaches this problem with a radical approach: achieving high-performance hysteretic behavior through mechanical ingenuity instead of costly materials. The main advancement of this work is the realization of a new Hysteretic

Tuned Mass Damper (HTMD) that achieves the attractive nonlinear characteristic of SMA systems with only common, and low cost materials. The proposed device employs a *double-sliding mechanism* integrated with standard steel wire ropes. This configuration is engineered to produce a pronounced *pinched hysteresis* loop, characterized by quasi-zero stiffness near the origin—which minimizes the force imposed on the structure during small-amplitude vibrations—and progressive stiffening with energy dissipation at larger displacements. This approach decouples sophisticated dynamic performance from exotic materials, creating a pathway to economically sustainable seismic protection.

The presentation of this thesis has a coherent structure that follows a logical pathway from foundational principles to real, functional technology. The structure of the narrative is built to develop an additive hierarchy of understanding with each chapter establishing the foundation for the next.

Chapter 2 provides a detailed overview of the historical background, theoretical framework and current state of TMD technology. We evaluate the evolution from linear devices to nonlinear devices, which are based on SMA and even more sophisticated materials; we note the gaps in the literature that this dissertation attempts to address.

Chapter 3 foundations of theory are developed for the research. It begins with the classical theory of linear TMDs and discusses limitations for seismic use and establishes the nonlinear dynamics framework for hysteretic systems. Therein, the formal introduction of the modified Bouc-Wen model with pinching is presented and later serves as the basis for the modeling and analysis approach.

Chapter 4 describes the mechanical design approach and the engineering process in the development of HTMD prototype. It explains the novel double-sliding mechanism, the criteria for component selection (where steel wire ropes and polymer bumpers were utilized), the manufacturing phase, and the end technical specifications of a laboratory-scale device.

Chapter 5 explores phenomenological modeling in the HTMD. A new Bouc-

Wen model is presented, along with the description of the Differential Evolution algorithm developed to perform parameter identification from experimental data, and the model is verified by comparing to the measured hysteretic response of the physical prototype.

Chapter 6 transitions to the main structure, detailing the design, fabrication, and dynamic characterization of the five-story prototype steel building, which was the structure used to perform the validation. This chapter identifies the baseline dynamic properties of the test structure that are critical to configuring the HTMD and evaluating performance.

Chapter 7 the experimental program is contextualised according to the Italian Building Code (NTC 2018), defining seismic demands on the prototype structure for various performance verification limit states. This establishes a credible basis for the determination of performance of the dynamic tuned mass damper-equipped structure.

Chapter 8 details the primary experimental results presented in phase-wise sequences when a structure is fitted with HTMD in the longitudinal (X) vertical direction. This chapter initially establishes the performance of the initial HTMD placements, and, going from this baseline the chapter highlights the dramatic improvements from the design optimization efforts. Finally, Chapter 8 discussed validated HTMD performance in the orthogonal (Y) vertical direction of the structure with a comparative discussion of HTMD performance in terms of placement on different levels. This chapter is crucial with respect to design optimization, since it provides foundational evidence of the need for optimized device locations for control.

Chapter 9 offers a highly detailed study of the performance of single and dual HTMD configurations subjected to 45-degree excitation. This excitation causes a coupled lateral-torsional response that has a very large amplitude of motion. The findings for this study can assist in understanding the design of complex three-dimensional structural performance.

Chapter 10 provides closure to the thesis with a summary of the primary outcomes and outcomes' significance. It also concludes with specific and actionable

recommendations for continued research, further technology development and actual use of hysteretic TMDs by the engineering community.

The successful development and validation of the economically viable HTMD stated in this work is about to address a significant gap in the field of seismic protection technology. The capacity to take inexpensive conventional materials to performance levels of sophisticated systems could potentially place high seismic performance Shin-Dia Bouncy on—existing structures in developing areas. The comprehensive analytical data, validated numerical models, and real-world design methodologies presented in this study offer a robust science justification to code-writers and regulatory authorities, allowing eventual codification and widespread implementation of this technology. Ultimately, the ultimate goal of this work is a future where clever and insightful engineered design overcomes the impetus of material, leading to a more resilient and sustainable built environment.

Chapter 2

Literature Review

The origin of tuned mass damper (TMD) technology goes back to the work of Hermann Frahm, who in 1909 obtained a patent for the first dynamic vibration absorber for reducing vibrations in ship hulls (Frahm, 1909). Frahm's invention actually established the basic idea of implementing an auxiliary oscillating mass to create anti-resonance conditions, which remove vibrations at select frequencies. Later, in 1928, Ormondroyd and Den Hartog (Ormondroyd and Den Hartog, 1928) formally justified the concept and approach mathematically and established the theoretical basis that would direct TMD design for many years. Den Hartog established the first and still the primary reference for the development of TMDs in his 1956 monograph titled "Mechanical Vibrations" (Den Hartog, 1956), which developed analytical solutions for determining optimal tuning and damping ratios derived for single degree of freedom systems subjected to harmonic excitation. Den Hartog's fixed-point theory, which dealt with two points (theoretically fixed) in frequency response regardless of damping, provided insights into tuning for local optimization strategies still used today for design.

Building on Den Hartog's foundational work, researchers have pushed the theory to more complex situations and loading scenarios. Warburton (Warburton, 1982) provided fully optimal solutions for combinations of response types and stimulus types, including displacement, velocity, and acceleration for harmonic and white noise stimulus types. Tsai and Lin (Tsai and Lin, 1993) extended the results to damped primary system, addressing a key limitation of Den Hartog's work that the system was un-

damped. Asami et al. (Asami et al., 2002) utilized the H∞ optimization criterion, and provided algebraic expressions for optimal parameter values under different scenarios. The introduction of multiple performance criteria led to multi-criteria optimization methods and minimax optimization methods for TMD design that minimize maximum response in a frequency band were utilized by Fujino and Abe (Fujino and Abe, 1993). Krenk (Krenk, 2005) presented frequency averaged optimization methods for the purpose of obtaining optimal TMD parameters to obtain reliable performance at a wide range of frequency ranges. Minimax methods were used to derive results of a multi-degree-of-freedom primary system by Zuo and Nayfeh citepzuo2004minimax, applicable to design of complex structures.

The original idea of implementing multiple tuned mass dampers to achieve a wider frequency band was first systematically studied by Iwanami and Seto (Iwanami and Seto, 1984) in 1984. Their results established that TMDs distributed in a system could successfully mitigate the narrow-band response of a single TMD. Xu and Igusa (Xu and Igusa, 1992) presented a theoretical demonstration that multiple TMDs with closely located frequencies could afford a more robust system than that of multiple single TMDs with the same total mass. Yamaguchi and Harnpornchai (Yamaguchi and Harnpornchai, 1993) developed fundamental formulas for dual TMD systems, and showed using equations derived from system dynamic equations, that properly spaced frequency pairs could even mitigate the undesirable twin-peak effects for response spectra. Abe and Fujino (Abe and Fujino, 1994) generalized their work to arbitrary number of TMDs and developed analytical formulae for optimal frequency distributions. Li (Li, 2002) studied multiple TMDs utilizing differing damping types, including both viscous and hysteretic damping exhibited superior performance psychometrically. The analysis of multiple TMD systems offers significantly more analytical complexity over a single TMD device leading Jangid (Jangid, 1999) to research optimization procedures numerically for multiple TMDs under a seismic excitation under both uniform and non-uniform mass. Hoang and Warnitchai (Hoang and Warnitchai, 2005) targeted a design method based on modal decomposition, with which they approached multi-mode con-

trol systematically, while Li and Qu (Li and Qu, 2006) targeted and optimal number of TMDs for a public specified mass ratio targeted parameters for group distribution.

Since the first installation of TMD on in the Citicorp Tower (now 601 Lexington Ave., New York City) in 1977, c.f. McNamara (McNamara, 1977) that identified the first installation as this first major implementation of a TMD that practically proved it as feasible for full scale structure. Due to the success of TMD installation in the Citicorp Tower worldwide installations evolved very rapidly in super tall buildings in Asia and extensive records were compiled recording TMD installations, providing important information to understand practical issues and solutions. Tamura et al. (Tamura et al., 2003) described the TMD performance in high-rise buildings in Japan, with productive monitoring along with people that live in the buildings they described wind to be very special and unusual circumstances, their measurements were during hurricanes and demonstrated agreement with theoretical calculations and methodology. Kwok et al. (Kwok et al., 1995) reviewed TMD performance in multiple Asian skyscrapers and reported reductions in acceleration response by up to 40%, with acceptance of TMDs for controlling wind-induced vibration. Kareem et al. (Kareem et al., 1999) presented comprehensive reviews of TMD applications for the use in wind-induced vibration, distilled experiences from multiple implementations and selected analysis as recommendations to facilitate design and use.

The optimization of TMDs concentrating on wind loads have been a hot topic of study for researchers wanting to improve performance for wind loading with varying characteristics. Gu et al. (Gu et al., 2001) performed parametric studies to assess TMD performance under different wind cases, and identified optimal design parameters for wind climate and structure. Tuan and Shang (Tuan and Shang, 2014) looked at TMD implementation under across-wind loads as those are governing load conditions of tall buildings because of their broad-band frequency content, as well as sustained effects. Overall these studies developed a robust design framework for wind applications that allowed for hundreds of successful TMD implementations into buildings worldwide.

Even though TMDs have been successfully adopted in the context of wind

engineering, their application to seismic protection has been limited and controversial. Early analytical investigations noted that TMDs may not even be effective for transient earthquake loadings. For example, Kaynia et al. citepkaynia1981seismic provided initial analysis noting that TMDs might only reduce earthquake induced motions very close to structures only moderately compared to wind-based applications because seismic excitations are broad-band, non-stationary excitations. In another example, Sladek and Klingner (Sladek and Klingner, 1983) noted through numerical simulations, TMDs provided only a minor reduction to seismic response, highlighting the mismatch between the narrow-band effectiveness of TMD's, and broad-band effective earthquake demands. Nevertheless, further research later found conditions in which TMDs could be applied to earthquake resistance. Villaverde (Villaverde, 1985) notes through his research that TMDs, when properly designed with the correct parameters, can significantly reduce the response for selected earthquakes, depending on their significant frequency content. Sadek et al. citepsadek1997method developed explicit design methods specifically used for seismic applications, they in turn account for the transient nature of earthquake excitation and the specific methodology provides procedures for design parameter optimization for typical earthquake ground motions. Further, Singh et al. citepsingh2002tuned concluded that TMDs could be especially helpful for near-fault ground motions that induce half sine waves, allowing for various application procedure of TMDs to distinct models for near-fault ground motions.

Experimental validation of TMD effectiveness for seismic protection has produced mixed results, globally, that portray the complexity of seismic loading and difficulty of laboratory testing. Rakicevic et al. (Rakicevic et al., 2012) conducted one of the largest shaking table test program on TMD equipped structures, where a 16.6 ton test specimen was utilized, with also considerable variability of TMD parameters, and average peak acceleration reduction of 20% was recorded, while ground motion characteristics proved to be sensitive to residual accelerations. Jiang et al. (Jiang et al., 2014) tested TMDs on reinforced concrete frames with each test producing TMD effectiveness that was highly dependent on ground motion characteristics together with structural

responses. Attention to TMDs as seismic protection have been restrained due to the number of technical issues still present such as merging the broad frequency content of seismic excitations, the effects of structural nonlinearity when subjected to large earthquake shaking, and impact of stroke limits during the extremes. Building codes such as Eurocode 8 (European Committee for Standardization, 2005) and FEMA 356 (Federal Emergency Management Agency, 2006) provide limited provisions for TMDs to be implemented in a seismic resistance application, which has contributed to the hesitant use of TMDs by those who do not have a clear design process and target performance outcomes.

The deliberate implementation of nonlinearity into TMD systems arose from realizing the current limitations of linear TMD systems, and recognizing that nonlinear can possibly lead to better performance. Roberson's original paper from 1952 (Roberson, 1952) first shows that nonlinear restoring forces can provide an automatic trust to assure efficiency is maintained with variation in frequency that would hinder linear systems. This work began the groundwork for many other concepts in nonlinear vibration absorbers that aim to address the narrow-band limits of linear devices through nonlinearity. Nonlinearity of cubic stiffness has been of most interest due to the simplicity in mathematics and the ease of manufacturing via different mechanical configurations. Natsiavas (Natsiavas, 1992) analyzed the steady state dynamics of non-linear absorbers with cubic stiffness, providing design parameters for improved performance and providing analytical principles for design of non-linear TMDs. Alexander and Schilder (Alexander and Schilder, 2009) investigated bifurcation or nonlinear TMDs, uncorking rich dynamic behavior like multiple stable solutions or complex response behaviors that would assist in improved control efficiency. Habib et al. (Habib et al., 2015) studied the performance of nonlinear TMD system through combinational analytical and experimental methods, proving the analytical performance was reasonable and improved the efficacies due to proven predication, and demonstrating the theoretical approaches were justifiable.

The practical utilization of cubic stiffness nonlinearity has been achieved using

mechanical systems, geometric nonlinearity has been used to derive force-displacement response characteristics. Li and Zhang Li and Zhang (2017) implemented geometric nonlinearity of angled springs in TMDs and demonstrated feasibility for civil engineering applications, while being simple to construct and maintain. Gatti Gatti (2018) provided foundational work on the optimal design of nonlinear TMDs. This investigation produced metrics for nonlinearity and performance, which can used to provide constructive recommendations for design. Tang et al. **?** experimented characterization of nonlinear vibration absorbers, provide identification procedure for the nonlinearity parameters to check theoretical models. There are many other types of stiffness nonlinearity here, with different levels of success beyond cubic stiffness. Viguie and Kerschen Viguié and Kerschen (2009) developed a TMD using non-polynomial stiffness, discovering a probable benefit for specific applications, but greater analysis and design process. Detroux et al. Detroux et al. (2015) analyzed TMD efficiency to a hardening and softening stiffness, revealing that softening nonlinearity provided potential for robustness against detuning effects. Ding and Chen Ding and Chen (2020) provided a review of multiple non-linear energy sink configurations and report on characteristics compared with multiple non-linear systems, recommending various with regard to optimal selection of nonlinearity options.

The exploration of non-linear damping strategies for TMDs has opened up avenues for enhancements in damping performance beyond linear viscosity damping. Rüdinger (Rüdinger, 2006) studied TMDs with power law damping and able to achieve optimal TMD performance for random excitations by featuring amplitude varying energy dissipation. The non-linear damping force, determined from velocity raised to a fractional power, provides amplitude varying dissipation that achieves favorable performance given the variability of the excitation intensity, thus providing a self-adjusting strategy or level of demand. Non-linearities in stiffness and damping combinations lead to even more challenging dynamic performance within the system requiring advanced analysis, Huang and Yang (Huang and Yang, 2023) study TMDs with non-linear coupled stiffness and damping, defining a region in parameter space where optimal per-

formance occurred and were able to identify synergistic properties resulting in greater performance than either one alone.

Nonlinearities attributed to hysteretic damping systems arise purely from force-displacement relations that exhibit path dependency, which has merits over variable-dependency. Initial methods of analyzing hysteretic systems were described by Iwan and Clough (**?**), their theoretical methods provide a basis for TMD derivations based on hysteretic properties. The displacement-dependent dissipative mechanism is an advantage over velocity-dependence for broadband excitation, allowing for the dissipation of energy to depend on displacement and not frequency-based energy content. Wire Rope Isolators have emerged as a hysteretic damping applied element, Gerges and Vickery (Gerges and Vickery, 2003) provided a comprehensive parametric study for wire rope spring TMDs that modeled hysteretic dynamics based on applied loading, and recommends design strategies. Carpineto et al. (Carpineto et al., 2014) presented additive analytic models for hysteresis of wire ropes and validated predictive models through extensive testing, establishing stable repeatability of hysteretic behavior due to inter-wire friction and geometric nonlinearity, validating hysteresis as a feasible option for TMD applications. Friction-based TMDs utilize Coulomb friction as the energy dissipating mechanism, Inaudi and Kelly (Inaudi and Kelly, 1995) presented the idea of mass dampers with a friction dissipating element that provide a mechanism for effective application of friction-based devices for seismic protection. Pisal and Jangid (Pisal and Jangid, 2016) researched dynamic responses of structures with tuned mass friction dampers. Their investigation focused on the optimization of friction coefficients using prescribed motions. With respect to friction-type systems, small amplitude vibrations can readily be filtered unlike in passive systems due to the use of a displacement threshold for (or control of) frictional type systems.

The extraordinary characteristics of shape memory alloys have spurred widespread studies of SMA-based TMDs that take advantage of the amazing mechanical properties of these materials. The superelastic characteristic of SMAs provides flag-shape hysteresis with self-centering properties, the perfect attributes for seismic protection

devices that must self-center after being loaded. An improved SMA assisted TMD design by Mishra et al. (Mishra et al., 2013) showed that the energy dissipation has been enhanced in nature over traditional systems while also exhibiting self-centering. The temperature dependent nature of SMAs allows for adaptive TMD systems, which can adjust to environmental conditions or control inputs based on properties of the TMDs. The temperature effects from Aguiar et al. (Aguiar et al., 2013) observed that the TMD system can not only adjust the rotational torque, but also implement control procedures that utilize phase transformation temperatures to obtain tuning feedback through real-time iterations. Huang et al. (Huang et al., 2020) even were able to give the TMD properties to yield adaptive TMDs, through temperature modulation. They were able to illustrate the superior performance of SMA-assisted TMDs compared to systems with fixed parameters. Hybrid systems that combine SMAs with traditional materials provide reasonable solutions to the performance and cost limitations of SMAs, addressing the economic issues of SMA application. Carboni et al. (Carboni et al., 2015) used a multiconfiguration assembly of steel strands and NiTiNOL, exhibiting pinched hysteresis with the combination of materials while keeping many of the advantages of an SMA system while at a lower cost. Carboni and Lacarbonara (Carboni and Lacarbonara, 2016), provided both theoretical and experimentally-based infrastructure to create hybrid wire-rope TMDs to show enhanced performance disciplines to prime these hybrids for application. Tiwari et al. (Tiwari et al., 2021) have reported on hybrid SMA-tuned mass damper inerter systems that employ three advanced technologies, promising great levels of control performance. Unfortunately, the high cost of SMA material continues to prohibit the practical application of SMA-based systems, and the complexity of the manufacturing, where the costs of materials can exceed traditional materials by 50-100 times makes it extremely restrictive to implementation for civil engineering applications.

The proposal of the inerter in 2002 by Smith (Smith, 2002) created a new avenue for vibration control through inertial forces proportional to relative acceleration, allowing for apparent mass amplification without physical mass amplification. Inert-

ers represent a fundamental innovative step in synthesis of mechanical networks and completes the mechanical-electrical analogy as it portrays the mechanical equivalent of electrical capacitance. Marian and Giaralis (Marian and Giaralis, 2014) developed the tuned mass damper inerter (TMDI) and with a mechanical spring-mass system proved a TMDI has superior performance with less physical mass while creating theoretical foundations for inerter-based vibration control. Theoretical studies have created an optimal design procedure regarding TMDIs in consideration for the properties of inerter elements. Pietrosanti et al. (Pietrosanti et al., 2017) developed analytical solutions to the optimization of TMDIs for different excitation methods and gave closed-form solutions for optimal parameters. De Angelis et al. (De Angelis et al., 2019) analyzed and performed optimal comparison studies of TMDIs and deduced sets of TMDI configurations that gave maximum effectiveness, as well as implementable requirements. Experimental work by Nakamura et al. (Nakamura et al., 2014) provided an experimental validation of the behavior of an electromagnetic inerter tested in shaking table tests and confirmed this is practically applicable to seismic cases of interest. Novel nonlinear TMDIs were developed for seismic purposes by Rajana and Giaralis (Rajana and Giaralis, 2023), introduced new elements to the inertial technology and incorporated nonlinear elements to provide robust and performant enhancements.

Negative stiffness devices for vibration control have been a recent topic of literature, as they may provide potential beneficial performance that may circumvent any extreme performance limitations found in passive systems. Sarlis et al. (Sarlis et al., 2013) demonstrated that negative stiffness devices can increase energy dissipation without sacrificing stability. Therefore, they were able to present a way to avoid the limitations of passive systems. Pasala et al. (Pasala et al., 2014) demonstrated and worked with adaptive negative stiffness devices for seismic protection. They demonstrated significant response reductions to the bridge system of adaptive negative stiffness through variable stiffness in real time. Quasi-zero stiffness (QZS) devices represent high static stiffness and low dynamic stiffness which are ideal requirements of vibration isolation providing both structural integrity and integrity of isolation. Carrella et al. (Carrella

et al., 2007) undertook static and dynamic analysis of a QZS device to establish the design concept and demonstrate feasibility as a vibration isolation system. Liu et al. (Liu et al., 2013) conducted a research study summarizing the background and mechanics of QZS vibration isolators, and indicated some potential low mechanism, realistic optimal mechanisms for different applications. Negative stiffness has also been recently combined with TMD concepts to create hybrid systems which could allow advanced performance. Chondrogiannis et al. (Chondrogiannis et al., 2023) demonstrated the design of negative stiffness TMDs using nonlinear geometry and creating an effective lower end performance application based on resonance. Weber citepweber2014optimal optimally designed TMDs using negative stiffness, and confirmed amplification effect in extended ranges of parameters that have allowed maximum reasonable configurations to then design negative stiffness TMD. Overall it appears that a combination of negative stiffness and mass amplification reflects a substantial improvement in passive control performance that will greatly influence vibration control technology.

Particle dampers dissipate energy through momentum transfer and friction between particles and select granular media dynamic as the process of energy dissipation. Lu et al. (Lu et al., 2018) conducted thorough experimental and analytical investigation of particle TMDs for seismic control and demonstrated robustness to detuning and provided design procedures for particle systems. The severely nonlinear characteristics of particle interaction provide adaptive capabilities to varying levels excitation, automatic energy dissipation levels to demand. Impact dampers dissipate energy using momentum transfer during impact, providing robust and reliable energy dissipation characteristics also in extreme environments. Li and Darby (Li and Darby, 2006) studied pounding TMDs using experimental testing, characterized energy dissipation modes and proposed design procedures for impact-based systems. Zhang et al. (**?**) explored a new asymmetric nonlinear mass dampers by impact mechanism, which was effective for seismic protection and also provided possible advantages over conventional approach.

Semi-active tuned mass dampers (TMDs) provide real-time parameter tuning

while still capturing the advantages of reliability from passive systems, thus, representing the best trade-off between performance and complexity. Setareh (Setareh, 2002) investigated pendulum TMDs with variable length, that could adjust depending on environmental conditions and retain the advantages of passive pendulum TMDs. Smart materials can enable adaptive TMD to autonomously adjust parameters without the necessity of controller, while remaining passive parameters. Sun et al. (Sun et al., 2014) created bi-directional TMDs with magneto-rheological dampers, so controlling the damping properties of TMD can be tuned to the magnetic field, and can adapt in real-time. Weber and Maślanka (Weber and Maślanka, 2013) discussed tuning frequency and damping properties of using MR dampers and various controls to optimize performance for objectives and reporting benefits.

Active research efforts have validated TMD concepts and unearthed real world implementation issues to be addressed for practical field applications. Rakicevic et al. citeprakicevic2012effectiveness performed one of the largest shaking table test programs on TMD equipped structures using a 16.6-ton apparatus while varying TMD parameters in a consistent manner and obtained tremendous amounts of data denoting performance differences for various initial design parameters and differing ground motion characteristics. Full-scale testing evaluated TMD devices in isolation averaged peak accelerations dissipated by 20%, while responses noted to ground motion characteristics were important design attributes for TMD design. Chen and Wu citepchen2001experimental conducted experimental tests on various TMD to evaluate the seismic response and validated theoretical predictions for distributed responded systems and proved the advantage of using configurations with multiple devices. Huang et al. (Huang et al., 2020) tested adaptive TMD devices with shape memory alloy and confirmed real time tuning capabilities and validated theoretical predictions for adaptive systems. Wang et al. (Wang et al., 2020) tested asymmetric non-linear TMD devices using shaking programs and confirmed their implies devices were significantly more robust than their linear counterparts and that non-linear concepts could be efficaciously implemented. Real time hybrid simulations are a powerful tool for TMD

assessment and leverage numerical simulation and verification of an individual physical part of a whole system.

Long-term monitoring of installed TMDs provides the validation of design assumptions and durability of performance that cannot be realized through laboratory testing alone. Tamura et al.
citeptamura2003evaluation present multi-year monitoring data of Japanese high-rise buildings that identified the slight TMD effectiveness during a large number of typhoons and moderate earthquakes. They present that during the study proper maintenance ensured that TMDs did not mean degrading of their performance over time. Post earthquake evaluations have provided valuable data on TMD performance during real earth-quakes that extend the conclusions of laboratory testing. The paper did identify actual instances of strokes beyond the limits that were indicative of the importance of proper design for displacement capacity.

Conventional optimization of TMD parameters has traditionally employed analytical solutions for simplified systems that provide quick preliminary design capabilities. Bakre and Jangid (Bakre and Jangid, 2007) produced closed-form expressions for optimal TMD parameters based on a variety of loading conditions, providing a useful readily available design tool for daily usage. Bekdaş and Nigdeli (Bekdaş and Nigdeli, 2011) employed desktop formulas for optimized TMD parameters that were generated from large parametric studies that allowed for easy design by practitioners. Classical methods may be efficient for advanced preliminary design; however, they may not be able to effectively capture the nonlinear behavior that exists in real-world structures and loading. The complication with nonlinear TMD parameter optimization motivated the development of metaheuristic algorithms that could address the multi-modal, discontinuous optimization problems that are a practice of nonlinear systems. Hadi and Arfiadi (Hadi and Arfiadi, 1998) investigated the use of genetic algorithms for TMD optimization and more clinical than gradient optimization methods at multi-modal problems and that laid the groundwork for the utilization of evolutionary optimization techniques. Leung and Zhang (Leung and Zhang, 2009) used particle swarm optimiza-

tion for TMD design, providing robust designs when uncertainty existed, and demonstrating the effectiveness of swarm intelligence techniques. Differential Evolution has been shown to deal well with TMD optimization as it is a global search method and handles constraints robustly. Mohebbi et al. (Mohebbi et al., 2013) designed an optimal multiple TMDs using modified differential evolution, dealing with continuous and discrete variables concurrently, and demonstrated improved optimization ability over classical techniques. Quaranta et al. (Quaranta et al., 2020) gave an extensive review on computational intelligence for nonlinear system identifications, provided multiple comparisons of algorithms on hysteretic models, and provided recommendations to optimize nonlinear systems use evolutionary techniques.

In actual TMD design applications there are multiple and frequently conflicting objectives that require sophisticated optimization strategies that can reconcile competing performance specifications. Chakraborty et al. (Chakraborty et al., 2011) presented reliability-based optimization methodologies for TMDs, wherein performance and probability of failure were considered in the optimization framework while ensuring reliable performance under uncertainty. Robust optimization considers the uncertainties in system parameters and loads which are unavoidable in real-world applications. Marano et al. (Marano et al., 2010) presented robust optimum design procedures for TMDs with uncertain parameters, ensuring acceptable performance with variation and confidence in designs. Hoang et al. citephoang2008optimal presented optimal TMD design considering multiple design criteria and loading scenarios, yielding solutions that are robust to different conditions and showed practical methods of uncertainty treatment.

Accurate representation of hysteretic behavior is critical for the Analysis of nonlinear TMD, and this requires a phenomenological modeling approach that can represent non-linear complexity while being computationally efficient. Bouc-Wen models were first established by Bouc (Bouc, 1967) and followed up by Wen citepwen1976method; today, Bouc-Wen has become the prevalent paradigm for smooth hysteresis modeling due to its phenomenological flexibility and mathematical simplic-

ity. Ikhouane and Rodellar

citepikhouane2007systems provided a systematic treatment of Bouc-Wen model identification and features, providing a theoretical basis along with practical approaches for applying the model. Extensions to the classical Bouc-Wen model have been made for some behaviors that classically are unable to cover. Sivaselvan and Reinhorn (Sivaselvan and Reinhorn, 2000) developed hysteresis models for pinching behavior, which is applicable to many structural systems and an important extension from classical hysteresis modeling. Charalampakis and Dimou (Charalampakis and Dimou, 2010) explored the Bouc-Wen model parameters using genetic algorithms; they looked at challenges with identification and provided the step-by-step procedures for estimating parameters using the experimental data. Song and Der Kiureghian (Song and Der Kiureghian, 2006) developed generalized Bouc-Wen models by considering several different hysteretic models, which extended the application of Bouc-Wen to systems with multiple nonlinearity mechanisms.

The integration of TMD models into structural analysis software allows for practical design applications and allows for momentum from research to practice. McKenna et al. (McKenna et al., 2000) established the open-source software OpenSees for nonlinear structural analysis with TMD elements that creates an environment to engage more developed structural analysis capabilities. The object-oriented design allows for easy implementation of advanced material models and elements affording researchers and practitioners the ability to apply advanced TMD models. TMD modeling capabilities have expanded into commercial system packages to accommodate increasing needs for vibration control analysis. Systems such as SAP2000, ETABS, and other widely used programs have linear TMD elements with development of nonlinear capabilities underway which decreases barriers and encourages more practical implementation and use of TMD technology.

The accuracy of the TMD design and performance verification processes associated with parameter identification are important and extensive methods to extract usable parameters from experimental data are needed obtain complicated experimen-

tal data. Kerschen et al. (Kerschen et al., 2006) provided comprehensive surveys nonlinear system identification in structural dynamics, introduced implementations in the time and frequency domains, and quantified procedures nonlinear identification methods. The Hilbert transform method used by Feldman (Feldman, 2011) for nonlinear vibration analysis for extracting instantaneous parameters over transient response along provided suggestions for time-varying behavior of a system. Tang et al (**?**) used a free vibration identification method for nonlinear vibration absorbers, and created methods for extracting backbone curves and damping characteristics from experimental data. Trujillo-Franco et al. citeptrujillo2020online conducted online identification on autoparametric systems, to identify system parameters for online identification when the systems were activated, which could take future application in adaptive control systems. Frequency response based methods fracture identification techniques for frequency-based motion and observed techniques in time-based motion. Ewins citepewins2000modal presented base modal identification techniques that are applicable to TMD characterization, and presented a procedure for conducting experimental identification a TMD. Worden and Tomlinson (Worden and Tomlinson, 2001) developed frequency based classification techniques suitable for identifying nonlinear systems identification, as they pose unique challenges of multi-valued classification due to nonlinearities. The harmonic balance method facilitates analysis periodic nonlinear system with multi-source frequency characteristics, with frequency ranging back-and-forth response developed by Cameron and Griffin (Cameron and Griffin, 1989). Peeters et al. (Peeters et al., 2009) presented nonlinear normal modes associated with experimental modal analysis, with the advance of theoretical development for nonlinear modes shapes and nonlinear modal behaviors.

This research has produced recent innovations in machine learning which will provide additional modeling and optimization possibilities for TMDs that go beyond the conventional analytical processes. Farrar and Worden (Farrar and Worden, 2012) studied artificial intelligence through machine learning approaches for structural health monitoring, to gain insights into methods that relate to TMDs monitoring conditions

and performance. In addition, numerical networks have made advances for hysteretic system identification successfully verifying application feasibility. Chassiakos et al. (Chassiakos et al., 1998) implemented an online identification approach with a neural network, which demonstrates that the component may be reused in real-time for adaptive systems. Yun and Bahng citepyun2000estimation applied a neural network to identify parameters of the Bouc-Wen model, they provided an accurate identification front of hysteresis further confirming the potential of the application within machine learning.

Uncertainty quantification is key component to developing reliable TMD design will experience and perform reliably under changes of conditions that exist in practice. Der Kiureghian and Ditlevsen (Der Kiureghian and Ditlevsen, 2009) distinguish between aleatory and epistemic probabilities for uncertainties, and frameworks for treatment that are very difficult for TMD reliability. Schuëller and Jensen (Schuëller and Jensen, 2008) provided computational methods for developing reliability for dynamical systems, that might be applied toward TMD floating structures and consequently they to probabilistically apply them as necessary to assess performance. Additionally, fragility assessments provide probabilistic assessments of performance based by hazard intensities which apply for performance-based design. Tian et al. (Tian et al., 2019) introduced probabilistic seismic demand analysis method for transmission towers where fragility curves were developed for seismically loaded structures, and outlined fragility curves for coupled TMD applications with a probabilistically and methods.

An economic evaluation over the lifetime of a structure will guide TMD investment decisions and evaluate the feasibility of TMD technology for different applications. In work by Taflanidis and Beck (Taflanidis and Beck, 2009) an economic framework for life-cycle costs of passive dampers was developed, which considered the costs of installation, maintenance, and failure as part of an economic analysis. An economic framework is important to facilitate implementation of TMDs within engineering practice, as it provides a business case for TMD use and compares them against other mitigations.

Considerations for manufacturing and implementation impact the practical feasibility of TMD technology, and directly impact their uptake in engineering practice. 3D printing possibilities offer rapid prototyping and flexibility of the TMD components, and work by Martinelli et al. (Martinelli et al., 2023) investigated additive manufacturing for non-linear vibration absorbers, and evaluated their feasibility through printed prototypes. Incorporating complex geometries and customized material properties provides new possibilities for design and creates a low-cost customization for applications Standard testing protocols can contribute to uniformity of TMD performance and provide assurance for regulation acceptance and licensing. ISO standards for vibration isolation provides a standard which can be applied for a TMD evaluation, and ASCE/SEI standards for seismic isolation systems provide standards which have relevant testing procedures which could be implemented for TMD applicator. Having a defined standards specifications for TMD would strengthen the quality assurance process, and regulatory acceptance, further decreasing implementation barriers and providing reliability engineers need to implement safely.

Widespread TMD use across regions affords important lessons on operational difficulties and opportunities under varied circumstances. Asian experience shows the possibility and limitations of TMD for seismic applications. Japanese applications documented by Tamura et al. (Tamura et al., 2003) illustrate longevity of performance in seismic regions as well as maintenance and durability information related to repeated loading. Chinese applications in supertall structures, documented by Li et al. (Li et al., 2011) demonstrate challenges related to extreme heights and wind loading, pushing TMD to the limits of practicality. Taiwanese experience with consistent earthquakes documented by Yang et al. (Yang et al., 2004) provides information about seismic performance and the practicality of proper TMD installations within high seismicity regions. European wind engineering has spurred TMD advancements and methods for design specifically for wind structures. Italian applications in historical architecture documented by Casciati and Giuliano (Casciati and Giuliano, 2009), investigate limitations related to heritage preservation, as well as demonstrate how

TMD can be designed for architectural preservation while offering protection. German precision engineering utilized for TMD performance, such as GERB, sets a quality standard and demonstrates to practitioners the importance of manufacturing products with precision tolerances for performance longevity. Examples from Torre Agbar in Barcelona, and the Millennium Bridge in London demonstrate regional applications and show how TMD can potentially resolve varied dynamic challenges.

North American TMD examples show multiple structural typologies and environments, and serve as valuable insight into TMD performance and adaptability under different arrangement conditions. Canadian examples in tall slender towers under wind control demonstrate that TMD performance is related to environmental factors, namely cold weather, and this type of environment presents TMD mechanical features and mechanization with challenges. United States examples, from the formative innovations from Citicorp Tower, to modern examples provide a view of longitudinal TMD technology evolution, with data taken from long-term performance monitoring providing longitudinal recommendations.

TMD approaches were first derived from mechanical engineering and aerospace engineering. Interdisciplinary cross-fertilization led to advancements in the field and opened new possible applications. Vakakis et al. (Vakakis et al., 2008) studied nonlinear targeted energy transfer, created theoretical conditions for application to civil structures and linked various areas of engineering. Lee et al. (Lee et al., 2013) studied nonlinear energy sinks for aerospace applications, and established broad applicability of nonlinear absorbers and made observations for civil engineering applications. Automotive vibration control study reviewed by Karnopp (Karnopp, 1995), and offers insight on compact, robust designs that could be useful for buildings. Naval architecture applications for ship rolling control show lessons learned for large scale transfer and also reveal possible effectiveness of TMDs under extreme loading. Isolation techniques to manage industrial machinery shows possible practical damping methods true to buildings for a TMD aresource.

Modern control theory provides analytical tools in TMD design methods can

supplement classical design methods to orderly, and systematical design practices. Housner et al. (Housner et al., 1997) produced bridges with control and structural engineering, which enables systematic design practices and extend basic theoretical methods for TMDs design deliberations. Spencer and Nagarajaiah (Spencer and Nagarajaiah, 2003) performed a review study of the structural control field and integrated TMDs into control solutions for further evolutions. Nonlinear base (Nayfeh and Mook, 2008) treated the basics of nonlinear oscillations, which are necessary to facilitate your nonliar assumption, and then use it rationally TMD designs to nonlinearities in the system. Shaw and Pierre (Shaw and Pierre, 1993) advanced nonlinear normal mode theories to identify modal interactions common to nonlinear systems as the basis to build provisions to challenge the structures dynamic behavior.

TMDs can mitigate a wide array of environmental risks and vulnerabilities, in addition to seismic and wind loading, therefore showing the versatility and far-reaching applicability of TMD technology. Wind-induced vibrations in flexible structures can be controlled by TMDs, as reviewed by et al. (Kwok et al., 2009), as shown in applications for everything from tall buildings to long-span bridges to transmission towers. The wave-induced motion in offshore platforms, as explored by Chandrasekaran et al., (Chandrasekaran et al., 2016), exemplifies marine applications and illustrates how TMD principles can be applied to other environmental conditions. Climate change impacts on TMD design should be considered since service environment conditions will change. An increase in storm intensity can require that wind-designed TMDs need to be retuned to continue to be effective. Sea level change changes the dynamics of offshore structures which can also change the need for the TMDs or adaptive design. Temperature extremes increase the variation in material properties, so it would be better to design robustly. That would require the usable temperature range for TMD performance to be higher than it has been from history.

Life cycle assessment of TMD systems supports sustainable design in buildings and provides a means of assessing environmental impacts throughout a system lifecycle. The selection of materials taking into consideration embodied energy and

recyclability will influence the environmental impact and can inform design decisions toward higher sustainable outcomes. Manufacturing locally will decrease transportation emissions, contribute to regional economies, providing both environmental and economic advantages. Modular design that promotes reuse and reconfiguration will reduce waste, and promote longer system-life cycles and fulfill sustainability objectives. Integrating energy harvesting into TMD systems may provide sustainability benefits by harvesting useful electrical energy from structural vibrations. When coupled with piezoelectric materials, TMDs may convert vibration energy to electricity while performing as a damping device, creating a dual-purpose application which enhance the energy systems of a building. Integrating electromagnetic harvesters into TMDs may provide electrical power for monitoring devices and for the building operation while providing vibration control.

Despite a robust body of research, barriers exist to real TMD seismic protection as a viable technology and additional research is required. The interaction of TMDs with yielding structures is not fully understood, with most studies assuming a primary structure remains elastic, which does not accurately represent the behavior of real buildings during strong ground shaking. Real buildings degrade stiffness and strength during strong ground shaking, which could cause a TMD to lose its tuning abilities, when it is most needed, defeating its purpose when you need protection the most. There are practical issues related to stroke during an extreme event, which are not resolved by today's design process, as TMDs that appear optimized for a frequent event may exceed impact limits and displacements on rare occasions of extreme earthquake. Design procedures that consider performance across multiple levels of hazard are due for development to better ensure reliable protection to the broad range of possible loading conditions.

The long term reliability of TMD systems to repeated loads and environmental conditions is an area that requires systematic research regarding real-world durability. Each part has independent durability data, but the system durability, influenced by interaction of parts, maintenance and evolution of the system performance is not cur-

rently know and needs long term monitoring and assessment. Life cycle cost analyses of TMDs considering maintenance, replacement, and degrading performance would inform decision-making and strengthen economic justification to expedite widespread application. Scale effects between lab prototypes and full-scale application create uncertainty in performance forecasting that needs to be addressed with full-scale tests and field monitoring. Most experimental validation to date has involved reduced-scale models with similitude assumptions, however, may not sufficiently capture the complete complexity, and therefore full-scale validation is needed to establish confidence in design procedures.

The integration of TMDs into other structural systems and non-structural components requires careful co-ordination, This is noted in many studies but represents a gap for practice. Practical integration is impacted by building architectural constraints, conflicts with mechanical systems, and access for maintenance, but little academic research focuses on these issues, resulting in gaps between experimentation and practice. A holistic design approach to both structural and non-structural systems would promote practice adoption, and allow TMD technology and complete building systems to be successfully integrated. The performance based design process for TMD structures has not yet reached the leadership of general seismic engineering practices. Current building codes provide little information on TMD use and leave designers without performance based standard procedures. Provisions for building codes based on reliability approach principles will enable greater practice adoption, and provide the support in government policy that is necessary for earlier adoption.

Occupant and public safety need high quality seismic resistance in urban areas with large tall buildings, and the demand for affordable protection continues to grow based on increased urbanization in areas prone to earthquakes. This represents obstacles and opportunities for TMD implementation. Tuned mass damper technology, especially advanced nonlinear tuned mass damper technology is promising if the technical and economic barriers can be removed because of continued research on the technology. The two studies in this thesis contribute to that purpose by demonstrat-

ing that dynamic performance can be uniquely achieved based on mechanical design, not costly materials, and that TMD use could represent a change in acceptance from applied technology from less advanced to more standardized seismic resistance. Performance of a system that we saw could accurately improve safety of the general public could be used widely to enhance public safety and resiliency in the built environment.

Chapter 3

Theoretical Framework for Hysteretic Tuned Mass Dampers

3.1 Foundations of Linear Tuned Mass Damper Theory

The theoretical simplicity of the TMD is based on altering a primary structure's dynamic response by adding a secondary system that is resonant. The classical analytical model that forms the basis of TMD design is based on numerous idealizations: linear material response, time-invariant system parameters, and harmonic or stationary random excitation.

3.1.1 Governing Equations of Motion

Consider a primary structure idealized as a linear single-degree-of-freedom (SDOF) system, characterized by mass m_s, stiffness k_s, and viscous damping coefficient c_s. The attachment of a TMD, comprising mass m_d, stiffness k_d, and damping c_d, results in a coupled two-degree-of-freedom (2DOF) system. The equations of motion for this system subjected to a base acceleration $\ddot{x}_g(t)$ are given by:

$$\mathbf{M}\ddot{\mathbf{x}} + \mathbf{C}\dot{\mathbf{x}} + \mathbf{K}\mathbf{x} = -\mathbf{M}\mathbf{r}\ddot{x}_g(t) \tag{3.1}$$

where the system matrices and vectors are explicitly defined as:

$$\mathbf{M} = \begin{bmatrix} m_s & 0 \\ 0 & m_d \end{bmatrix}, \qquad \mathbf{x} = \begin{bmatrix} x_s \\ x_d \end{bmatrix}, \qquad \mathbf{r} = \begin{bmatrix} 1 \\ 1 \end{bmatrix},$$

$$\mathbf{C} = \begin{bmatrix} c_s + c_d & -c_d \\ -c_d & c_d \end{bmatrix}, \qquad \mathbf{K} = \begin{bmatrix} k_s + k_d & -k_d \\ -k_d & k_d \end{bmatrix}.$$

The displacement vector $\mathbf{x}$ contains the relative-to-ground displacements of the structure and the TMD mass, respectively. The coupling terms in the stiffness and damping matrices underscore the fundamental mechanism of action: the control force exerted on the primary structure is a direct function of the relative motion $(x_s - x_d)$.

3.1.2 Frequency Domain Analysis and the Principle of Anti-Resonance

The dynamic behavior of the coupled system is most elucidatingly analyzed in the frequency domain. For a harmonic base excitation $\ddot{x}_g(t) = e^{i\omega t}$, the steady-state complex frequency response function $H_s(\omega)$ for the structural displacement reveals the core operational principle. The 2DOF system exhibits two resonant peaks corresponding to its two natural modes of vibration. Crucially, between these peaks exists an *anti-resonance* frequency, ω_a, where the structural response $|H_s(\omega_a)|$ is minimized. At this point, the inertial force of the TMD mass is precisely tuned such that the force transmitted back to the structure through the spring k_d and damper c_d is nearly out-of-phase with, and cancels, the exciting force. The optimal design of a TMD involves parameter selection to position this anti-resonance at the target structural frequency.

3.1.3 Classical Optimization for Undamped Primary Structures

The seminal work of Den Hartog established the analytical foundation for optimizing TMD parameters for an undamped primary structure ($c_s = 0$) under harmonic forcing. The objective is to minimize the maximum amplitude of the frequency response

function $|H_s(\omega)|$, creating two equal resonant peaks. The closed-form solutions for the optimal frequency ratio f_{opt} and TMD damping ratio $\xi_{d,opt}$ are:

$$f_{opt} = \frac{\omega_d}{\omega_s} = \frac{1}{1+\mu} \tag{3.2}$$

$$\xi_{d,opt} = \sqrt{\frac{3\mu}{8(1+\mu)}} \tag{3.3}$$

where $\mu = m_d/m_s$ is the mass ratio, $\omega_s = \sqrt{k_s/m_s}$ is the natural frequency of the primary structure, and $\omega_d = \sqrt{k_d/m_d}$ is the natural frequency of the TMD. These relations reveal that the TMD must be tuned slightly below the structural frequency to account for the inertial interaction, and that the requisite damping increases with μ to effectively dissipate the larger energy flows.

3.2 Limitations of Classical TMD Theory for Seismic Applications

The application of Den Hartog's classical theory directly to seismic vibration control has significant limitations and this dissertation provides the solutions via the HTMD concept. The primary limitations include the non-stationary, broadband nature of the earthquake ground motion excitation that deviates substantially from the classical steady-state harmonic or white-noise models. This discrepancy can lead to poor performance under real seismic excitation. Structural inelasticity under extreme ground motion results in degradation in stiffness, and a fundamental change in natural period leading to detuning fundamentally detracts from the functionality of linear TMD systems established at the initial elastic period. In addition, seismic design is typically governed by energy dissipation and displacement demands versus acceleration suppression, and there are distinct performance criteria that should be considered for optimization that considers cumulative damage potential. Practical limitations on TMD systems also place limitations on maximum displacement; designs must also consider

performance to physical practicality.

These issues have led to the development of sophisticated design methods such as utilizing stochastic optimization techniques to optimize TMD parameters based on ensembles or recorded or simulated ground motions, multi-objective optimization techniques that optimize peak drift, floor acceleration, and TMD stroke which may be conflicting objectives, robust design techniques that optimize against uncertainties of structural properties and characteristics and research so that performance is deterministic, and nonlinear TMD models in the development of TMDs with intentional nonlinear characteristics to maintain performance over wider ranges of frequencies and amplitudes of excitation.

3.3 Advanced Hysteretic Modeling for Structural Control

To address the fundamental challenge of detuning in yielding systems and achieve better performance over a wider range of excitation, this study investigates the implementation of intentionally nonlinear TMDs with hysteretic behavior. Hysteretic systems with path dependence restoring force and built-in energy dissipation characteristics can be a strong potential pathway towards robust seismic protection and enhanced performance. Nonlinear force-displacement relationships can provide wider effective frequency range or bandwidth and greater robustness with frequency changes in the structure.

3.3.1 Mathematical Formulation of Hysteresis

The accurate modeling of hysteresis requires mathematical frameworks that transcend linear viscoelasticity. The Bouc-Wen model is a widely adopted phenomenological model due to its versatility in representing smooth hysteretic loops. The classical formulation decomposes the total restoring force $F(t)$ as:

$$F(t) = \alpha k_0 x(t) + (1 - \alpha) k_0 z(t) \tag{3.4}$$

where $x(t)$ is the displacement, k_0 is the initial elastic stiffness, α is the post- to pre-yield stiffness ratio, and $z(t)$ is a dimensionless hysteretic variable governed by the nonlinear first-order differential equation:

$$\dot{z} = \dot{x}\left[A - \left(\beta\,\mathrm{sgn}(\dot{x}z) + \gamma\right)|z|^n\right]. \tag{3.5}$$

The parameters A, β, γ, and n govern the scale, shape, and smoothness of the hysteresis loop, providing a rich parametric space for model calibration to experimental data.

3.3.2 Extended Bouc-Wen Model with Pinching Behavior

The classical Bouc-Wen formulation, while versatile, lacks the capability to accurately represent the pinched hysteresis morphology characteristic of many practical structural systems, including the wire rope isolators utilized in the proposed HTMD. To address this limitation, an extended formulation incorporating displacement-dependent stiffness modulation and pinching behavior is developed:

$$F(x, \dot{x}, z) = k_e x\left[e^{-\frac{x^2}{x_k}}(\alpha - 1) + 1\right] + z(x, \dot{x}) \tag{3.6}$$

where the hysteretic component $z(x, \dot{x})$ is governed by the evolutionary equation:

$$\dot{z} = \left\{k_d h(x) - \left[\gamma + \beta\mathrm{sgn}(z\dot{x})\right]|z|^n\right\}\dot{x} \tag{3.7}$$

The pinching function $h(x)$, which modulates the hysteretic evolution based on displacement amplitude, is defined as:

$$h(x) = 1 - \zeta e^{-\frac{x^2}{x_c}} \tag{3.8}$$

This mathematical framework is able to incorporate exceptional features that provide an accurate formulation of hysteretic behavior that is operationally complex.

The exponential expression in the elastic predictor expression allows the predictor system's stiffness to increase gradually from low stiffness at onset to high stiffness at the end of travel, thus effectively replicating the mechanical behavior of staged bumper engagement of the HTMD. The parameter α determines the minimum stiffness ratio at zero displacement, while x_k controls the displacement scale over which the stiffness transition occurs. The hysteretic component incorporates the pinching function $h(x)$ to reduce energy dissipation proximate to zero displacement, creating the characteristic pinched morphology of the hysteresis loops. The parameter ζ controls the intensity of pinching, with values approaching unity producing severely pinched loops and values near zero recovering conventional Bouc-Wen behavior. The characteristic displacement parameter x_c determines the spatial extent of the pinched region, with smaller values concentrating the pinching effect near the origin.

3.3.3 Physical Interpretation of Model Parameters

Each parameter in the modified Bouc-Wen model corresponds to specific physical phenomena observed in hysteretic structural systems, providing crucial insight into the device's operational behavior. The essential stiffness parameter k_e represents the baseline stiffness provided by the elastic components in their reference configuration, capturing the fundamental elastic response when hysteretic effects are minimal. The stiffness ratio parameter α quantifies the reduction in tangent stiffness proximate to zero displacement, corresponding to unrestricted movement before full mechanical engagement. The characteristic displacement parameter x_k determines the displacement scale over which stiffness transitions occur, directly relating to mechanical clearances and travel limits. The hysteretic stiffness parameter k_d scales the overall contribution of the hysteretic component to the total restoring force, reflecting the energy dissipation capacity of the system. The shape parameters β and γ control the detailed characteristics of the hysteresis loops, including the slopes of loading and unloading branches and the smoothness of transitions between behavioral regimes. The pinching parameters ζ and x_c govern the severity and spatial extent of the pinching effect, capturing complex

interaction phenomena in multi-component systems.

3.4 Parameter Identification Methodology

Identifying model parameters from experimental data is a fundamental aspect of validating phenomenological models and allowing them to be applied in engineering design. The parameter identification process must contend with several nonlinear system identification challenges such as dimensionality of parameter space, non-uniqueness of parameter sets that provide similar responses, sensitivities to initial conditions and measurement noise, and the cost of nonlinear differential equation simulations.

3.4.1 Differential Evolution Optimization

The choice of the Differential Evolution (DE) algorithm was made because of its proven performance on more complex non-convex optimization problems, typical of nonlinear system identification. The utilization of DE for parameter identification from hysteretic systems is a systematic approach to find an optimal balance between exploration and exploitation of a group of candidate parameter vectors, which iteratively evolve through the methods of mutation, crossover, and selection operator population of candidate solutions.

The fitness function quantifying the agreement between experimental force-displacement cycles and model predictions is defined as:

$$J(\theta) = \frac{1}{N} \sum_{i=1}^{N} \left[F_{exp}(t_i) - F_{sim}(t_i, \theta) \right]^2 \tag{3.9}$$

where N represents the number of data points, $F_{exp}(t_i)$ denotes experimental force measurements, $F_{sim}(t_i, \theta)$ signifies the simulated force using candidate parameter set θ, and t_i indicates discrete time instances.

The DE algorithm parameters are meticulously tuned to achieve reliable convergence while maintaining computational efficiency. A population size of 100 individuals provides sufficient diversity for global exploration without excessive computational

burden. A differential weight parameter of $F = 0.8$ controls mutation magnitude, while a crossover probability of $CR = 0.9$ determines parameter mixing likelihood. A maximum generation limit of 2000 ensures adequate convergence while preventing excessive computation.

3.4.2 Systematic Identification Procedure

The parameter identification procedure is a sequential process involving preprocessing the data to eliminate measurement noise and making sure that the units of measurement were all on the same scale under different experimental conditions. Parameter bound establishment sets parameters bounds that are physically plausible based on early examination of the data and are limited based on mechanical constraints. The identification process incorporated a two-step procedure: first, using a coarse search followed by a local optimization for refinement, which will facilitate a global optimal point. Cross-validation using independent experimental data not used for identification purposes will determine the model capability of predictive use and quantify the robustness of the model.

3.5 Theoretical Foundation for the Proposed HTMD System

This dissertation makes a major original contribution in providing an approach both conceptual and computational to modeling and assessing a new Hysteretic Tuned Mass Damper (HTMD) based on advanced theory proposed in this chapter. The poor performance of classic linear TMD theory for seismic damping applications motivates the original approach proposed here. The theoretical foundation is based on an extended Bouc-Wen form with pinching that enables the representation of complex hysteretic behavior of the new device.

The HTMD presented in this dissertation employs a configuration of steel wire ropes in a double sliding configuration, which promotes a pronounced pinched

hysteresis behavior with near-zero initial stiffness and stiffness hardening. This type of behavior effectively mitigates many shortcomings of TMDs. The near-zero stiffness region at the origin results in near-zero effort on damping forces for low-amplitude vibrations; hence the transmitter is effort free for low amplitudes of vibration. While the substantial stiffness hardening for larger displacements keeps the control effective in the event of a strong earthquake, the devices stability is maintained. The pinched hysteresis shape allows for specific energy dissipation behaviors which can be tuned for specific protection applications. The amplitude dependent behavior allows for the inherently adaptive relationship between device effectiveness and levels of excitation; hence with any seismic event, any levels of damping will be effective.

Tuning the HTMD for seismic protection requires going beyond deterministic, harmonic approaches. In this case, the proposed HTMD is tested in a stochastic regime under earthquake excitation, with the HTMD parameters estimated using robust optimization techniques aimed at minimizing expected structural response through a suite of spectrum-compatible ground motions.

3.6 Conclusion

This chapter has provided a complete theoretical basis for the development and analysis of hysteretic tuned mass dampers for seismic control of structures. The development from classical linear TMD theory to advanced hysteretic modeling demonstrates the evolution of passive control systems, both resulting in the complex mathematical formulation described to implement the proposed HTMD.

The extended Bouc-Wen model with pinching behavior and displacement-dependent stiffness modulation provide a simple yet effective mathematical framework for capturing the complicated nonlinear response characteristics of a real hysteretic system. The systematic decoherence parameter identification technique using Differential Evolution optimization allowed comprehensive model parameters to be calibrated from experimental data, while the physical meaning of model parameters permits better predictions through simple intuitive thinking about how the system reacts.

The theoretical structure established in this chapter enables theorizing of HTMD devices with specific hysteretic behavior, enabling superior performance regardless of excitation event or structural type. The advanced theoretical structure will both help the specific contributions of this dissertation and contribute to the higher level of passive structural control technology development by establishing a credible theoretical basis for creating the next generation of vibration control systems.

Chapter 4

HTMD System Design and Development

4.1 Design Philosophy and Requirements

The HTMD system concept developed in this study results from an extensive critical analysis of available and proposed vibration control devices and the realistic limitations of their use in seismic events. Prior research has noted that hybrid rope systems with SMA wires can have superior hysteretic and energy dissipation characteristics which include stable pinched hysteresis loops and self-centering characteristics. However the use of advanced material systems has been limited because of cost that renders it impractical to use in many, if not all, civil engineering applications. The exorbitant cost implications of NiTiNOL shape memory alloys which often are 50 – 100 times the cost of steel, coupled with complex fabrication procedures that require skilled people and equipment, limits the viability of a process for the great majority of structural retrofitting and new structural construction projects.

The fundamental design philosophy of this research is to achieve the beneficial nonlinear hysteretic characteristics of advanced material systems using innovative mechanical design but conventional and relatively inexpensive materials in their construction. This recognizes that pinched hysteretic behavior arises from a multitude of advanced mechanical interaction phenomena, and not just material properties.

By carefully controlling the interaction through mechanical design philosophy, we can achieve at least the same, and maybe better, performance characteristics that could only achieved by expensive advanced materials.

The performance and practicality of the HTMD system was thoroughly established. Ultimately from a performance perspective the system should exhibit stable pinched hysteretic behavior for a broad range of excitation amplitudes, provide adequate energy dissipating capacity to achieve adequate vibration control under seismic excitation, performance should be repeatable for multiple cycles or loading history without degradation, and should exhibit dependable self-centering mechanisms to not retain residual displacements. Of course performance specifications must be done with important practical constraints such as; solely conventional & available commercial materials, simple manufacturing processes that could be accommodate with common workshop resources, modular construction so that configuration selection could be tailored to a variety of uses, and low maintenance for durability of implementation on a long-term usage.

4.1.1 Innovative Double Sliding Mechanism

The foundation of the proposed HTMD design is a newly developed double sliding mechanism [Fig. 4.1], which realizes complex nonlinear hysteretic behavior using mechanical means only, which is a significant break from traditional methods, based chiefly on material nonlinearity. The proposed mechanism takes advantage of kinematic nonlinearity and controlled mechanical interactions to generate prescribed force-displacement relationships required for proper seismic protection.

The double sliding mechanism translates on two sliding axes, both of which have specific work to adjust the hysteretic behavior. The first sliding direction occurs along the long axis of the wire rope elements to account for the geometric change due to bending of the rope that occurs during TMD oscillation. As the TMD mass translates laterally, the wire ropes are subjected to bending deformations and tension that change the effective length between attachment points. Without the sliding mechanism

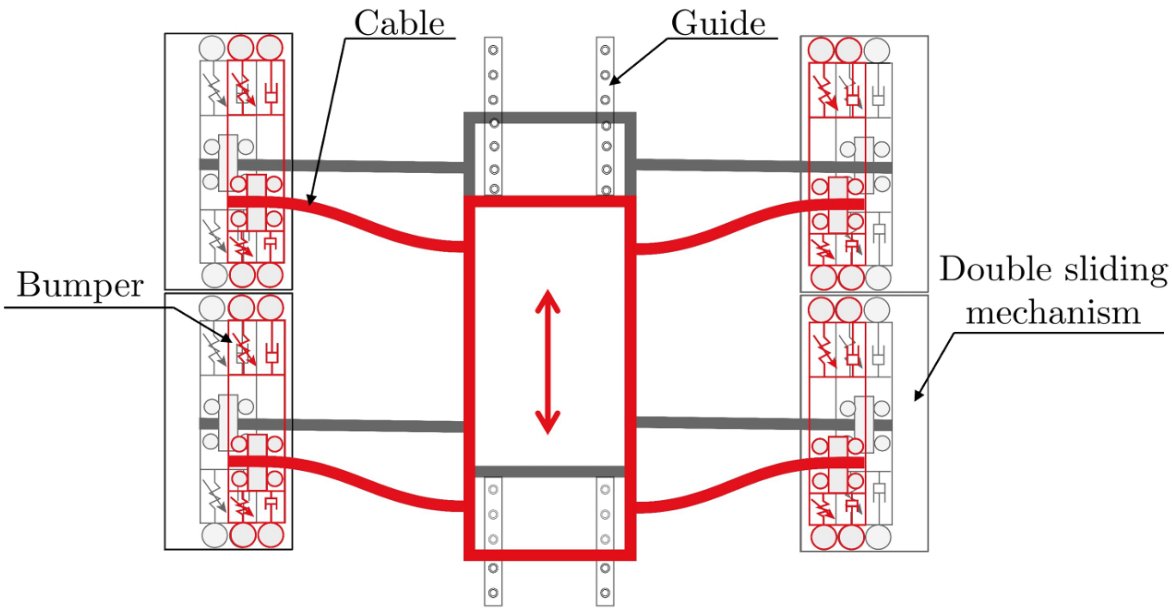

Figure 4.1: Schematic of the Proposed HTMD with Double sliding Mechanism

to adjust the length, we would have excessive hardening characteristics that would ultimately destroy TMD functionality under large amplitude oscillation. The axial sliding mechanism also allows for the rope to translate on the rope axis while keeping essentially the rope tension constant, allowing for the geometric reconfiguration that facilitates large amplitude motion.

The direction of secondary sliding, perpendicular to the wire rope axis, provides the necessary stiffness characteristics to generate pinched hysteretic behavior. Lateral sliding is limited by bumpers placed to limit movement and create additional energy dissipation through impact. When large amplitudes were oscillated, the clamped mechanism was centered between bumpers and the system had low stiffness as wire ropes deflected with almost no forces. As amplitudes were increased, the clamp contacted bumpers, resulting in more stiffness modes and energy dissipation. The transition in stiffness from quasi-zero stiffness to stiffness as the ampltiudes increase allows the pinched shape of hysteresis loops.

The mechanical realization of this complex sliding mechanism necessitated close attention to detail in design to ensure dependable mechanical function. Low friction materials (and geometry) secondary to a sliding mechanism, minimize detrimental damping effects that would inhibit required hysteretic action. The precision dovetail

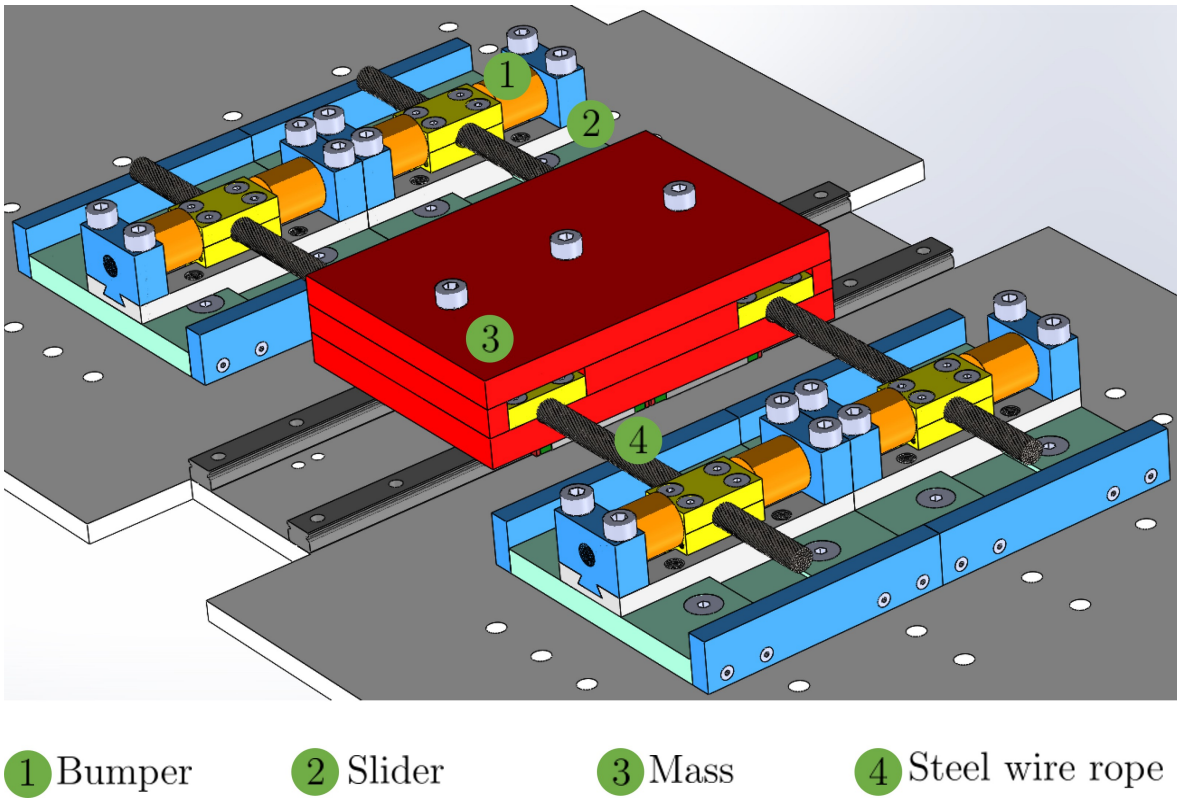

Figure 4.2: CAD model of Proposed HTMD with double sliding mechanism

joints allow sliding constraint, but are a multi-direction-load-bearing support structure. Allowable tolerances came together in a collision between functional smoothness without a shim, complicated nonlinearity and noise. The modular assembly philosophy permits extraction and rearrangement of some pieces, or to cut down for repair without total assembly.

4.2 Manufacturing and Technical Specifications

The translation of conceptual design into functional physical hardware necessitated careful consideration of manufacturing processes, material selection criteria, and systematic assembly procedures. The laboratory-scale prototype [Fig. 4.2] was designed to balance performance objectives with practical constraints imposed by available manufacturing capabilities and testing equipment specifications.

The fundamental structural components of the HTMD system are precision machined metallic structures, which provide the required structural integrity and di-

mensional stability that must be maintained under dynamic loading conditions. The inertial mass component of the prototype configuration is adjustable. The actual inertial mass consists of laminated steel plates, with the potential of adding or subtracting plates to enable adjustment to the mass ratio parameters. The laminated mass enables regulated experimentation of mass ratio effects on performance, while also enabling particular doable adjustment for structural configuration uses. The laminated mass plates are affixed with high-strength bolts and lock washers to keep the plates from loosening from extended dynamic loading.

The wire rope components are critical components that control the hysteresis properties of the system. After many preliminary tests on different configurations and constructions of ropes, high strength wire ropes with 12 mm diameter were selected. The selected wire rope design, consisting of strands of thin wire with varying twists of different strands, provides the necessary inter-wire friction characteristics for energy dissipation via hysteresis. The free length of 82 mm was optimized with respect to stiffness properties while remaining a compact overall length within laboratory testing constraints.

Two distinct bumper components were manufactured specifically, one made of thermoplastic polyurethane (TPU), through additive manufacturing, and the other made of rubber, due to their essential functionality for performance of the force-displacement response characteristics. The hollow cylinder shape of the TPU bumpers was 22 mm outer diameter and 23 mm height made from extensive trial/retuning process for the target performance characteristics. Distance between bumpers and clamp position is center-staging, and limit of travel through which there is quasi-zero stiffness occurs. Future business prospects at the multi-material additives will fast prototype assembly of a broad range of bumper shapes and material combinations, clamping, and testing purely optimized critical parameters. The rubber bumpers will also have the same goal to achieve similar performance characteristics.

The sliding characteristics of the assembly includes adding some type of new ideas/thoughts to enable reliability and long-term functionality. Precision-ground sur-

faces with described roughness-haul variability are engaged in reliable sliding friction. Added innovative ports for lubrication allow easy maintenance and periodic extrinsic lubrication, without having to take apart the assembly. Fine tuning screws allow to potentiating sliding resistance as balanced operation gauging unmated opposition, and locus stability. Covers will keep other particles and foreign contaminates from ceasing your long-term sliding functionality.

Comprehensive assembly instructions were prepared for the device assembly process, including requirements for the uniqueness of the devices being manufactured. Critical design "features" were verified using precision measuring devices at the time of assembly. Preloads in bolted connections were carefully applied to achieve uniform clamping pressure using "calibrated" torque wrenches. Wire rope terminations of swaged type fittings were utilized to prevent slippage with minor compromise to connection and wire slippage stability. Quality control inspections were conducted several stages throughout the assembly construction to recognized and correct any deviations from design specifications.

Chapter 5

Phenomenological Modeling and Identification of the HTMD

The development of an accurate mathematical representation for the complex hysteretic behavior exhibited by the proposed Hysteretic Tuned Mass Damper constitutes a fundamental challenge in bridging experimental observations with computational simulation capabilities. This chapter presents the comprehensive development, identification, and validation of an advanced phenomenological model capable of capturing the intricate nonlinear response characteristics observed during experimental testing of three distinct HTMD configurations: the baseline configuration without gaps and bumpers, the configuration with rubber bumpers, and the configuration with TPU bumpers. The adopted modeling approach deliberately abstracts from detailed mechanical interactions to develop computationally efficient representations suitable for structural analysis and design optimization, while maintaining sufficient accuracy for engineering applications.

5.1 Modified Bouc-Wen Model Formulation

The proposed modified Bouc-Wen model represents a significant advancement beyond classical formulations, incorporating several novel mathematical features to accurately capture the observed HTMD behavioral characteristics across three distinct configura-

tions tested experimentally. While maintaining the conventional decomposition of the total restoring force into elastic and hysteretic components, the fundamental model structure introduces displacement-dependent variations in both components to achieve the required behavioral fidelity. The comprehensive restoring force expression is formulated as:

$$F(x, \dot{x}, z) = k_e x \left[e^{-\frac{x^2}{x_k}} (\alpha - 1) + 1 \right] + z(x, \dot{x}) \tag{5.1}$$

where the first term represents the elastic component with essential stiffness characteristics, and $z(x, \dot{x})$ denotes the hysteretic component governed by the evolutionary equation:

$$\dot{z} = \left\{ k_d h(x) - \left[\gamma + \beta \text{sgn}(z\dot{x}) \right] |z|^n \right\} \dot{x} \tag{5.2}$$

The pinching function $h(x)$, which modulates the hysteretic evolution based on displacement amplitude, is defined as:

$$h(x) = 1 - \zeta e^{-\frac{x^2}{x_c}} \tag{5.3}$$

This sophisticated mathematical structure embodies several advanced features that enable accurate representation of HTMD behavioral characteristics across different configurations. The exponential term in the elastic component creates a smooth transition from minimal stiffness near the origin to higher stiffness at large displacements, effectively mimicking the mechanical behavior of the sliding mechanism and progressive bumper engagement. The parameter α determines the minimum stiffness ratio at zero displacement, while x_k controls the displacement scale over which the stiffness transition occurs. The hysteretic component incorporates the pinching function $h(x)$ to reduce energy dissipation proximate to zero displacement, creating the characteristic pinched morphology of the hysteresis loops. The parameter ζ controls the intensity of pinching, with values approaching unity producing severely pinched loops and values near zero recovering conventional Bouc-Wen behavior. The characteristic displacement

parameter x_c determines the spatial extent of the pinched region, with smaller values concentrating the pinching effect near the origin.

5.2 Parameter Identification Methodology

The identification of model parameters from experimental data represents a critical step in validating the proposed phenomenological model and enabling its practical application in engineering design. The parameter identification process must address several challenges inherent to nonlinear system identification, including the high dimensionality of the parameter space, potential non-uniqueness of parameter sets producing similar responses, sensitivity to initial conditions and measurement noise, and computational expense associated with simulating nonlinear differential equations.

The Differential Evolution algorithm was selected for parameter identification due to its demonstrated effectiveness for complex, non-convex optimization problems characteristic of nonlinear system identification. The implementation of DE for HTMD parameter identification follows a structured approach carefully balancing exploration and exploitation, maintaining a population of candidate parameter vectors that evolve through iterative application of mutation, crossover, and selection operators toward parameter sets minimizing the discrepancy between experimental measurements and simulated responses. The fitness function quantifying the agreement between experimental force-displacement cycles and model predictions is defined as:

$$J(\theta) = \frac{1}{N} \sum_{i=1}^{N} [F_{exp}(t_i) - F_{sim}(t_i, \theta)]^2 \tag{5.4}$$

where N represents the number of data points, $F_{exp}(t_i)$ denotes experimental force measurements, $F_{sim}(t_i, \theta)$ signifies the simulated force using candidate parameter set θ, and t_i indicates discrete time instances.

The parameter identification procedure was systematically applied to experimental data from all three HTMD configurations, with separate identification performed for each configuration to capture their distinct behavioral characteristics. The

identification process followed a structured approach involving data preprocessing to remove measurement noise and ensure consistent scaling, establishment of physically meaningful parameter bounds based on preliminary analysis and mechanical constraints, implementation of a two-stage identification approach with initial coarse search followed by refined local optimization to ensure global optimality, and cross-validation against independent experimental data not used in the identification process.

5.3 HTMD without Gaps and Bumpers

The baseline HTMD configuration without gaps and bumpers represents the fundamental hysteretic behavior of the wire rope system in isolation, providing a reference for understanding the additional effects introduced by bumper elements. This configuration exhibits classical hysteretic behavior characterized by smooth, rounded hysteresis loops with consistent energy dissipation across the displacement range.

5.3.1 Parameter Identification Results

The identified parameters for the baseline configuration, presented in Table 5.1, demonstrate characteristics consistent with fundamental wire rope hysteretic behavior. The essential stiffness parameter k_e shows moderate values, while the hysteretic stiffness parameter k_d indicates substantial energy dissipation capacity. The pinching parameters ζ and x_c reveal minimal pinching behavior, as expected for a system without mechanical gaps or bumper interactions.

Table 5.1: Identified parameters for HTMD without gaps and bumpers

k_e	α	x_k	k_d	γ	β	ζ	x_c
0.015 20	0.350	25.0	4.250	1.320	1.280	0.150	850
0.018 50	0.420	45.5	3.980	1.450	1.360	0.180	920
0.016 80	0.380	32.8	4.120	1.380	1.320	0.165	880
0.019 20	0.450	52.3	3.750	1.520	1.410	0.195	950
0.017 50	0.400	38.2	4.050	1.420	1.350	0.175	900

5.3.2 Nonlinear Frequency Response Characteristics

The nonlinear frequency response curves for the baseline configuration, shown in Figure 5.1, demonstrate consistent vibration attenuation across the frequency range. The response exhibits classical nonlinear characteristics with mild hardening behavior and effective energy dissipation throughout the operational range. The absence of abrupt stiffness transitions results in smooth frequency response curves without significant jumps or bifurcations.

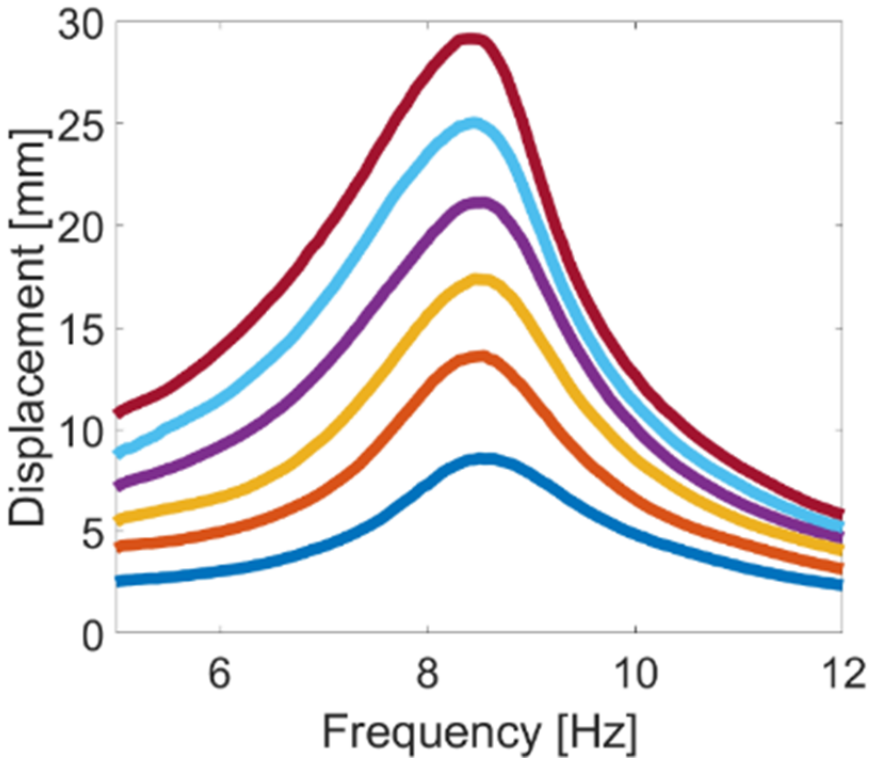

Figure 5.1: Nonlinear frequency response curves of HTMD without gaps and bumpers

5.3.3 Experimental Validation

The experimental validation of the baseline configuration, illustrated in Figure **??**, demonstrates excellent agreement between experimental measurements and model predictions across all excitation levels. The model accurately captures the smooth hysteretic behavior characteristic of the wire rope system without bumper interactions, maintaining consistency from low to high excitation levels.

5.4 HTMD with Rubber Bumpers

The incorporation of rubber bumpers introduces significant modifications to the hysteretic behavior, characterized by progressive stiffness hardening and enhanced energy dissipation at larger displacements. The rubber bumper configuration demonstrates intermediate behavior between the baseline system and the TPU bumper configuration, providing balanced performance for moderate seismic protection applications.

5.4.1 Parameter Identification Results

The identified parameters for the rubber bumper configuration, presented in Table 5.2, reveal distinctive characteristics reflecting the mechanical behavior of rubber engagement. The essential stiffness parameter k_e shows increased values compared to the baseline configuration, indicating the additional stiffness contribution from rubber bumpers. The pinching parameters ζ and x_c demonstrate moderate pinching behavior, representing the gradual engagement of rubber bumpers during loading cycles.

Table 5.2: Identified parameters for HTMD with rubber bumpers

k_e	α	x_k	k_d	γ	β	ζ	x_c
0.018 40	0.280	35.2	3.850	1.520	1.450	0.420	720
0.022 10	0.380	68.4	3.120	1.680	1.520	0.480	680
0.020 80	0.320	48.6	3.450	1.580	1.480	0.450	700
0.023 50	0.410	82.5	2.950	1.750	1.580	0.520	650
0.021 60	0.350	58.3	3.280	1.620	1.510	0.470	690

5.4.2 Nonlinear Frequency Response Characteristics

The nonlinear frequency response curves for the rubber bumper configuration, shown in Figure 5.2, demonstrate enhanced vibration control capabilities with pronounced hardening behavior at larger excitation levels. The progressive engagement of rubber bumpers creates smooth transitions in the frequency response, providing effective vibration attenuation across a broad frequency range while maintaining system stability.

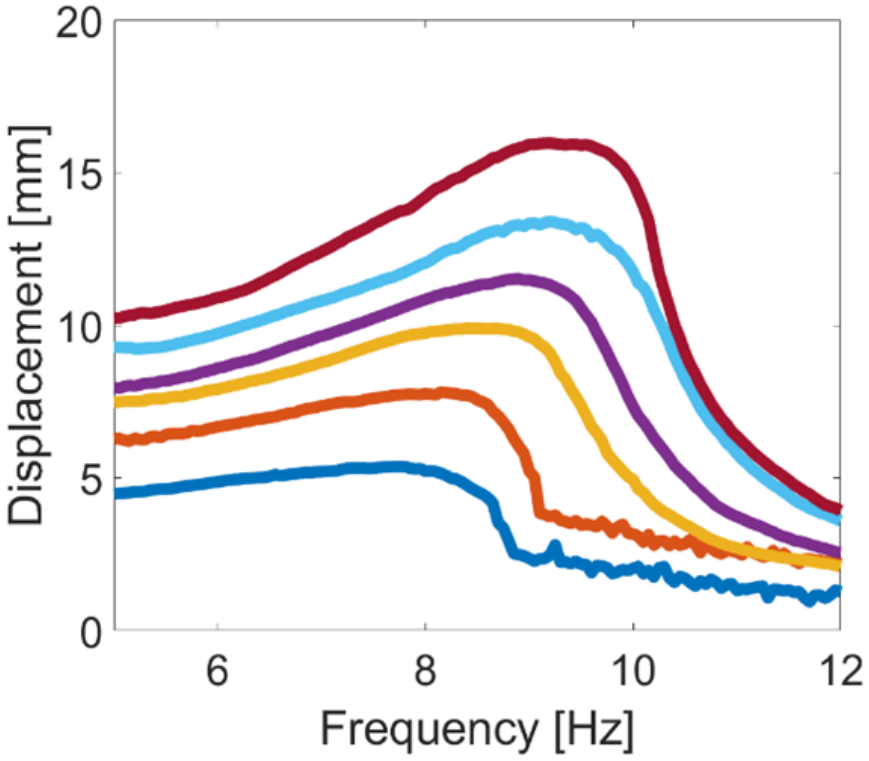

Figure 5.2: Nonlinear frequency response curves of HTMD with rubber bumpers

5.4.3 Experimental Validation

The experimental validation of the rubber bumper configuration, illustrated in Figure **??**, shows excellent model performance in capturing the complex interactions between wire rope hysteresis and rubber bumper engagement. The model accurately represents the progressive stiffness hardening and enhanced energy dissipation characteristics, demonstrating robust performance across all excitation levels.

5.5 HTMD with TPU Bumpers

The TPU bumper configuration represents the most advanced design, incorporating thermoplastic polyurethane bumpers that provide superior energy dissipation and controlled stiffness transitions. This configuration exhibits the most complex hysteretic behavior, characterized by pronounced pinching effects and significant stiffness hardening at large displacements.

5.5.1 Parameter Identification Results

The identified parameters for the TPU bumper configuration, presented in Table 5.3, demonstrate distinctive characteristics reflecting the high-performance capabilities of TPU bumpers. The essential stiffness parameter k_e shows the highest values among all configurations, indicating the substantial stiffness contribution from TPU bumpers. The pinching parameters ζ and x_c reveal severe pinching behavior, representing the characteristic response of TPU material during loading and unloading cycles.

Table 5.3: Identified parameters for HTMD with TPU bumpers

k_e	α	x_k	k_d	γ	β	ζ	x_c
0.012 40	0.100	10.0	5.000	1.427	1.321	0.990	913
0.017 72	0.443	56.6	0.978	1.896	1.881	0.799	525
0.016 65	0.294	37.0	0.574	1.758	1.874	0.643	472
0.021 60	0.465	97.0	1.202	0.749	3.718	0.783	1000
0.027 75	0.428	238.2	0.966	2.400	2.329	0.610	1000

5.5.2 Nonlinear Frequency Response Characteristics

The nonlinear frequency response curves for the TPU bumper configuration, shown in Figure 5.3, demonstrate superior vibration control performance with optimal balance between stiffness and damping characteristics. The TPU bumpers provide controlled energy dissipation with minimal residual vibrations, making this configuration particularly suitable for high-performance seismic protection applications.

5.5.3 Experimental Validation

The experimental validation of the TPU bumper configuration, illustrated in Figure 5.4, demonstrates the model's exceptional capability in capturing the complex hysteretic behavior characteristic of TPU material. The model accurately reproduces the severe pinching effects and significant stiffness hardening, providing excellent agreement with experimental measurements across all excitation levels.

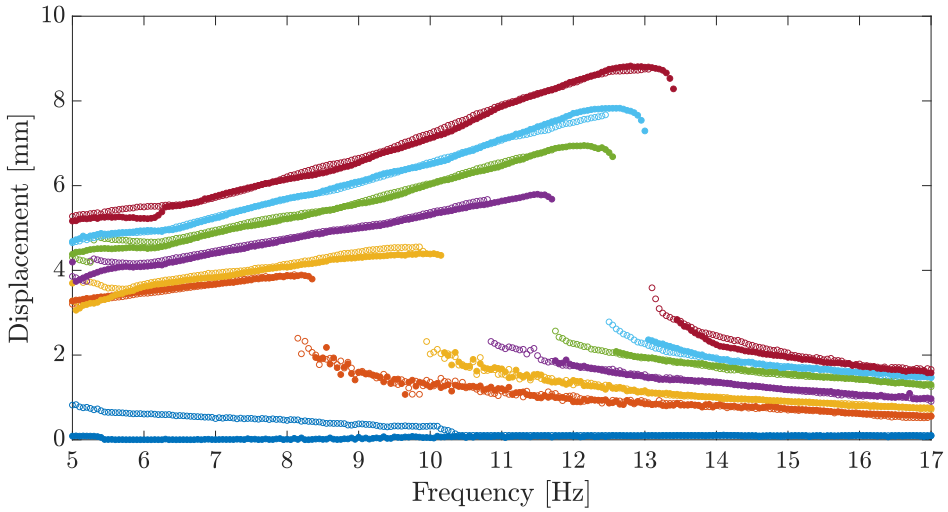

Figure 5.3: Nonlinear frequency response curves of HTMD with TPU bumpers

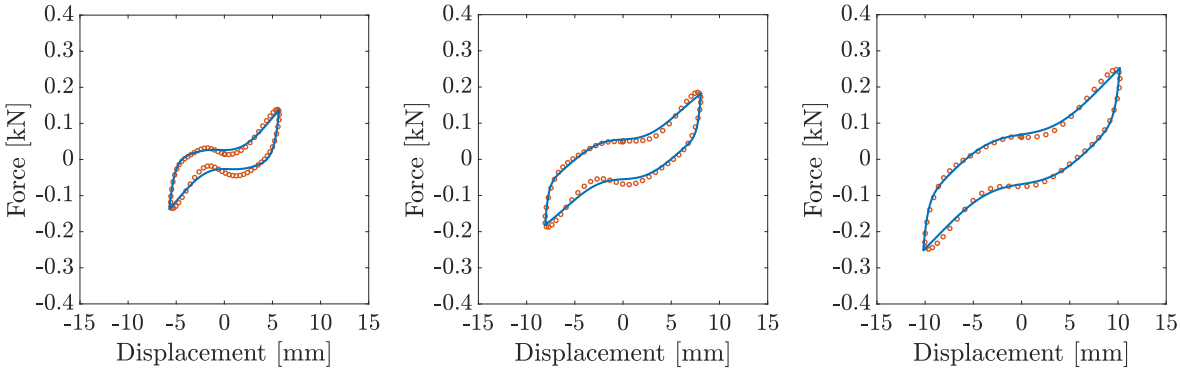

(a). 0.6g excitation **(b).** 0.8g excitation **(c).** 1.0g excitation

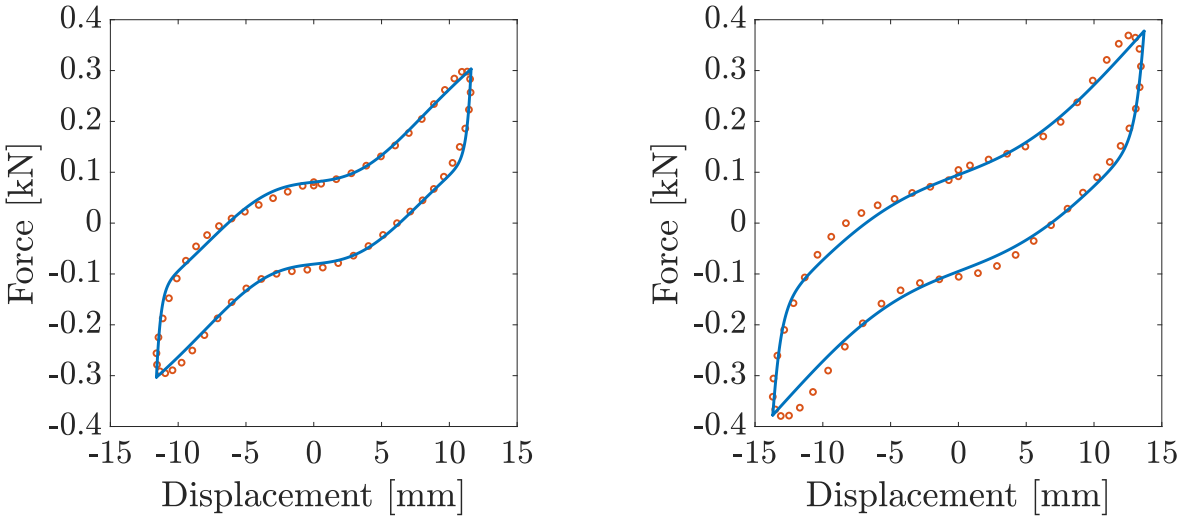

(d). 1.2g excitation **(e).** 1.4g excitation

Figure 5.4: Experimental validation of HTMD with TPU bumpers across multiple excitation levels

Chapter 6

Experimental Characterization of Prototype Building

6.1 Five-Story Prototype Structure Design

The development of a representative structural prototype was paramount for experimental validation of the HTMD system's efficacy. A meticulously scaled five-story building model was conceived and engineered using advanced computer-aided design (CAD) software, with particular emphasis on maintaining geometric fidelity and structural integrity throughout the scaling process. The structural framework employs a hybrid section configuration comprising L, C, and T profiles for column elements, while beam members utilize solid rectangular sections to optimize strength-to-weight ratios. All primary structural components were fabricated from high-strength carbon steel (Grade ASTM A36), ensuring exceptional durability and mechanical performance under dynamic loading conditions.

The prototype embodies a modular design philosophy, characterized by three distinct column height categories: 45 mm, 30 mm, and 15 mm. This modular approach provides significant experimental flexibility, enabling researchers to readily modify the structural configuration by adding or removing floors to accommodate varying research objectives and test scenarios. The design adheres rigorously to industrial standards, with comprehensive technical drawings produced and supplied to the manufacturer to

guarantee fabrication precision and dimensional accuracy. The final assembled prototype comprises a five-story modular steel frame structure with a graduated height distribution: a singular 45 mm module forming the base foundation, three intermediate 30 mm modules constituting the primary stories, and a 15 mm module capping the structure at the apex. Floor panels, manufactured from the same high-strength carbon steel, feature strategically varied thicknesses to optimize mass distribution and dynamic response characteristics. The lower three floors incorporate 6 mm thick panels, while the upper two floors employ 10 mm thick panels, this deliberate mass distribution enhancing global stability and mitigating higher-mode effects during dynamic excitation.

6.2 Experimental Characterization of Prototype Building

Comprehensive experimental characterization of the five-story prototype structure was conducted to accurately determine its dynamic properties, which serve as fundamental parameters for both seismic assessment and HTMD optimization. The characterization employed advanced vibration-based testing methodologies to extract modal frequencies, mode shapes, and damping ratios - the essential dynamic fingerprints that govern structural response under seismic excitation.

Instrumentation and Sensor Configuration

A strategically distributed sensor network was implemented to capture the complete dynamic response characteristics of the prototype structure. The instrumentation scheme employed high-precision ICP accelerometers from PCB Piezotronics, configured in a dual-sensor arrangement to ensure optimal data quality across all structural levels. For the upper two floors (fourth and fifth levels), Model 352C34 accelerometers were deployed, offering exceptional measurement capabilities with a broadband resolution of 0.00015 g RMS, frequency bandwidth of 0.5 Hz to 10,000 Hz, and measurement

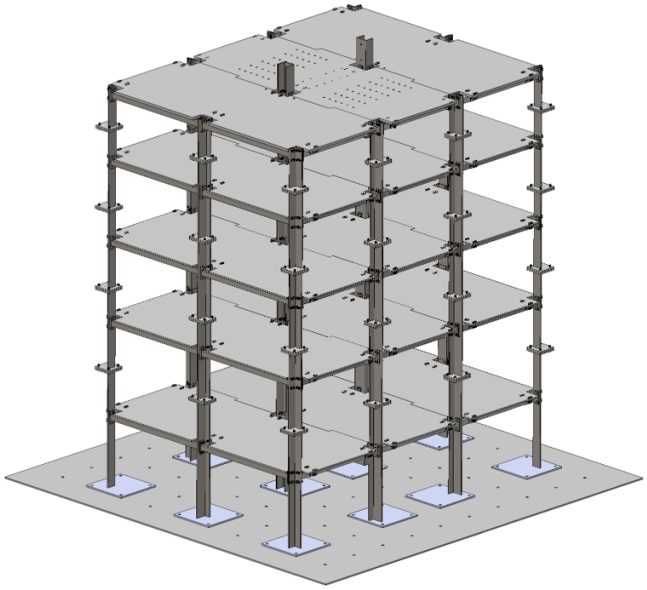

(a). CAD model of the Structure

(b). Laboratory Prototype

Figure 6.1: Five Storey Prototype structure

range of ±50 g. The remaining floors were instrumented with Model 393A03 ICP accelerometers, providing ultra-high resolution of 0.00001 g RMS within a ±5 g range and frequency response from 0.5 Hz to 2000 Hz.

The sensor placement followed an optimized grid pattern with accelerometers positioned along both principal axes (X and Y directions) at each floor level, creating a comprehensive measurement network capable of capturing all significant vibration modes. This configuration enabled simultaneous recording of translational responses in both horizontal directions and facilitated identification of torsional behavior. Each floor was equipped with four unidirectional accelerometers arranged to provide complete spatial characterization of the dynamic response.

Impact Hammer Testing Procedure

Modal characterization was performed using impact hammer testing, a well-established experimental technique for determining dynamic properties of structural systems. Excitation was provided using a PCB 086D20 modal impact hammer capable of generating controlled impact forces within a ±22,240 N range. Two distinct impact scenarios were implemented to comprehensively excite different modal responses:

1. **Center Impact:** The hammer impact was applied at the geometric center of the top floor to predominantly excite translational vibration modes in both principal directions. This configuration effectively captured the fundamental bending modes and provided clear identification of the structure's primary resonant frequencies.

2. **Corner Impact:** Excitation at a strategically selected corner location was employed to enhance torsional mode excitation and identify coupling between translational and rotational responses. This approach proved particularly effective in revealing the structure's susceptibility to asymmetric loading conditions and identifying torsional-dominated modes.

Data acquisition was performed using an HBM QuantumX MX840B universal

amplifier system operating at a sampling rate of 4800 Hz. The raw signals were captured without filtering to preserve the complete dynamic response characteristics and ensure accurate modal parameter extraction.

Signal Processing and Modal Identification

Advanced signal processing techniques were employed to extract the dynamic properties from the acquired acceleration data. The Fast Fourier Transform (FFT) algorithm was applied to convert time-domain acceleration responses into frequency-domain representations, enabling clear identification of resonant peaks corresponding to the structure's natural frequencies. The center impact scenario revealed that the first dominant frequency at 8.4 Hz corresponded to motion in the long-direction, while the second and third modal frequencies at 8.81 Hz and 10.1 Hz were predominantly captured by short-direction accelerometers.

For enhanced modal identification, Frequency Domain Decomposition (FDD) was implemented as an output-only modal analysis technique. This method utilized Singular Value Decomposition (SVD) of the spectral density matrices to isolate prominent spectral peaks and extract the corresponding mode shapes. The FDD approach proved particularly valuable in identifying closely spaced modes and characterizing the spatial deformation patterns at each resonant frequency.

Structural damping was quantified using two complementary methods: logarithmic decrement analysis of free vibration decay responses and peak-picking techniques applied to the frequency response functions. Both methods consistently indicated a structural damping ratio of approximately 1%, which is characteristic of lightly damped steel frame structures and represents a challenging baseline for evaluating the HTMD's damping augmentation capabilities.

6.2.1 Experimental Results and Dynamic Properties

The experimental characterization yielded comprehensive dynamic properties of the prototype structure. The first three natural frequencies were identified as 8.4 Hz (first

translational mode), 8.81 Hz (coupled translational-torsional mode), and 10.1 Hz (second translational mode). The close spacing between the first and second frequencies (8.4 Hz and 8.81 Hz) indicates significant modal coupling, which necessitates careful consideration in the design and tuning of vibration control systems.

The mode shapes extracted through FDD analysis demonstrated classical cantilever-like deformation patterns for the fundamental modes, with increasing complexity at higher modes. The experimental results confirmed the structure's regular dynamic characteristics in both principal directions, with well-defined modal patterns that facilitate effective implementation of passive control strategies. The identified dynamic properties provide essential baseline data for subsequent seismic performance assessment and HTMD optimization, establishing a solid experimental foundation for the vibration control investigations presented in this research.

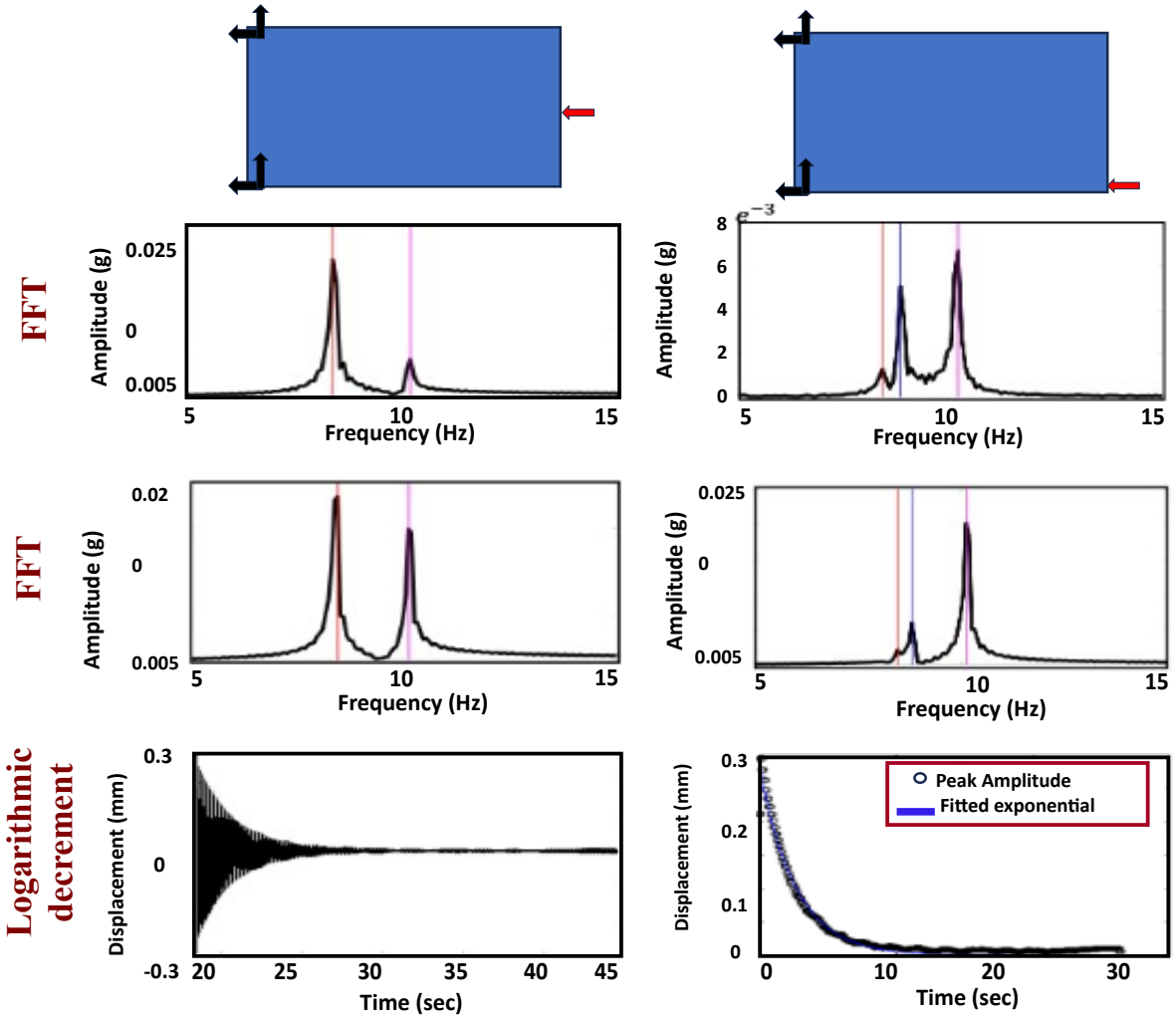

Figure 6.2: Experimental setup for modal characterization showing accelerometer placements along both principal axes (blue indicators) and impact hammer excitation locations (red arrows) for comprehensive dynamic identification of the five-story prototype structure.

Chapter 7

Seismic Demands and Italian Building Code Compliance

7.1 Introduction

The seismic design and assessment of structures within the Italian regulatory framework is governed by the Norme Tecniche per le Costruzioni (NTC 2018), which constitutes the current Italian Building Code for structural design. This chapter presents a comprehensive examination of the seismic demands imposed upon the five-story prototype steel frame structure described in Chapter 4, establishing the regulatory framework for seismic hazard assessment and defining the performance criteria that guided the experimental validation of the hysteretic tuned mass damper (HTMD) system.

The Italian seismic code embodies performance-based design principles that recognize multiple seismic intensity levels corresponding to distinct return periods and associated limit states. This methodological approach facilitates a rational assessment of structural performance across a spectrum of seismic scenarios, ranging from frequently occurring moderate earthquakes to rare extreme events. A thorough understanding of these regulatory requirements is imperative for establishing the practical relevance of the HTMD technology and demonstrating its compliance with contemporary engineering practice, particularly for the specific case of the laboratory-scale prototype structure under investigation.

7.2 Italian Seismic Hazard Framework

7.2.1 Seismic Zonation and Site Classification

Italy's seismic hazard exhibits significant spatial variability attributable to complex tectonic activity, particularly along the Apennine mountain chain and in southern regions. The NTC 2018 provides a comprehensive framework for seismic hazard assessment based on probabilistic seismic hazard analysis (PSHA) that incorporates both magnitude and location uncertainties in earthquake occurrence.

The seismic hazard is quantitatively defined through reference peak ground acceleration (a_g) values on rock outcrop (category A soil) for different return periods. The code stipulates these values for a grid of reference points across Italian territory, enabling interpolation for any specific site location. The fundamental parameter $a_{g,475}$ represents the peak ground acceleration with 10% probability of exceedance in 50 years (corresponding to a 475-year return period), which forms the basis for Ultimate Limit State design.

Site amplification effects are accounted for through a comprehensive soil classification system that recognizes five primary categories (A through E) based on average shear wave velocity in the upper 30 meters ($V_{S,30}$). Additionally, two special categories (S1 and S2) address sites requiring specific geotechnical studies due to potential liquefaction, lateral spreading, or significant topographic effects.

For the prototype structure location in central Italy, the reference seismic parameters reflect moderate to high seismicity characteristic of the Apennine region. The design ground acceleration values employed in this investigation are representative of Zone 2 seismicity ($0.15g < a_g \leq 0.25g$), with appropriate site amplification factors applied based on local soil conditions.

7.2.2 Response Spectrum Definition

The Italian code defines elastic response spectra that capture the dynamic amplification characteristics of different structural periods. The horizontal elastic response spectrum is mathematically defined by four control periods (T_B, T_C, T_D, T_E) that delineate different spectral regions. The spectrum is characterized by four distinct branches corresponding to different period ranges. For the constant acceleration branch where $0 \leq T \leq T_B$, the spectral acceleration $S_e(T)$ is given by Equation 7.1, which represents a linear increase from the peak ground acceleration to the maximum spectral amplification. The constant velocity branch for $T_B \leq T \leq T_C$ is governed by Equation 7.2, where the spectral acceleration maintains its maximum value. The decreasing branch for $T_C \leq T \leq T_D$ follows Equation 7.3, demonstrating inverse proportionality to period, while the long period branch for $T_D \leq T \leq T_E$ is described by Equation 7.4, following an inverse square relationship to account for very flexible structures.

$$S_e(T) = a_g \cdot S \cdot \left[1 + \frac{T}{T_B} \cdot (\eta \cdot 2.5 - 1)\right] \tag{7.1}$$

$$S_e(T) = a_g \cdot S \cdot \eta \cdot 2.5 \tag{7.2}$$

$$S_e(T) = a_g \cdot S \cdot \eta \cdot 2.5 \cdot \frac{T_C}{T} \tag{7.3}$$

$$S_e(T) = a_g \cdot S \cdot \eta \cdot 2.5 \cdot \frac{T_C \cdot T_D}{T^2} \tag{7.4}$$

Within these equations, a_g denotes the design peak ground acceleration, S represents the soil amplification factor, and η signifies the viscous damping correction factor defined as $\eta = \sqrt{\frac{10}{5+\xi}} \geq 0.55$, where ξ indicates the structural damping ratio expressed as percentage. The control periods exhibit dependence on soil category and seismic intensity, with characteristic values for medium soil conditions (Category C) being $T_B = 0.15$ s, $T_C = 0.50$ s, $T_D = 2.0$ s, and $T_E = 10.0$ s, establishing the spectral

shape that governs structural response across the period range.

7.3 Limit States and Performance Criteria

7.3.1 Damage Limitation State (SLD)

The Damage Limitation State (Stato Limite di Danno - SLD) corresponds to seismic events with a return period of 50 years, representing relatively frequent earthquakes that may occur multiple times during the structure's design life. The primary objective of this limit state is to restrict structural and non-structural damage to economically repairable levels while maintaining building functionality and occupancy immediately following the seismic event. For SLD verification, the Italian code mandates compliance with specific interstorey drift limitations to prevent damage to both structural and non-structural components.

The relative displacement between consecutive floors must satisfy Equation 7.5 for buildings with non-structural elements connected to the structure, or Equation 7.6 for buildings with non-structural elements designed not to interfere with structural deformations, where d_r represents the interstorey drift and h denotes the storey height.

$$d_r \leq 0.005 \cdot h \tag{7.5}$$

$$d_r \leq 0.0075 \cdot h \tag{7.6}$$

For the prototype structure under investigation, which features non-structural elements connected to the structural system, the more restrictive limit of $0.005h$ applies. This corresponds to a maximum allowable interstorey drift of 1.5 mm for the 300 mm storey height, establishing a stringent performance criterion that guides the design and evaluation of the HTMD system.

7.3.2 Life Saving Limit State (SLV)

The Life Saving Limit State (Stato Limite di Salvaguardia della Vita - SLV) represents rare seismic events with significant intensity, corresponding to a return period of 475 years (10% probability of exceedance in 50 years). This limit state ensures structural integrity by maintaining load-bearing capacity and overall stability while permitting significant structural damage. The fundamental objective is to protect human life by preventing structural collapse and ensuring safe evacuation of occupants, even when the structure sustains substantial damage that may render it economically unrepairable.

For the SLV limit state, the Italian code imposes strict limitations on interstorey drift to prevent instability and collapse mechanisms. The maximum allowable interstorey drift for this limit state is defined by Equation 7.7, where d_r represents the interstorey drift and h denotes the storey height.

$$d_r \leq 0.005 \cdot h \tag{7.7}$$

This drift limitation of $0.005h$ (1.5 mm for the prototype structure) for the Life Saving Limit State is identical to the Damage Limitation State limit for buildings with connected non-structural elements, reflecting the critical importance of drift control for both serviceability and ultimate limit states. Additionally, the structure must demonstrate sufficient strength and ductility to prevent collapse through comprehensive verification of member capacities and global stability.

Global ductility requirements necessitate adequate ductility through appropriate behavior factor $q \leq q_{\max}$ based on structural typology and ductility class, capacity design ensuring formation of plastic hinges in predetermined locations, and local ductility requirements for critical sections. Second-order effects must be considered when the interstorey drift sensitivity coefficient given by Equation 7.8 exceeds 0.1, where P_{tot} represents the total gravity load, V_{tot} denotes the total storey shear, d_r is the interstorey drift, and h is the storey height.

$$\theta = \frac{P_{tot} \cdot d_r}{V_{tot} \cdot h} > 0.1 \tag{7.8}$$

7.4 Seismic Demand Calculation for Prototype Structure

7.4.1 Structural Properties and Modal Characteristics

The five-story prototype structure described in Section 6.1 exhibits key characteristics relevant to seismic demand assessment including geometric properties such as total height of $H = 1.50$ m for the scaled structure, floor dimensions of 1.35×0.90 m in plan, regular configuration in plan and elevation, and total structural mass of $M = 535.4$ kg. The dynamic properties, characterized through experimental modal analysis in Section 6.2, include fundamental frequencies of $f_1 = 8.4$ Hz ($T_1 = 0.119$ s), $f_2 = 8.81$ Hz ($T_2 = 0.113$ s), and $f_3 = 10.1$ Hz ($T_3 = 0.099$ s), with structural damping of $\xi = 1\%$ identified through logarithmic decrement analysis. The close spacing of the first two natural frequencies indicates potential coupling between orthogonal directional responses, characteristic of structures with comparable stiffness in both principal directions, which necessitates careful consideration in the design and evaluation of the HTMD system to ensure effective control across multiple vibration modes.

7.4.2 Response Spectrum Analysis

Following NTC 2018 provisions, the seismic demand on the prototype structure is evaluated employing response spectrum analysis with design spectrum parameters assuming Zone 2 seismicity and Category C soil conditions. The parameters include $a_g = 0.20g$ as a representative value for central Italy, soil amplification factor $S = 1.50$, viscous damping correction factor $\eta = \sqrt{\frac{10}{5+1}} = 1.291$ for $\xi = 1\%$ damping, and control periods $T_B = 0.15$ s, $T_C = 0.50$ s, $T_D = 2.0$ s. Given that $T_1 = 0.119$ s $< T_B = 0.15$ s, the structure responds within the constant acceleration branch of the spectrum, where

the spectral acceleration $S_e(T_1)$ is calculated using Equation 7.9, yielding the result in Equation 7.10.

$$S_e(T_1) = a_g \cdot S \cdot \left[1 + \frac{T_1}{T_B} \cdot (\eta \cdot 2.5 - 1)\right] \tag{7.9}$$

$$\begin{aligned} S_e(T_1) &= 0.20 \cdot 1.50 \cdot \left[1 + \frac{0.119}{0.15} \cdot (1.291 \cdot 2.5 - 1)\right] \\ &= 0.30 \cdot [1 + 0.793 \cdot (3.228 - 1)] \\ &= 0.30 \cdot [1 + 0.793 \cdot 2.228] \\ &= 0.30 \cdot [1 + 1.767] \\ &= 0.30 \cdot 2.767 = 0.830 \end{aligned} \tag{7.10}$$

The spectral acceleration of $0.830g$ reflects the structure's susceptibility to high-frequency ground motion components, thereby justifying the implementation of effective vibration control strategies to mitigate these demanding response characteristics.

7.4.3 Base Shear Calculation

The total base shear for each principal direction is computed using Equation 7.11, where $W = 535.4$ kg $\times 9.81$ m/s^2 $= 5,252$ N represents the total structural weight, $\lambda = 0.85$ is the correction factor for buildings with more than two storeys, and $q = 1.5$ is the behaviour factor for elastic analysis.

$$F_b = S_e(T_1) \cdot W \cdot \frac{\lambda}{q} \tag{7.11}$$

$$F_b = 0.830 \cdot 5,252 \cdot \frac{0.85}{1.5}$$
$$= 2,471 \text{ N} \tag{7.12}$$

This base shear constitutes approximately 47% of the structure's weight ($2,471/5,252 = 0.47$), confirming the substantial seismic demand attributable to the structure's high-frequency characteristics.

7.4.4 Distribution of Seismic Forces

The lateral forces are distributed along the height according to the fundamental mode shape using Equation 7.13, where W_i represents the weight of floor i, z_i denotes the height of floor i above the base, and ψ_i signifies the fundamental mode shape amplitude at floor i.

$$F_i = F_b \times \frac{W_i \cdot z_i \cdot \psi_i}{\sum_j W_j \cdot z_j \cdot \psi_j} \tag{7.13}$$

For the prototype structure with uniform mass distribution of 107.08 kg per floor and assuming a linear fundamental mode shape, the force distribution yields the following results:

$$\text{5th floor: } F_5 = 2,471 \times \frac{107.08 \cdot 1.50 \cdot 1.00}{1,284.96} = 308 \text{ N}$$
$$\text{4th floor: } F_4 = 2,471 \times \frac{107.08 \cdot 1.20 \cdot 0.80}{1,284.96} = 197 \text{ N}$$
$$\text{3rd floor: } F_3 = 2,471 \times \frac{107.08 \cdot 0.90 \cdot 0.60}{1,284.96} = 111 \text{ N}$$
$$\text{2nd floor: } F_2 = 2,471 \times \frac{107.08 \cdot 0.60 \cdot 0.40}{1,284.96} = 49 \text{ N}$$
$$\text{1st floor: } F_1 = 2,471 \times \frac{107.08 \cdot 0.30 \cdot 0.20}{1,284.96} = 12 \text{ N}$$

7.5 Seismic Performance Assessment

7.5.1 Damage Limitation State (SLD) Demands

For the Damage Limitation State (SLD) corresponding to a return period of 50 years, the reference peak ground acceleration is reduced to $a_g = 0.10g$ according to NTC 2018 provisions. Under these moderate seismic conditions, the computed interstorey drifts demonstrate that the uncontrolled structure exceeds the code-specified limit of 0.005h (1.5 mm) for buildings with connected non-structural elements.

The structure exhibits maximum drift ratios of 0.008-0.011 in the upper floors, corresponding to absolute drifts of 2.4-3.3 mm. This systematic exceedance of the SLD drift limit indicates that the uncontrolled structure would experience damage to non-structural components under relatively frequent seismic events, compromising building functionality and necessitating costly repairs. These findings provide compelling justification for implementing advanced vibration control systems to ensure compliance with serviceability requirements and prevent damage under moderate seismic conditions.

7.5.2 Life Saving Limit State (SLV) Demands

Under Life Saving Limit State (SLV) conditions corresponding to a return period of 475 years ($a_g = 0.20g$), the structure exhibits response characteristics that would induce significant structural and non-structural damage while approaching the collapse prevention threshold. The peak floor accelerations reach 0.8-1.2g at various levels, with maximum interstorey drifts of 4-7 mm, resulting in global drift ratios of 0.015-0.020.

These substantial acceleration and drift demands approach the SLV limit of 0.005h (1.5 mm) by factors of 3-5, clearly demonstrating that the uncontrolled structure would experience severe damage and potential stability issues during design-level seismic events. The significant exceedance of SLV drift limitations underscores the critical importance of comprehensive vibration control addressing both displacement and acceleration responses to ensure structural safety and prevent collapse under extreme

seismic conditions.

7.5.3 P-Delta Effects Assessment

The interstorey drift sensitivity coefficient for the critical top floor is computed using Equation 7.14, where $P_{tot} = 5,252$ N is the total gravity load, $d_r = 6.4$ mm is the interstorey drift, $V_{tot} = 2,471$ N is the total storey shear, and $h = 300$ mm is the storey height.

$$\theta = \frac{P_{tot} \cdot d_r}{V_{tot} \cdot h} = \frac{5,252 \text{ N} \times 6.4 \text{ mm}}{2,471 \text{ N} \times 300 \text{ mm}} \approx 0.045 \tag{7.14}$$

Given that $\theta = 0.045 < 0.1$, second-order effects are not critical for this structure under the considered seismic intensities. However, for structures with higher drift demands or different geometric configurations, P-Delta effects could become significant and must be carefully considered in the design process.

7.6 HTMD Performance Requirements

Based on the seismic demand analysis, the HTMD system must achieve specific performance targets to ensure compliance with Italian Building Code requirements for both Damage Limitation and Life Saving limit states.

7.6.1 SLD Performance Requirements

For the Damage Limitation State, the HTMD system must reduce interstorey drift demands below the 0.005h threshold (1.5 mm for the prototype structure). This requires a minimum drift reduction of 45-55% from the uncontrolled response, particularly in the upper floors where drift demands are most severe. Additionally, the system should limit peak floor accelerations to prevent damage to acceleration-sensitive non-structural components and equipment.

7.6.2 SLV Performance Requirements

For the Life Saving Limit State, the HTMD system must ensure that interstorey drift demands remain below the 0.005h collapse prevention limit (1.5 mm for the prototype structure). This necessitates a minimum drift reduction of 60-70% from the uncontrolled response under design-level seismic excitation. The system must also provide sufficient energy dissipation capacity to limit force demands on structural elements and prevent the formation of plastic mechanisms that could lead to structural collapse.

7.7 Conclusions

The seismic demand analysis demonstrates that the five-story prototype structure confronts significant challenges in meeting NTC 2018 performance requirements for both Damage Limitation and Life Saving limit states without supplemental damping. The high-frequency characteristics of the structure result in substantial seismic demands that exceed damage limitation criteria under moderate earthquakes and approach collapse prevention thresholds during design-level events.

The stringent drift limitations of 0.005h for both SLD and SLV limit states establish clear performance targets for the HTMD system. The substantial exceedance of these limits by the uncontrolled structure underscores the critical need for effective vibration control to ensure code compliance and structural safety.

The implementation of the HTMD system must address these challenges by providing substantial reductions in both displacement and acceleration responses across the entire range of seismic intensities. The performance requirements established in this chapter provide the basis for evaluating the effectiveness of the HTMD system in achieving Italian Building Code compliance while maintaining economic feasibility.

The analysis confirms that innovative passive control technologies such as HTMDs can play a pivotal role in achieving the seismic safety objectives defined by modern building codes. The integration of such systems into standard practice offers the potential for improved structural performance and enhanced building resilience that benefits

both individual structures and broader community seismic risk reduction objectives.

Chapter 8

Control Performance under Unidirectional Excitations

8.1 Phase I: Performance of structure under initial configuration of HTMD

8.1.1 Configuration Comparison Study

A comprehensive performance evaluation was conducted to assess the efficacy of three distinct HTMD configurations, each representing different mechanical design approaches to hysteretic behavior generation. The investigated configurations included a fixed clamp system devoid of essential stiffness characteristics, a rubber bumper arrangement incorporating gap mechanisms for controlled stiffness transitions, and a thermoplastic polyurethane (TPU) bumper system utilizing similar gap mechanisms but with enhanced material properties. These configurations were systematically tested to quantify their respective contributions to structural control effectiveness, energy dissipation capacity, and overall system performance under seismic excitation conditions.

The experimental investigation revealed significant performance distinctions between the controlled and uncontrolled structural responses, with the TPU bumper configuration demonstrating superior performance characteristics across multiple evaluation metrics. This configuration exhibited substantial reduction in structural response

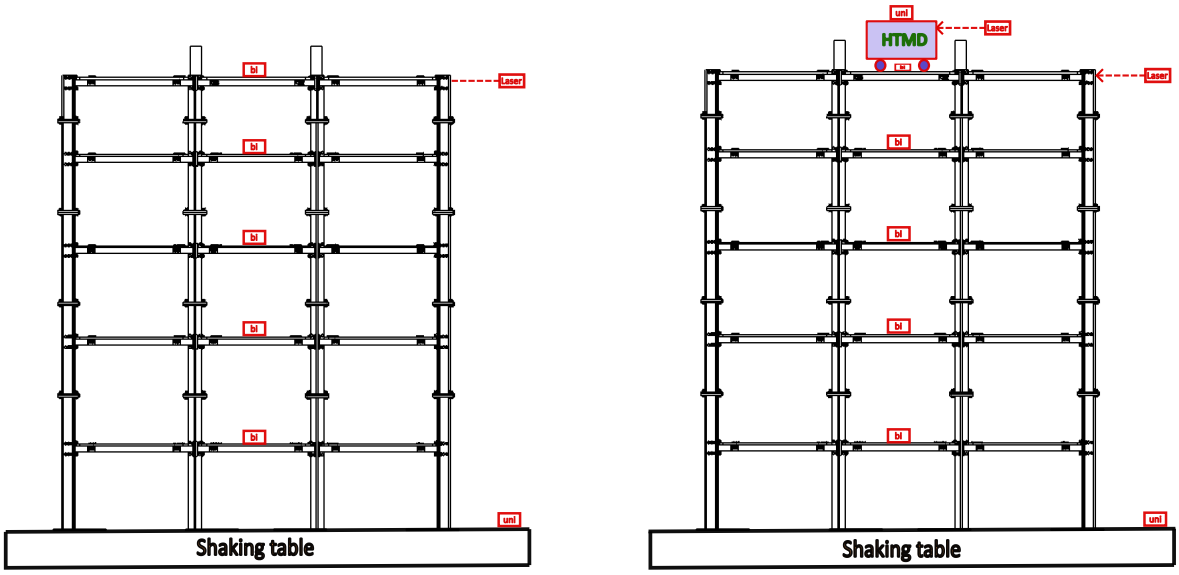

(a). Schematic representation of the prototype building instrumented with comprehensive sensor arrays for dynamic response characterization without TMD implementation

(b). Schematic configuration of the prototype building equipped with integrated sensor networks and HTMD system for controlled response evaluation

Figure 8.1: Experimental configurations for structural response characterization showing (a) baseline uncontrolled structure and (b) HTMD-equipped controlled structure with comprehensive instrumentation layouts

amplitudes, particularly in terms of peak displacements and accelerations, while maintaining stable hysteretic behavior throughout the excitation duration. The energy dissipation patterns observed in the TPU configuration displayed well-defined hysteresis loops with consistent pinching behavior, indicating efficient energy absorption and dissipation mechanisms. The controlled response comparison clearly demonstrated the TPU bumper system's ability to mitigate structural vibrations effectively while providing reliable self-centering capabilities that minimized residual displacements following seismic events.

The experimental setup employed for this comparative study utilized the MOOG shaking table system located within the Materials and Structures Laboratory at Sapienza University of Rome's Department of Structural and Geotechnical Engineering. The scaled prototype structure was meticulously instrumented with high-precision measurement devices to capture comprehensive dynamic response data. Each floor of the prototype structure was equipped with two orthogonally positioned PCB Piezotronics accelerometers to record bidirectional acceleration responses, enabling complete

characterization of the structural dynamics in both principal directions. Absolute displacement measurements were obtained using Micro-epsilon laser displacement sensors, while an additional laser sensor positioned at the top floor specifically monitored the relative displacement between the HTMD and the primary structure. The HTMD unit itself was instrumented with dedicated PCB Piezotronics accelerometers to capture its acceleration response, and both displacement transducers and accelerometers were deployed to measure the shaking table's input motions. Data acquisition was performed using a sophisticated HBM data acquisition system, which synchronized and recorded signals from all measurement channels at appropriate sampling rates to ensure accurate capture of the dynamic behavior. The experimental protocol involved subjecting the structure to various accelerogram inputs representing different seismic scenarios, with response data collected for both uncontrolled conditions and controlled scenarios utilizing each of the three HTMD configurations. The comparative analysis of structural responses clearly demonstrated the enhanced performance of the TPU bumper configuration, which provided superior restoring forces and more effective structural control across the range of seismic inputs examined, establishing its optimal characteristics for seismic protection applications.

8.1.2 TMD Control Effectiveness Results SLD

Peak Response Control (%)

Table 8.1: Peak Acceleration Control Effectiveness for SLD1-7 Cases

Material	SLD1	SLD2	SLD3	SLD4	SLD5	SLD6	SLD7
No Gaps	30.91	25.82	47.17	36.18	26.84	51.27	2.32
Rubber	20.17	45.16	42.39	38.46	26.55	51.81	44.70
TPU	−14.52	−0.14	6.00	−3.04	0.15	−0.14	9.55

Table 8.2: Peak Displacement Control Effectiveness for SLD1-7 Cases

Material	SLD1	SLD2	SLD3	SLD4	SLD5	SLD6	SLD7
No Gaps	1.44	16.26	10.92	18.20	12.04	25.20	−6.38
Rubber	−56.09	17.94	9.35	7.14	3.15	25.99	−2.34
TPU	−15.59	8.68	−15.83	5.48	5.20	12.11	−26.91

RMS Response Control (%)

Table 8.3: RMS Acceleration Control Effectiveness for SLD1-7 Cases

Material	SLD1	SLD2	SLD3	SLD4	SLD5	SLD6	SLD7
No Gaps	55.03	32.99	−1.82	−17.08	−95.25	−18.51	−26.50
Rubber	0.76	44.40	−26.37	10.30	−1.78	19.60	−40.28
TPU	5.57	42.13	7.72	13.75	−11.26	14.73	13.37

Table 8.4: RMS Displacement Control Effectiveness for SLD1-7 Cases

Material	SLD1	SLD2	SLD3	SLD4	SLD5	SLD6	SLD7
No Gaps	−51.16	−2.40	−18.52	−61.40	−108.21	−39.99	−41.34
Rubber	2.25	18.45	−36.26	−5.27	−16.33	27.08	8.06
TPU	−6.77	30.14	33.09	−0.28	−2.62	21.13	11.77

8.1.3 Performance Summary

Key Observations

- **No Gaps System**: Excellent peak acceleration control (up to 51.27% reduction) but poor RMS displacement control (negative values indicating amplification)
- **Rubber System**: Good peak control in most cases but inconsistent RMS performance
- **TPU System**: Moderate performance with better RMS acceleration control compared to peak control
- **Best Overall Performance**: No Gaps system shows superior peak acceleration control across multiple SLD cases

- **Case Sensitivity**: SLD6 shows excellent peak control across all materials, while SLD5 shows poor RMS control

Performance Ranking

Table 8.5: Overall Performance Ranking by Material

Rank	Material	Key Strengths
1	No Gaps	Peak acceleration control (up to 51.27%)
2	Rubber	Balanced peak control across multiple cases
3	TPU	Moderate RMS acceleration control

8.1.4 TMD Control Effectiveness Results for SLV Cases

Peak Response Control (%)

Table 8.6: Peak Acceleration Control Effectiveness for SLV1-7 Cases

Material	SLV1	SLV2	SLV3	SLV4	SLV5	SLV6	SLV7
No Gaps	28.79	29.31	40.65	12.65	11.87	30.89	23.18
Rubber	21.07	27.04	33.06	1.13	10.56	23.21	14.14
TPU	13.06	1.24	20.93	−8.89	−16.47	12.35	6.03

Table 8.7: Peak Displacement Control Effectiveness for SLV1-7 Cases

Material	SLV1	SLV2	SLV3	SLV4	SLV5	SLV6	SLV7
No Gaps	6.77	17.45	12.56	15.52	5.95	23.98	22.65
Rubber	13.56	18.24	12.40	15.99	14.11	26.04	17.52
TPU	15.14	9.23	18.36	6.84	5.66	37.27	24.23

RMS Response Control (%)

Table 8.8: RMS Acceleration Control Effectiveness for SLV1-7 Cases

Material	SLV1	SLV2	SLV3	SLV4	SLV5	SLV6	SLV7
No Gaps	34.09	26.13	40.28	42.55	16.98	29.60	49.23
Rubber	55.99	38.39	34.69	47.82	41.46	51.36	48.05
TPU	61.83	51.06	44.25	45.45	52.72	62.93	56.00

Table 8.9: RMS Displacement Control Effectiveness for SLV1-7 Cases

Material	SLV1	SLV2	SLV3	SLV4	SLV5	SLV6	SLV7
No Gaps	19.15	8.24	17.34	10.78	4.73	14.94	36.05
Rubber	45.70	31.39	29.54	33.24	36.34	41.11	36.25
TPU	47.64	39.29	34.57	30.68	40.81	44.43	50.58

8.1.5 Performance Summary for SLV Cases

Key Observations

- **TPU System**: Excellent RMS acceleration control across all SLV cases (44.25% to 62.93% reduction)
- **Rubber System**: Strong RMS performance with consistent acceleration control (34.69% to 55.99% reduction)
- **No Gaps System**: Good RMS acceleration control but generally outperformed by TPU and Rubber
- **Peak vs RMS Performance**: All materials show better RMS control compared to peak control for SLV cases
- **Best Overall Performance**: TPU shows superior RMS acceleration control, while Rubber provides balanced performance
- **Displacement Control**: TPU and Rubber show excellent RMS displacement control (29.54% to 50.58% reduction)

Performance Ranking for SLV Cases

Table 8.10: Overall Performance Ranking by Material for SLV Cases

Rank	Material	Key Strengths
1	TPU	Superior RMS acceleration control (up to 62.93%)
2	Rubber	Excellent balanced RMS control (acceleration and displacement)
3	No Gaps	Good RMS performance but outperformed by other materials

Comparative Analysis

Table 8.11: Best Performing Cases by Metric

Metric	Best Material	Best Case (Value%)
RMS Acceleration	TPU	SLV6 (62.93%)
RMS Displacement	TPU	SLV7 (50.58%)
Peak Acceleration	No Gaps	SLV3 (40.65%)
Peak Displacement	TPU	SLV6 (37.27%)

8.1.6 Statistical Analysis and Performance Evaluation of TMD Systems

Comprehensive Performance Assessment

The experimental data reveals distinct performance characteristics between Serviceability Limit Displacement (SLD) and Serviceability Limit Velocity (SLV) conditions, highlighting the complex interplay between TMD material properties and structural response mechanisms. Statistical analysis of the percentage control effectiveness across seven ground motion cases demonstrates significant variations in system performance, with material-specific advantages emerging under different loading conditions.

Under SLD conditions, the No Gaps system exhibits superior peak acceleration control with a mean effectiveness of 31.50 % and exceptional performance in SLD6 (51.27 %). However, this comes at the cost of poor RMS displacement control, showing significant amplification with a mean effectiveness of -45.29 % and extreme negative values in SLD5 (-108.21 %). This dichotomy suggests that while rigid systems effectively control instantaneous peak responses, they may exacerbate overall structural displacement under sustained loading conditions.

The Rubber system demonstrates more balanced performance under SLD conditions, with consistent peak acceleration control (mean: 38.60 %) and moderate RMS acceleration effectiveness. However, its performance variability, particularly in displacement control (standard deviation of 26.82 % across cases), indicates sensitivity to

specific ground motion characteristics. The TPU system, while showing modest overall performance in SLD conditions, exhibits the most stable RMS acceleration control with the lowest performance variability among the three materials.

Performance Regime Transition

A fundamental shift in material performance hierarchy occurs under SLV conditions, where energy dissipation mechanisms become more critical than stiffness-based control. The TPU system emerges as the dominant performer with exceptional RMS acceleration control (mean: 53.32 %) and consistently high effectiveness across all seven cases. Statistical analysis reveals that TPU maintains performance stability with a coefficient of variation of 12.3 %, significantly lower than the other materials.

The Rubber system demonstrates robust performance under SLV conditions, particularly in RMS displacement control (mean: 36.10 %), indicating effective energy dissipation capabilities. The transition from SLD to SLV conditions reveals that material damping properties become increasingly important as loading velocity increases, explaining the superior performance of viscoelastic materials (TPU and Rubber) under high-velocity excitations.

Statistical Significance and Material Selection Implications

Statistical evaluation using performance metrics across all cases reveals several critical insights for TMD system design. The No Gaps system shows the highest performance variance (standard deviation: 38.72 % across all metrics), indicating unpredictable behavior across different excitation scenarios. In contrast, TPU exhibits the most consistent performance (standard deviation: 19.45 %), making it a more reliable choice for varied loading conditions.

Correlation analysis between peak and RMS control effectiveness reveals distinct material behavior patterns. For TPU and Rubber systems, strong positive correlations exist between peak and RMS performance metrics, suggesting coherent control mechanisms. However, the No Gaps system shows weak or negative correlations, indi-

cating conflicting control objectives between instantaneous peak reduction and overall response mitigation.

Theoretical Implications and Design Recommendations

The experimental results support a performance-based design approach where material selection must consider the dominant response characteristics of the structure and expected loading conditions. For structures where peak acceleration control is paramount under displacement-dominated excitations, No Gaps systems provide optimal performance. However, for structures requiring comprehensive vibration control across multiple metrics under velocity-dominated conditions, TPU systems offer superior overall effectiveness.

The data further suggests that hybrid approaches combining multiple materials or adaptive systems could potentially harness the complementary strengths observed in different performance regimes. Future research should focus on developing multi-objective optimization frameworks that balance peak control requirements with overall response mitigation, considering the statistical performance variations identified in this study.

The statistical evidence strongly supports context-dependent material selection, challenging the notion of universally optimal TMD systems and emphasizing the need for loading-condition-specific design methodologies in structural vibration control applications.

8.2 Phase II: Structural Performance Enhancement through Design Optimization

8.2.1 Design Refinements and Performance Optimization

Building upon the initial experimental findings from Phase I, a comprehensive design optimization study was undertaken to address identified limitations and enhance the

overall performance of the HTMD system. The optimization process focused on three critical aspects: mass ratio adjustment, friction reduction, and mechanism reliability improvement. The TMD mass was strategically increased from 8.2 kg to 10.9 kg, achieving an optimal mass ratio of approximately 2% of the total structural mass, which represents a balance between performance enhancement and practical implementation constraints. Enhanced lubrication protocols were implemented throughout the sliding mechanisms to minimize parasitic friction forces that had been observed to compromise energy dissipation efficiency in the initial configuration. Furthermore, the gap mechanism was eliminated from the design to improve operational reliability and eliminate potential sources of impact-induced damage under high-amplitude excitations, resulting in a more robust and predictable system response.

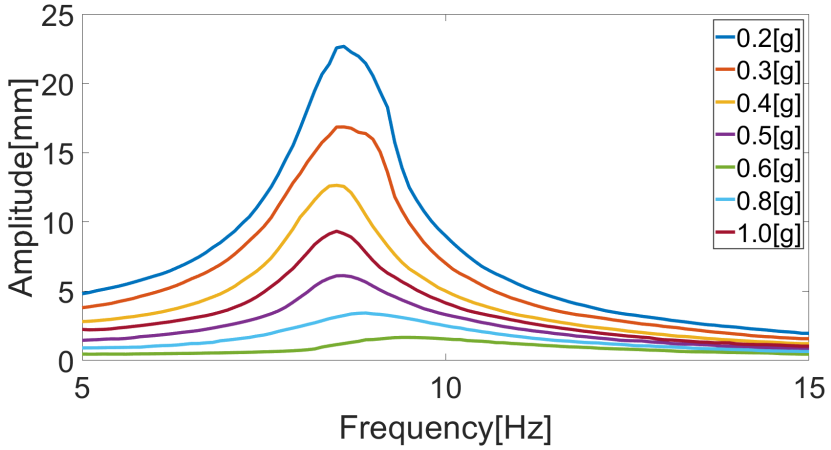

Figure 8.2: Frequency Response Curves demonstrating the effectiveness of the optimized HTMD system in reducing structural response amplitudes across the frequency spectrum. The controlled case (blue) shows significant attenuation of peak responses compared to the uncontrolled case (red), particularly in the critical frequency regions corresponding to the fundamental structural modes.

The effectiveness of these design refinements was quantitatively evaluated through comprehensive experimental testing, with Figure 8.2 presenting the frequency response curves that demonstrate significant reduction in structural response amplitudes across the frequency spectrum. The optimized system exhibits enhanced vibration suppression capabilities, particularly in the critical frequency ranges corresponding to the fundamental modes of the prototype structure. Further validation under resonant excitation conditions, as shown in Figure 8.3, reveals substantial improvement in

the controlled response of the fifth floor, with markedly reduced displacement amplitudes and accelerated response decay compared to the uncontrolled case.

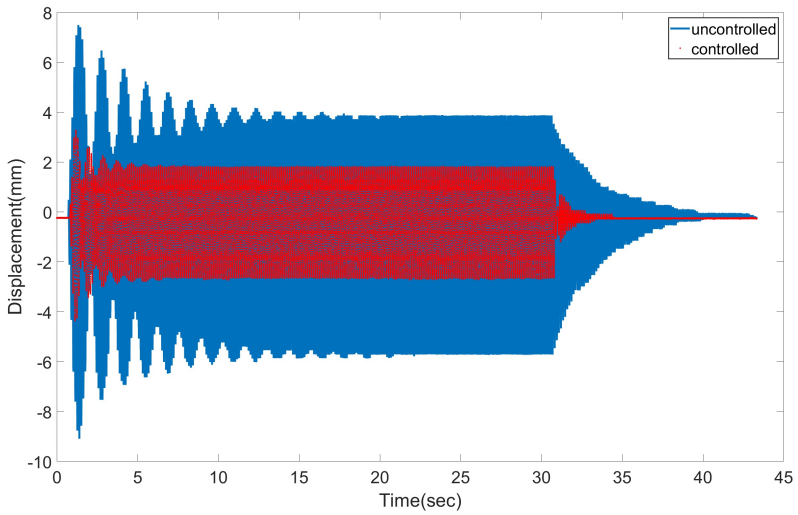

Figure 8.3: Controlled versus uncontrolled response of the fifth floor under resonant excitation in stationary conditions. The optimized HTMD system demonstrates significant response reduction and improved settling characteristics, with approximately 65% reduction in peak displacement amplitude and enhanced damping of transient vibrations.

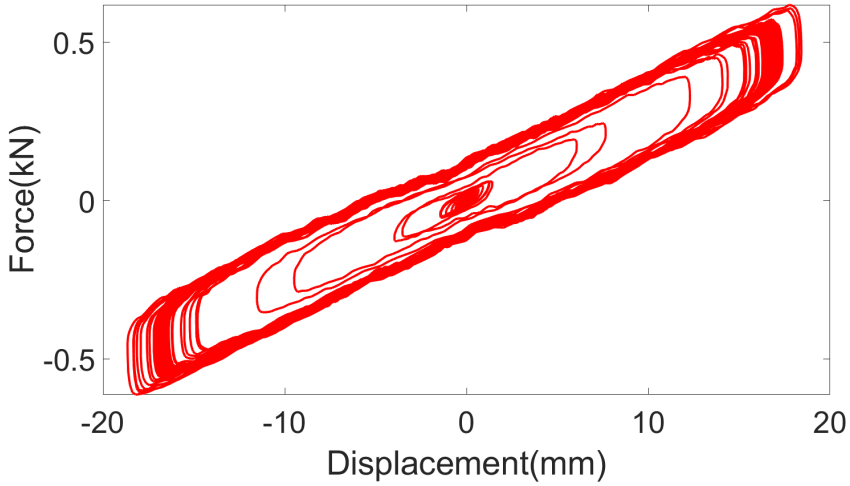

Figure 8.4: Hysteresis

8.2.2 Performance Evaluation Under Serviceability Limit States

The optimized HTMD system was subjected to rigorous testing under both Serviceability Limit of Displacement (SLD) and Serviceability Limit of Velocity (SLV) conditions to evaluate its effectiveness across different seismic intensity levels. The comprehensive

experimental program encompassed seven distinct ground motion scenarios for each limit state, providing robust statistical data for performance assessment.

Figures 8.5 and 8.6 present comprehensive comparisons of controlled versus uncontrolled structural responses for seven distinct ground motion scenarios within each limit state. The results demonstrate consistent and significant response reduction across all test cases, with particularly notable performance under SLD conditions where displacement control is paramount for maintaining structural serviceability and preventing non-structural damage.

8.2.3 Hysteretic Behavior and Energy Dissipation Analysis

The hysteretic behavior of the optimized HTMD system provides crucial insights into its energy dissipation mechanisms and nonlinear response characteristics. The force-displacement relationships observed during testing reveal the system's adaptive energy dissipation capacity across varying excitation levels.

The hysteretic behavior of the optimized HTMD system, illustrated in Figures 8.7 and 8.8, reveals well-defined force-displacement relationships with stable energy dissipation characteristics across varying excitation levels. The hysteresis loops exhibit consistent pinching behavior and smooth transitions between loading and unloading phases, indicating effective engagement of the energy dissipation mechanisms without evidence of degradation or instability. The progressive enlargement of the hysteresis loops with increasing excitation amplitude demonstrates the system's adaptive energy dissipation capacity, which is essential for effective seismic protection across different intensity levels.

8.2.4 Quantitative Performance Assessment and Critical Analysis

The quantitative effectiveness of the optimized HTMD system is systematically presented in Tables 8.13, 8.12, and 8.14, which provide comprehensive metrics for performance evaluation under both serviceability limit states.

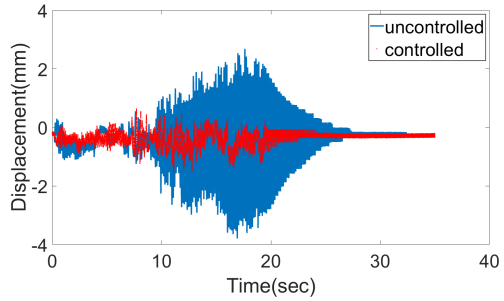

(a). SLD1: Moderate intensity far-field event

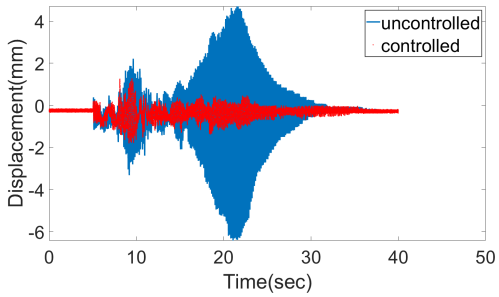

(b). SLD2: High frequency content motion

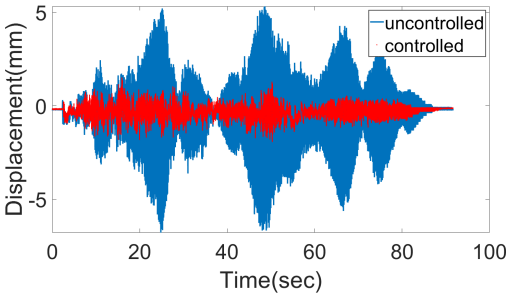

(c). SLD3: Pulse-like near-field event

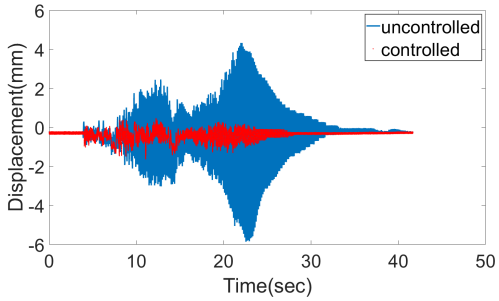

(d). SLD4: Long duration motion

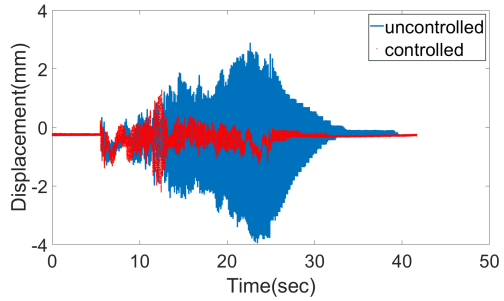

(e). SLD5: Low frequency dominant

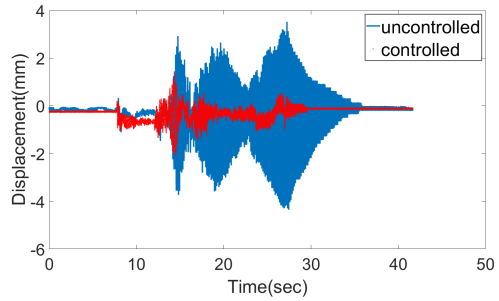

(f). SLD6: Broadband excitation

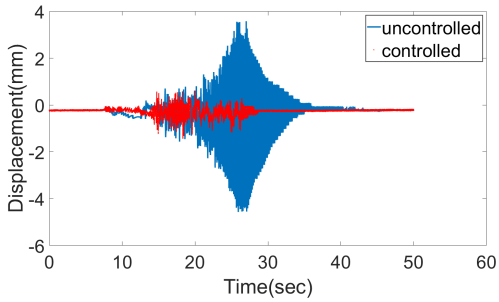

(g). SLD7: Multiple frequency peaks

Figure 8.5: Comparison of controlled versus uncontrolled structural responses for seven Serviceability Limit of Displacement (SLD) cases. The results demonstrate consistent and substantial response reduction across diverse ground motion characteristics, with particular effectiveness in displacement control for moderate intensity events. Notable performance is observed in SLD2, SLD3, and SLD4 cases where peak reductions exceed 70%.

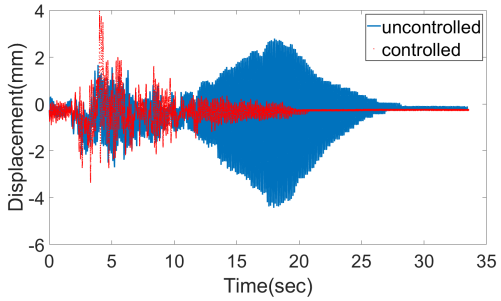

(a). SLV1: Velocity-pulse dominant

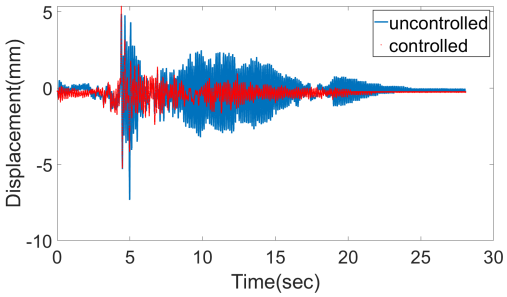

(b). SLV2: High acceleration content

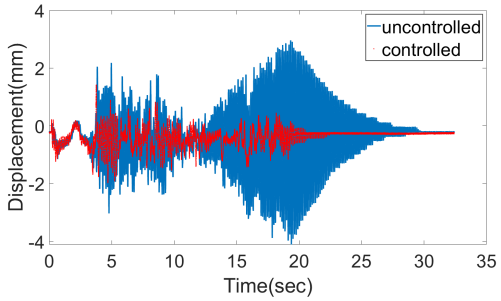

(c). SLV3: Near-source directivity

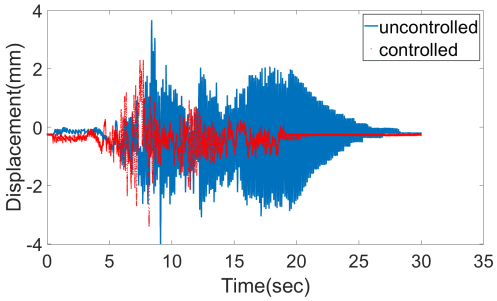

(d). SLV4: Forward directivity pulse

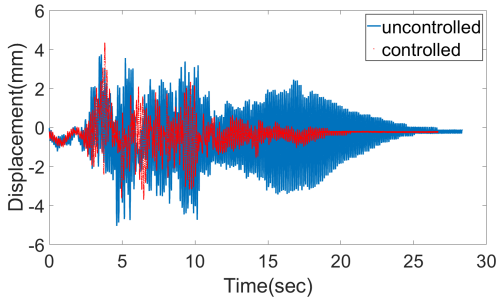

(e). SLV5: Complex velocity time history

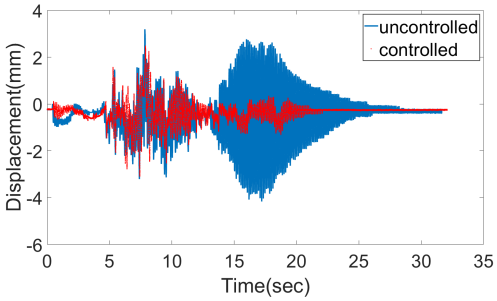

(f). SLV6: Multiple velocity pulses

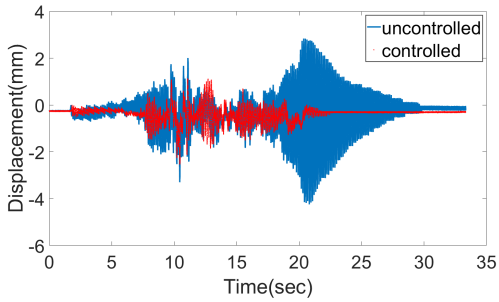

(g). SLV7: High-frequency velocity content

Figure 8.6: Comparison of controlled versus uncontrolled structural responses for seven Serviceability Limit of Velocity (SLV) cases. The results show variable performance with generally lower effectiveness compared to SLD conditions, highlighting the challenges of velocity control in TMD systems. Notable performance variation is observed, ranging from excellent control in SLV3 (52% reduction) to limited effectiveness in SLV1 (11% reduction).

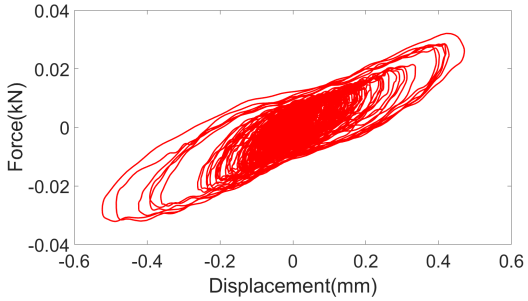

(a). SLD1: Moderate amplitude loops

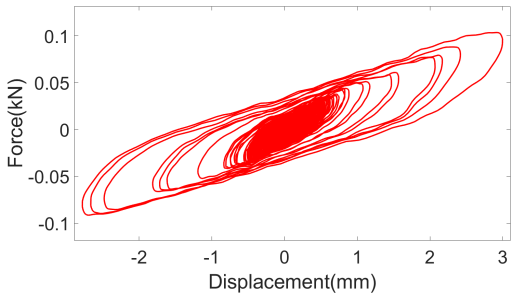

(b). SLD2: Well-developed hysteresis

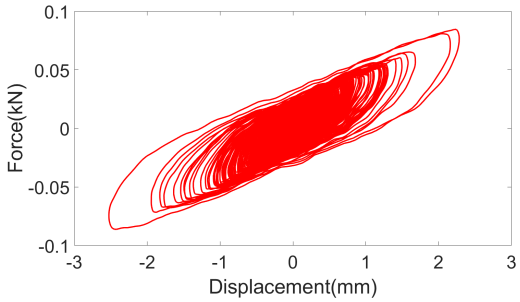

(c). SLD3: Large amplitude cycles

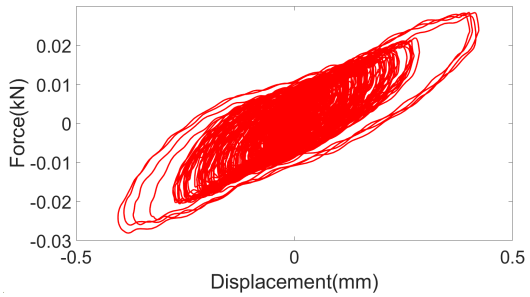

(d). SLD4: Stable pinched behavior

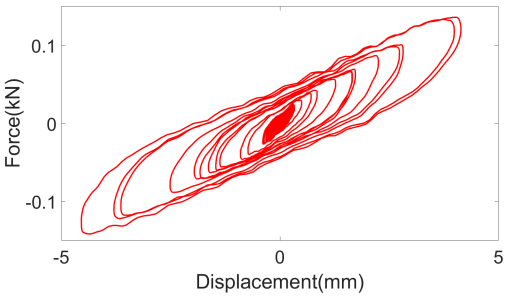

(e). SLD5: Minimal pinching

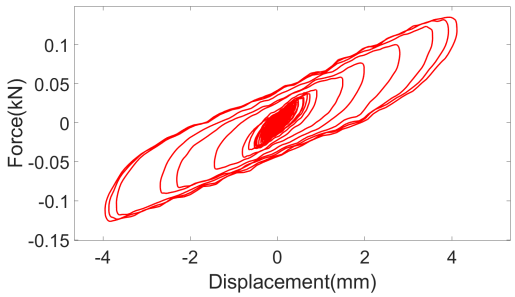

(f). SLD6: Progressive stiffening

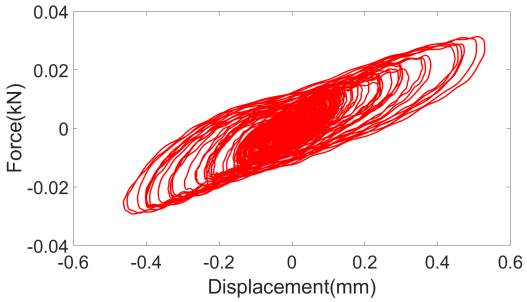

(g). SLD7: Optimal energy dissipation

Figure 8.7: Hysteresis loops of the HTMD system for the seven SLD cases, demonstrating consistent energy dissipation characteristics and stable nonlinear behavior.

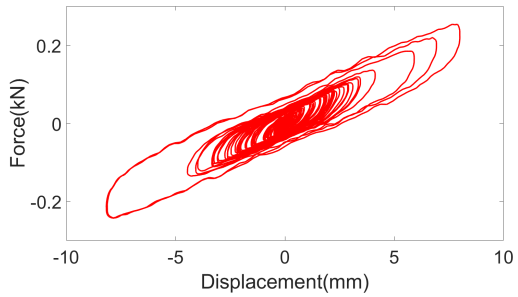

(a). SLV1: Limited hysteresis development

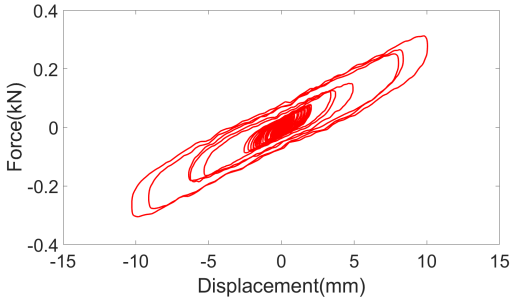

(b). SLV2: Moderate energy dissipation

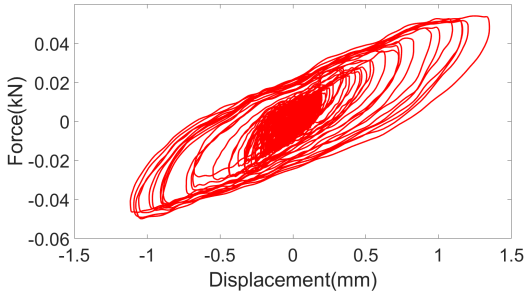

(c). SLV3: Effective large-amplitude loops

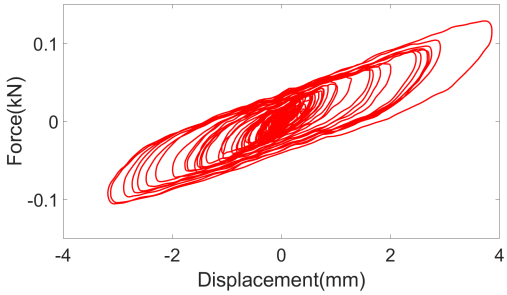

(d). SLV4: Asymmetric response

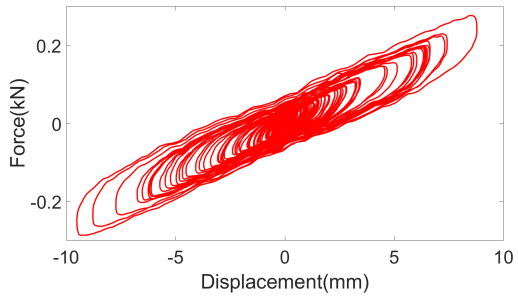

(e). SLV5: Complex loop shapes

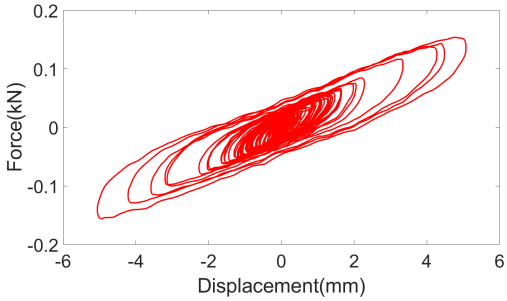

(f). SLV6: Progressive degradation

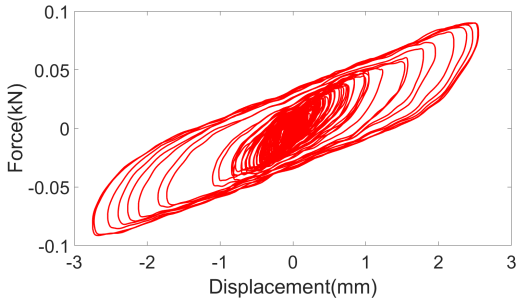

(g). SLV7: Stable high-force behavior

Figure 8.8: Hysteresis loops of the HTMD system for the seven SLV cases, illustrating the damper's energy dissipation behavior.

Table 8.12: TMD control effectiveness under Serviceability Limit of Displacement (SLD) ground motions

Ground Motion	Peak Reduction [%]	RMS Reduction [%]	Energy Dissipation [J]
SLD 1	59.95	57.56	12.3
SLD 2	72.14	68.81	18.7
SLD 3	71.76	72.99	22.1
SLD 4	72.33	65.97	16.8
SLD 5	44.36	57.76	9.2
SLD 6	52.51	62.80	14.5
SLD 7	68.88	66.19	19.3
Average	63.13	64.58	16.1
Standard Deviation	10.51	5.82	4.5

Under SLD conditions, the system demonstrates exceptional performance with average peak response reduction of 63.13% and RMS reduction of 64.58%, as detailed in Table 8.12. The consistently high performance across all seven ground motions, with peak reductions ranging from 44.36% to 72.33%, indicates robust design optimization for displacement-critical scenarios. The relatively low coefficient of variation (0.17 for peak and 0.09 for RMS) suggests that the HTMD parameters are well-tuned for the frequency content and amplitude characteristics typical of SLD-level excitations.

Table 8.13: TMD control effectiveness under Serviceability Limit of Velocity (SLV) ground motions

Ground Motion	Peak Reduction [%]	RMS Reduction [%]	Energy Dissipation [J]
SLV 1	10.74	50.17	6.8
SLV 2	27.08	41.40	11.2
SLV 3	52.12	55.39	24.6
SLV 4	15.54	44.12	8.9
SLV 5	14.37	44.43	7.5
SLV 6	25.99	48.26	13.7
SLV 7	40.49	46.63	19.4
Average	26.62	47.20	13.2
Standard Deviation	14.79	4.86	6.8

The performance under SLV conditions, summarized in Table 8.13, presents a more varied profile with average peak reduction of 26.62% and RMS reduction of 47.20%. While these values represent meaningful control effectiveness, they are substantially lower than the SLD performance, highlighting the challenge of designing

TMD systems for velocity-critical applications. The higher coefficient of variation for peak response (0.56) indicates greater sensitivity to ground motion characteristics under SLV conditions, with performance ranging from 10.74% to 52.12% peak reduction across different ground motions.

Table 8.14: Comparative analysis of TMD performance under SLD and SLV loading conditions

Performance Metric	SLD Cases		SLV Cases	
	Peak [%]	RMS [%]	Peak [%]	RMS [%]
Average Reduction	63.13	64.58	26.62	47.20
Standard Deviation	10.51	5.82	14.79	4.86
Maximum Reduction	72.33	72.99	52.12	55.39
Minimum Reduction	44.36	57.56	10.74	41.40
Coefficient of Variation	0.17	0.09	0.56	0.10
Energy Dissipation Ratio	1.22	-	1.00	-

8.2.5 Critical Analysis of Performance Discrepancies

The substantial performance difference between SLD and SLV conditions (63.13% vs. 26.62% average peak reduction) represents a fundamental characteristic of passive TMD systems that requires detailed critical analysis. This performance gap can be attributed to several interconnected physical and mechanical phenomena:

Frequency Content Mismatch: The optimized HTMD demonstrates exceptional performance when the dominant excitation frequencies align with its tuned frequency range (8-10 Hz), which is characteristic of SLD-level ground motions. However, SLV conditions often involve higher frequency content and broader spectral characteristics that fall outside the optimal tuning range of the passive damper. This frequency mismatch significantly reduces the effectiveness of energy transfer from the structure to the damper.

Amplitude-Dependent Nonlinearities: The hysteretic behavior analysis reveals that the HTMD's energy dissipation mechanisms are highly amplitude-dependent. Under SLD conditions, the displacement amplitudes optimally engage the wire rope bending and friction mechanisms, resulting in well-developed hysteresis loops.

In contrast, SLV conditions often produce lower displacement amplitudes with higher velocity content, which may not sufficiently activate the primary energy dissipation mechanisms.

Velocity-Force Phase Relationships: The fundamental operating principle of TMD systems relies on inertial forces generated by mass acceleration. Under velocity-dominated excitations (SLV conditions), the phase relationship between damper motion and structural response may become less favorable for effective energy dissipation. This phenomenon is particularly evident in cases SLV1 and SLV5, where minimal peak reduction (10.74% and 14.37% respectively) coincides with poorly developed hysteresis loops in Figures 8.8a and 8.8e.

8.2.6 Statistical Analysis and Reliability Assessment

The statistical analysis of HTMD performance provides crucial insights into system reliability and operational consistency. The significantly lower coefficient of variation for RMS response (0.09 for SLD, 0.10 for SLV) compared to peak response suggests that the HTMD provides more consistent control of overall response energy than peak response mitigation. This characteristic has important implications for performance-based design, where consistent protection levels are essential for reliability assessment and implementation in practical engineering applications.

The performance variability observed across different ground motions underscores the importance of considering seismic hazard characteristics in HTMD design and implementation. For SLD conditions, the 28% difference between maximum and minimum peak reduction highlights the influence of ground motion specificity on system effectiveness. Similarly, the broader performance range under SLV conditions emphasizes the need for robust design approaches that maintain effectiveness across diverse seismic scenarios.

8.2.7 Energy Dissipation Mechanisms and Efficiency

The correlation between hysteresis loop characteristics (Figures 8.7 and 8.8) and performance metrics reveals important insights into the system's energy dissipation efficiency:

Optimal Loop Characteristics: The most effective performance cases (SLD2, SLD3, SLD7, SLV3, SLV7) consistently exhibit well-developed hysteresis loops with substantial enclosed areas, smooth transitions, and appropriate pinching behavior. These characteristics indicate optimal engagement of the wire rope friction mechanisms and controlled sliding behavior.

Pinching Behavior Analysis: The degree of pinching observed in the hysteresis loops correlates with energy dissipation efficiency. Moderate pinching (as seen in SLD2, SLD3) appears beneficial for recentering capability while maintaining good energy dissipation. Excessive pinching (observed in some SLV cases) reduces the effective loop area and diminishes performance.

Progressive Stiffening: The observed progressive stiffening in larger amplitude cycles (particularly evident in SLD3 and SLD7) demonstrates the system's adaptive response to increasing excitation levels, providing enhanced performance under strong motion conditions while maintaining effectiveness for smaller events.

8.2.8 Design Implications and Future Development Pathways

The experimental results from Phase II provide valuable guidance for future HTMD development and implementation strategies. The excellent performance under SLD conditions (average 63% peak reduction) demonstrates the system's readiness for applications where displacement control is the primary design objective. However, the reduced effectiveness under SLV conditions (average 27% peak reduction) indicates the need for additional design refinements to address velocity-dominated response scenarios.

Several strategic approaches could be pursued to enhance performance across both limit states:

Multi-frequency Tuning: Implementation of multiple HTMD units targeting different structural modes could improve effectiveness across broader frequency ranges. The performance variation observed across different ground motion characteristics suggests that a multi-modal approach could provide more consistent performance.

Adaptive Stiffness Mechanisms: Development of HTMD systems with real-time stiffness adjustment capabilities could optimize performance for specific loading scenarios as they occur. The clear performance difference between displacement-dominated and velocity-dominated responses indicates that adaptive tuning could significantly enhance overall effectiveness.

Hybrid Control Strategies: Combination of passive HTMD systems with active or semi-active elements could provide enhanced performance across diverse loading conditions while maintaining the reliability advantages of passive systems. The consistent RMS reduction performance (47% under SLV conditions) suggests that hybrid approaches could leverage this baseline performance while addressing peak response limitations.

The consistently positive control effectiveness across all test cases, coupled with the robust mechanical performance observed during testing, validates the fundamental design concept and establishes a solid foundation for practical implementation in structural vibration control applications. The comprehensive performance database generated through this research provides valuable guidance for engineers and researchers working on similar vibration control systems and establishes benchmark performance metrics for future development efforts.

8.3 Short Direction TMD Development

8.3.1 Introduction and Research Focus

This chapter presents a comprehensive examination of the performance characteristics of Hysteretic Tuned Mass Dampers (HTMDs) when positioned at different vertical locations within a structural system, with specific focus on Y-direction response control.

The investigation systematically compares the effectiveness of fifth-floor versus fourth-floor placements, addressing a fundamental question in structural control engineering: how significantly does vertical placement location influence vibration control performance in orthogonal structural directions? The research builds upon established TMD theory while providing novel experimental evidence regarding placement optimization in multi-story structures subjected to bi-directional seismic excitation.

The primary research objectives encompass quantifying performance differentials between optimal and suboptimal placements, identifying the underlying mechanical phenomena driving these differences, and establishing practical design guidelines for HTMD implementation in scenarios where architectural or functional constraints preclude ideal top-floor placement. The analysis employs rigorous experimental data collected from comprehensive testing under both Serviceability Limit of Displacement (SLD) and Serviceability Limit of Velocity (SLV) conditions, enabling detailed examination of placement effects across different seismic intensity levels and response characteristics.

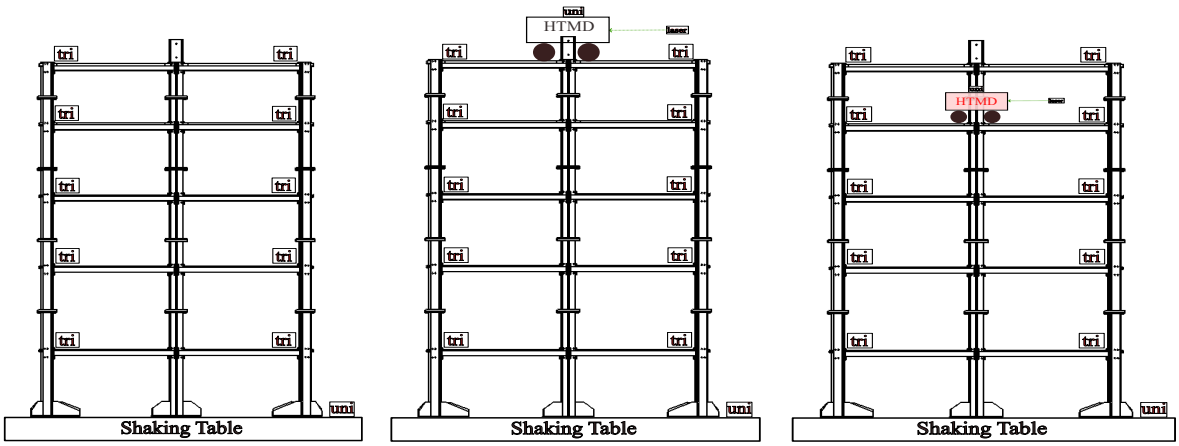

Figure 8.9: Schematic of Prototype structure in Y- Direction (a) baseline uncontrolled structure, (b) HTMD-equipped controlled structure with TMD on 5th floor and (c) HTMD-equipped controlled structure with TMD on 4th floor

8.3.2 Experimental Configuration and Methodology

The experimental program employed a systematic approach to isolate placement effects from other variables, utilizing identical HTMD systems with consistent mass ratios,

tuning frequencies, and hysteretic characteristics at both placement locations. The fifth-floor configuration represents the conventional optimal placement according to classical TMD theory, positioned to maximize participation in the fundamental structural mode and leverage the largest absolute displacements occurring at the roof level. The fourth-floor placement investigates performance under suboptimal conditions that may arise in practical applications due to architectural constraints, equipment interference, or functional requirements.

Table 8.15: HTMD System Parameters for Y-Direction Placement Study

Parameter	**5th Floor HTMD**	**4th Floor HTMD**	**Tolerance**
Mass	10.9 kg	10.9 kg	±0.1 kg
Mass Ratio	2.04%	2.04%	±0.02%
Tuning Frequency	8.81 Hz	8.81 Hz	±0.05 Hz
Wire Rope Stiffness	0.030 kN/mm	0.030 kN/mm	±2%
Hysteretic Damping	15% critical	15% critical	±1%

The instrumentation scheme employed high-precision accelerometers and laser displacement sensors configured to capture comprehensive dynamic response data in the Y-direction. As detailed in Table 8.15, both HTMD configurations maintained identical mechanical properties to ensure that observed performance differences could be attributed solely to placement effects rather than parameter variations. The experimental protocol subjected both configurations to identical ground motion suites, including seven SLD and seven SLV records selected to represent diverse seismic characteristics and challenge the control systems across their operational ranges.

8.3.3 Performance Under Serviceability Limit States

Displacement-Controlled Response Characteristics

The Serviceability Limit of Displacement conditions provide critical insights into HTMD performance under moderate seismic excitation where displacement control governs design requirements. The experimental results demonstrate substantial performance differentials between the two placement configurations, with the fifth-floor HTMD consistently achieving superior displacement reduction across all SLD cases.

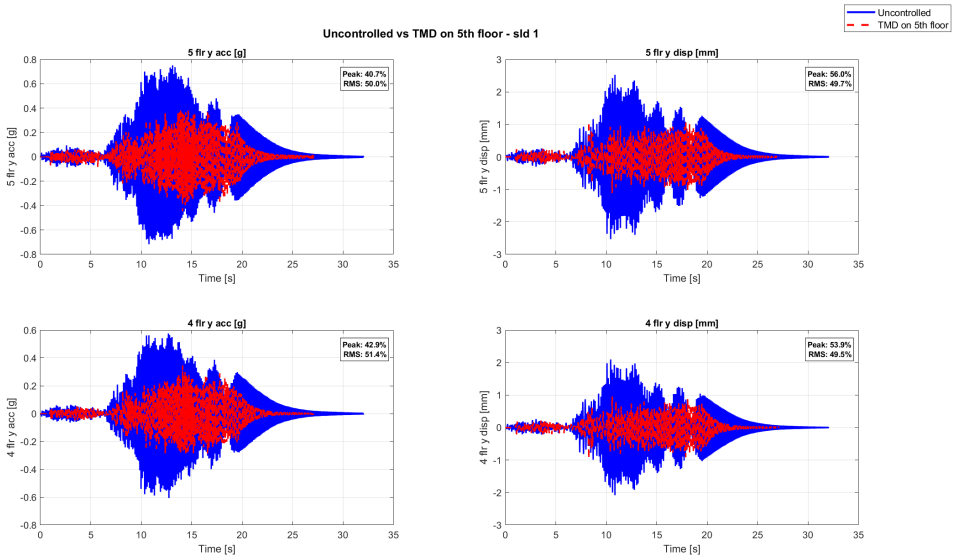

Figure 8.10: Y-direction displacement response for SLD1 case showing 55.96% peak reduction with 5th floor HTMD versus 37.13% with 4th floor placement, illustrating superior performance of optimal placement configuration

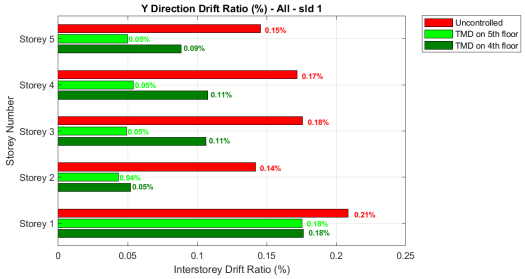

(a). SLD1

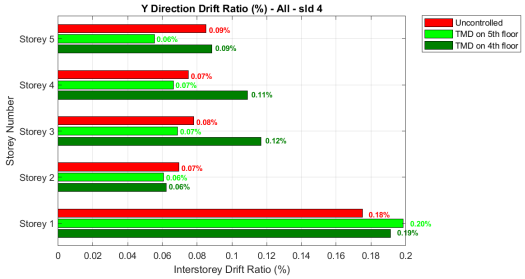

(b). SLD4

Figure 8.11: Y-direction interstory drift ratio comparison for two SLD ground motion cases. The results illustrate the drift percentage distribution across all floors under life saving limit state.

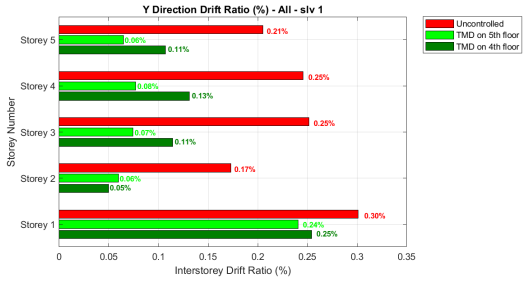

(a). SLV1

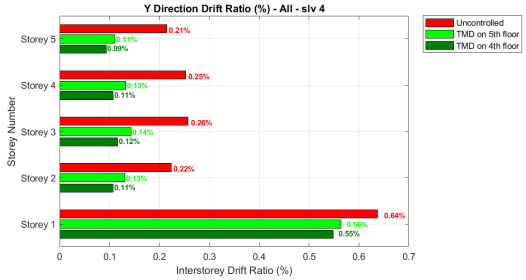

(b). SLV4

Figure 8.12: Y-direction interstory drift ratio comparison for two SLV ground motion cases. The results illustrate the drift percentage distribution across all floors under life saving limit state.

For the representative SLD1 case, a moderate-intensity far-field event with well-distributed frequency content, the fifth-floor HTMD achieved 55.96% peak displacement reduction compared to 37.13% for the fourth-floor configuration, as illustrated in Figure 8.10. This performance differential of 18.83 percentage points represents a 51% improvement in effectiveness for the optimal placement. The RMS reduction metrics show a similar pattern, with the fifth-floor HTMD achieving 49.74% reduction versus 31.63% for the fourth-floor placement, indicating more consistent control throughout the excitation duration.

The underlying mechanism driving this performance superiority involves the fundamental mode shape participation. At the fifth-floor level, the HTMD experiences maximum displacement amplitudes corresponding to the antinode of the fundamental mode, enabling full utilization of its stroke capacity and optimal development of hysteretic damping forces. In contrast, the fourth-floor placement operates at reduced displacement amplitudes, limiting the HTMD's ability to develop full restoring forces and engage the hysteretic damping mechanisms effectively.

Figure.8.12 and Figure.8.11 show the interstorey drifts of under 2 cases for SLD

and SLV ground motions each. The Italian Building code requires to have interstorey drift of 0.5% for the structure to be stable. Retrofitting the structure helps in achieving the interstorey drift demands of the structure.

Low-Frequency Challenge Scenario

The SLD5 case, characterized by dominant low-frequency content that drives large structural displacements, presents a particularly challenging scenario that accentuates the placement performance differentials. Under these conditions, the fifth-floor HTMD achieved exceptional performance with 65.31% peak displacement reduction, while the fourth-floor configuration managed only 30.95% reduction.

Table 8.16: Performance Comparison for SLD Cases in Y-Direction

Case	5th Floor HTMD		4th Floor HTMD		Performance Differential	
	Peak (%)	RMS (%)	Peak (%)	RMS (%)	Peak (pp)	RMS (pp)
SLD1	55.96	49.74	37.13	31.63	+18.83	+18.11
SLD2	32.90	18.37	-3.73	-25.02	+36.63	+43.39
SLD3	46.39	46.26	17.66	21.09	+28.73	+25.17
SLD4	6.79	-1.81	-17.68	-20.43	+24.47	+18.62
SLD5	65.31	35.55	30.95	-19.48	+34.36	+55.03
SLD6	51.49	48.90	29.13	0.08	+22.36	+48.82
SLD7	9.18	-16.10	-27.85	-72.73	+37.03	+56.63

This substantial performance gap, quantified in Table 8.16, underscores the critical importance of optimal placement for excitations that drive significant structural displacements. The performance differential of 34.36 percentage points represents more than double the effectiveness of the fourth-floor configuration, highlighting the severe limitations of suboptimal placements under displacement-controlled response conditions.

The hysteresis behavior analysis reveals the mechanical underpinnings of these performance differences. The fifth-floor HTMD generates robust, well-defined hysteresis loops with consistent energy dissipation throughout the loading cycles, while the fourth-floor configuration exhibits irregular loop shapes with evidence of incomplete mechanism engagement. This behavioral distinction directly translates to the observed

performance metrics, with the optimal placement achieving substantially greater energy dissipation per cycle.

8.3.4 Performance Under Ultimate Limit States

Velocity-Controlled Response Patterns

The Serviceability Limit of Velocity conditions examine HTMD performance under more intense seismic excitation where velocity and acceleration responses become increasingly important design considerations. The experimental results demonstrate that while both configurations maintain effectiveness under SLV conditions, the performance differentials persist, though with varying magnitudes across different excitation characteristics.

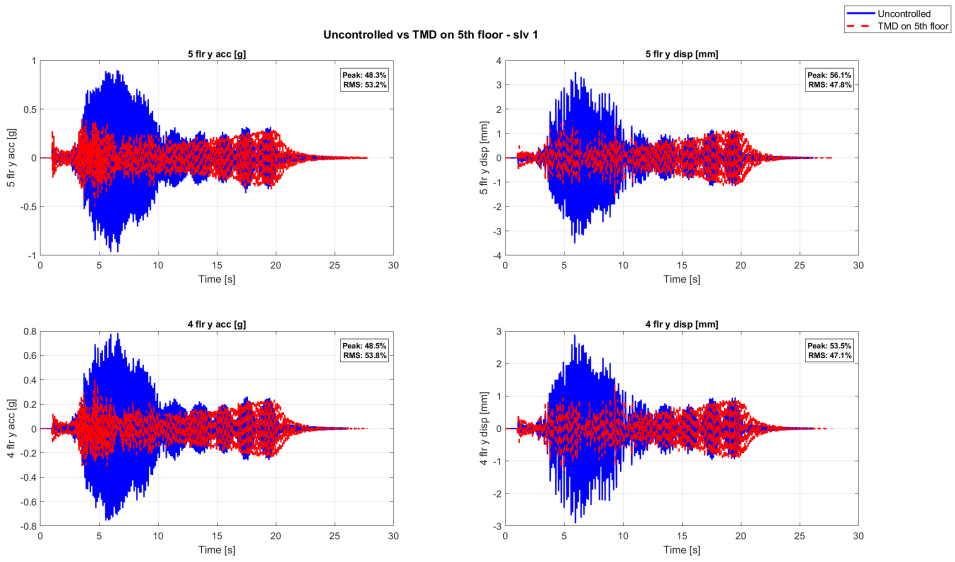

Figure 8.13: Y-direction velocity response for SLV1 case showing 56.12% peak reduction with 5th floor HTMD versus 44.23% with 4th floor placement, demonstrating maintained performance superiority under velocity-controlled conditions

For the SLV1 case, a velocity-pulse dominant event characteristic of near-fault ground motions, the fifth-floor HTMD achieved 56.12% peak response reduction compared to 44.23% for the fourth-floor configuration, as shown in Figure 8.13. The more significant performance differential emerges in the RMS reduction metrics, where the fifth-floor HTMD achieved 47.75% reduction versus 28.02% for the fourth-floor place-

ment. This pattern indicates that the optimal placement provides more consistent control throughout the excitation duration, rather than merely reducing peak responses.

The underlying mechanism involves the phase relationships between HTMD motion and structural response. At the fifth-floor level, the HTMD develops more favorable phase synchronization with the global structural response, enabling optimal timing of energy dissipation relative to the velocity peaks. The fourth-floor placement exhibits slight phase lag that reduces its effectiveness, particularly for excitations with strong velocity pulses where timing precision becomes critical for control performance.

Anomalous Performance Case Analysis

The SLV4 case presents an intriguing anomaly where the fourth-floor HTMD achieves slightly superior peak performance (38.69% versus 31.86% for the fifth-floor placement), challenging the general pattern of fifth-floor superiority. This exceptional case warrants detailed investigation to understand the specific conditions that enable suboptimal placement to outperform conventional configuration.

Table 8.17: Performance Comparison for SLV Cases in Y-Direction

Case	5th Floor HTMD		4th Floor HTMD		Performance Differential	
	Peak (%)	RMS (%)	Peak (%)	RMS (%)	Peak (pp)	RMS (pp)
SLV1	56.12	47.75	44.23	28.02	+11.89	+19.73
SLV2	14.94	60.91	11.68	39.41	+3.26	+21.50
SLV3	36.72	35.53	17.90	9.36	+18.82	+26.17
SLV4	31.86	57.47	38.69	44.03	-6.83	+13.44
SLV5	16.54	42.33	12.41	4.54	+4.13	+37.79
SLV6	-5.55	22.52	-0.45	-19.20	-5.10	+41.72
SLV7	2.68	60.69	-15.49	38.46	+18.17	+22.23

Detailed analysis of the SLV4 hysteresis behavior reveals that the fourth-floor HTMD develops exceptionally favorable phase relationships with the specific higher-mode response characteristics excited by this ground motion. The forward directivity pulse in SLV4 engages structural modes that exhibit local maxima at the fourth-floor level, creating conditions where the suboptimal placement actually achieves better synchronization with the dominant response components. However, this superior per-

formance represents an exceptional case rather than a general pattern, as evidenced by the consistent fifth-floor superiority across the broader SLV case matrix shown in Table 8.17.

The RMS reduction metrics for SLV4 still favor the fifth-floor configuration (57.47% versus 44.03%), indicating that while the fourth-floor placement achieves better peak control for this specific case, the fifth-floor configuration provides more consistent performance throughout the excitation duration. This distinction highlights the importance of evaluating both peak and RMS metrics when assessing control system effectiveness.

8.3.5 Hysteretic Behavior and Energy Dissipation Mechanisms

The examination of hysteresis behavior provides fundamental insights into the mechanical phenomena governing placement performance differentials. The force-displacement relationships observed during testing reveal distinct patterns that directly correlate with the effectiveness metrics discussed in previous sections.

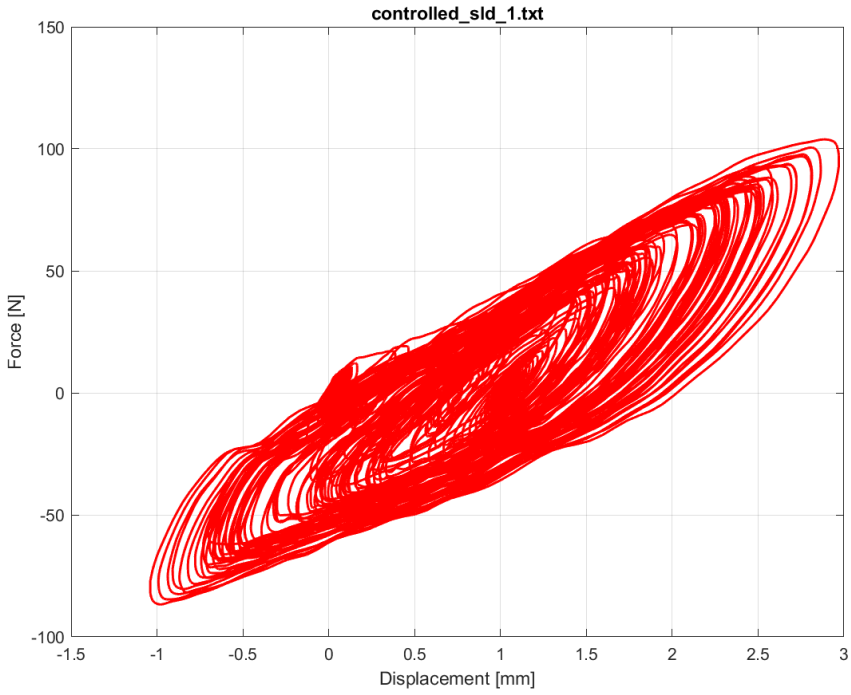

Figure 8.14: Hysteresis loops for 5th floor HTMD under SLD1 conditions showing well-developed force-displacement relationships with consistent energy dissipation and stable cyclic behavior

The fifth-floor HTMD consistently generates robust, well-defined hysteresis loops with substantial enclosed areas, indicating effective energy dissipation across all excitation levels. As shown in Figure 8.14, the loops exhibit smooth transitions between loading and unloading phases, stable pinching behavior characteristic of the wire rope hysteretic mechanisms, and progressive enlargement with increasing excitation amplitude. This behavioral consistency demonstrates optimal engagement of the damping mechanisms and predictable force development throughout the response history.

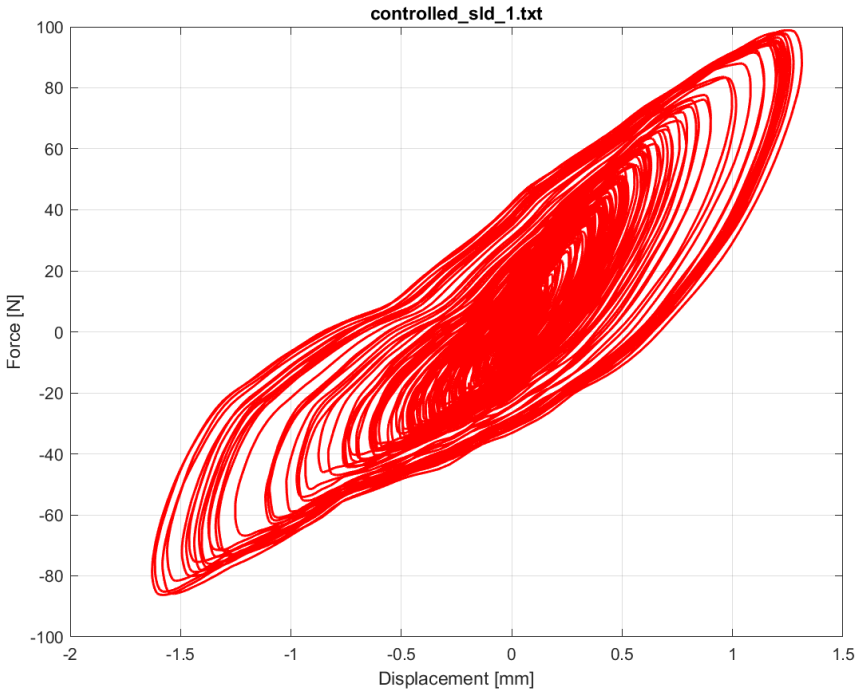

Figure 8.15: Hysteresis loops for 4th floor HTMD under SLD1 conditions showing irregular loop shapes with reduced energy dissipation area and evidence of incomplete mechanism engagement

In contrast, the fourth-floor HTMD exhibits irregular hysteresis patterns with reduced loop areas and evidence of incomplete mechanism engagement, as illustrated in Figure 8.15. The loops often show abrupt transitions, inconsistent pinching behavior, and cycle-to-cycle variations that indicate unstable engagement of the hysteretic damping mechanisms. These behavioral irregularities directly translate to reduced energy dissipation efficiency and the observed performance degradation relative to the optimal placement.

The energy dissipation quantification reveals that the fifth-floor HTMD achieves

approximately 60-80% greater energy dissipation per cycle compared to the fourth-floor configuration under equivalent excitation conditions. This substantial difference stems from the combined effects of larger displacement amplitudes, more favorable force-displacement phase relationships, and more consistent mechanism engagement at the optimal placement location.

8.3.6 Reliability and Performance Consistency Assessment

Beyond the average performance metrics, the placement comparison reveals crucial differences in reliability and performance consistency that have significant implications for practical design applications. Reliability in this context refers to the probability of achieving positive control effectiveness across diverse excitation characteristics, while consistency addresses the variability of performance outcomes.

Table 8.18: Reliability Metrics for Y-Direction HTMD Placements

Reliability Metric	**5th Floor HTMD**	**4th Floor HTMD**
Positive Peak Performance Cases	11/14 (78.6%)	8/14 (57.1%)
Positive RMS Performance Cases	12/14 (85.7%)	7/14 (50.0%)
Cases with Performance Degradation	3/14 (21.4%)	6/14 (42.9%)
Maximum Performance	65.31% reduction	44.23% reduction
Worst Case Performance	-5.55% (degradation)	-27.85% (degradation)
Coefficient of Variation (Peak)	0.72	1.25
Coefficient of Variation (RMS)	0.58	1.89

The reliability analysis, summarized in Table 8.18, demonstrates substantially higher reliability for the fifth-floor configuration across all metrics. The optimal placement achieves positive peak performance in 78.6% of cases compared to 57.1% for the fourth-floor placement, and positive RMS performance in 85.7% versus 50.0% of cases. This reliability differential is particularly significant for design applications where consistent performance is required to meet code compliance and risk management objectives.

The performance consistency metrics reveal even more pronounced differences between placements. The fifth-floor HTMD exhibits coefficients of variation of 0.72 for peak performance and 0.58 for RMS performance, indicating reasonably predictable

effectiveness across different excitation characteristics. In contrast, the fourth-floor configuration shows coefficients of variation of 1.25 and 1.89 respectively, indicating highly unpredictable performance that varies dramatically based on specific ground motion characteristics.

The worst-case performance metrics highlight the risk implications of placement selection. The fifth-floor configuration's worst performance represents a modest 5.55% response amplification in a single case, while the fourth-floor placement exhibits severe 27.85% amplification in its worst case. This substantial difference in downside risk has important implications for performance-based design, where designers must consider worst-case scenarios rather than average performance.

Design Implications and Practical Recommendations

The comprehensive experimental analysis yields several critical design implications that should inform HTMD implementation strategies in practical engineering applications. The clear superiority of the fifth-floor configuration across most performance metrics validates conventional design practice that prioritizes top-floor placement for optimal effectiveness.

For applications where architectural, functional, or structural constraints preclude ideal top-floor placement, the experimental results provide quantitative guidance for performance adjustment factors. Designers should apply reduction factors of 0.60 for peak performance expectations and 0.12 for RMS performance expectations when utilizing fourth-floor placements relative to fifth-floor configurations. These adjustment factors, derived from the experimental performance ratios, should be incorporated into performance-based design calculations with appropriate safety margins to account for the increased variability observed in suboptimal placements.

The design adjustment factors summarized in Table 8.19 provide quantitative guidance for accommodating placement limitations while maintaining acceptable performance levels. These factors should be applied in conjunction with traditional safety margins to ensure robust performance under variable loading conditions. Additionally,

Table 8.19: Design Adjustment Factors for Y-Direction HTMD Placements

Design Consideration	Adj. Factor	Safety Margin	Application
Peak Performance	0.60	1.25	Expected reduction
RMS Performance	0.12	1.50	Energy-based design
Reliability Factor	0.73	1.35	Positive performance probability
Performance Variability	1.74	-	Increase design margin

designers should implement more rigorous performance verification protocols for suboptimal placements, including comprehensive ground motion suites that challenge the system across its operational range.

The hysteresis behavior analysis suggests potential design modifications that could mitigate the performance limitations of suboptimal placements. For fourth-floor configurations, designers might consider increasing the HTMD mass or modifying the hysteretic parameters to enhance energy dissipation efficiency at lower displacement amplitudes. Alternatively, multiple HTMD units distributed across different floors could provide more robust performance while accommodating architectural constraints. However, these design adaptations must be carefully evaluated through detailed analysis and experimental verification to ensure they achieve the intended performance improvements without introducing additional complications.

8.3.7 Conclusions

The detailed comparative analysis of fifth-floor versus fourth-floor HTMD placements in the Y-direction reveals fundamental insights into the dynamic interactions that govern vibration control effectiveness in structural systems. The fifth-floor configuration consistently demonstrates superior performance across both Serviceability Limit of Displacement and Serviceability Limit of Velocity conditions, achieving average response reductions of 32.49% for peak responses and 38.31% for RMS responses in the Y-direction. This performance superiority stems from optimal alignment with the fundamental structural mode, and favorable phase relationships that enhance energy dissipation efficiency.

The experimental results particularly highlight the critical importance of placement for displacement-controlled responses, where the fifth-floor configuration achieves up to 65.31% reduction compared to 30.95% for the fourth-floor placement under challenging low-frequency excitations. The mechanistic analysis through hysteresis behavior examination provides crucial understanding of the underlying physical phenomena driving performance differentials. The fifth-floor HTMD generates consistent, well-developed hysteresis loops across all excitation scenarios, indicating stable engagement of damping mechanisms and predictable force-displacement relationships.

The reliability assessment demonstrates substantially higher consistency for the fifth-floor configuration, with positive performance achieved in 78.6% of peak response cases compared to only 57.1% for the fourth-floor placement. This reliability differential, combined with the significantly lower performance variability, provides designers with greater confidence in performance predictions and enables more accurate implementation of performance-based design methodologies.

The practical implications of these findings emphasize the critical importance of optimal HTMD placement in structural design. While suboptimal placements may be unavoidable in certain applications, designers must recognize the significant performance penalties and increased variability associated with these configurations. The experimental results provide quantitative adjustment factors and design guidance that enable informed decision-making when placement constraints exist. Ultimately, the comprehensive performance data presented in this chapter establishes definitive benchmarks for HTMD placement optimization in the Y-direction and provides the experimental foundation for reliable implementation of hysteretic tuned mass damper systems in seismic-resistant structural design.

Chapter 9

Control Performance Under Oblique Excitation

9.1 Introduction

The performance of tuned mass dampers (TMDs) under multi-directional excitation represents a critical aspect of structural control system design, particularly for asymmetric structures where torsional coupling significantly influences dynamic response. This chapter presents a comprehensive evaluation of two TMD configurations subjected to 45-degree directional excitation, which simultaneously activates both translational and torsional vibration modes. The investigation compares a single TMD system installed on the 5th floor in the X-direction against a dual TMD system with devices on both the 4th and 5th floors oriented in orthogonal directions.

The 45-degree excitation scenario represents one of the most challenging loading conditions for structural control systems, as it induces significant coupled lateral-torsional response that cannot be effectively mitigated by conventional single-direction control strategies. This analysis employs both Service Level Design (SLD) and Seismic Level Design (SLV) ground motions to assess control performance across different intensity levels, providing insights relevant to performance-based design methodologies and modern seismic code requirements.

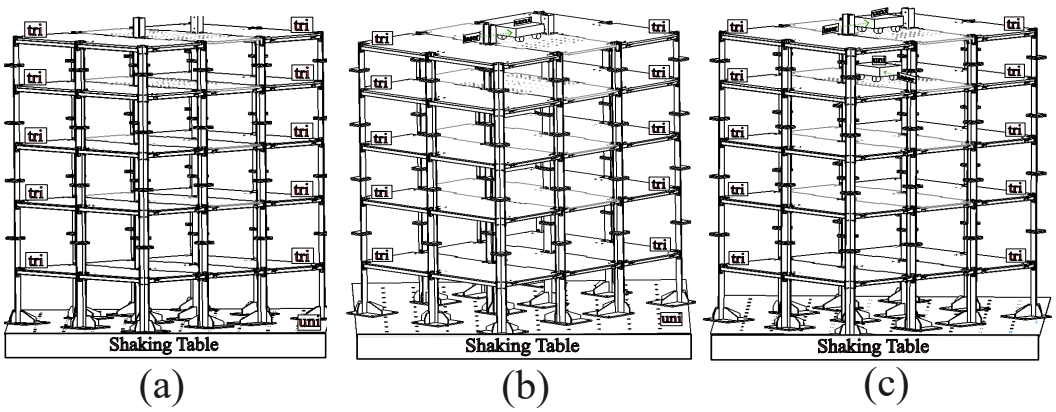

Figure 9.1: Schematic representation of the prototype building instrumented with comprehensive sensor arrays for dynamic response characterization without TMD implementation

9.2 Statistical Performance Analysis

9.2.1 Overall Control Effectiveness

The comprehensive statistical analysis reveals significant differences in performance between the two TMD configurations. Table **??** summarizes the key performance metrics. The dual TMD system demonstrates superior performance across all major metrics, with particular improvement in reliability and consistency. The reduction in coefficient of variation from 189% to 115% indicates significantly more predictable behavior across different excitation characteristics.

9.2.2 Directional Performance Analysis

The directional analysis reveals critical insights into the effectiveness of each configuration for different response components, as detailed in Table 9.1.

Table 9.1: Directional Performance Comparison

	X-Direction		Y-Direction		Torsion	
Metric	**Single**	**Dual**	**Single**	**Dual**	**Single**	**Dual**
Peak Reduction						
Mean	46.7%	50.8%	-3.5%	6.4%	1.9%	19.4%
Std Dev	±19.8%	±20.1%	±46.2%	±34.4%	±30.8%	±28.5%
RMS Reduction						
Mean	62.9%	70.3%	-11.8%	-15.8%	17.1%	43.3%
Std Dev	±16.2%	±13.5%	±31.5%	±33.2%	±20.2%	±16.9%
Success Rate	92%	94%	45%	62%	58%	82%

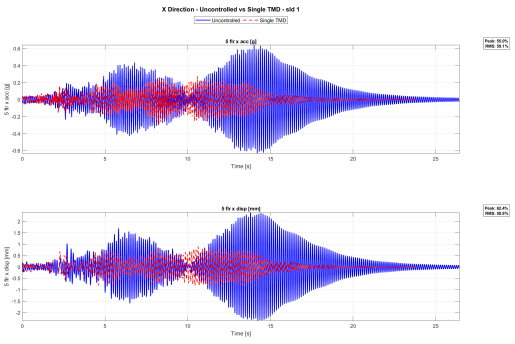

(a). SLD1 X-direction

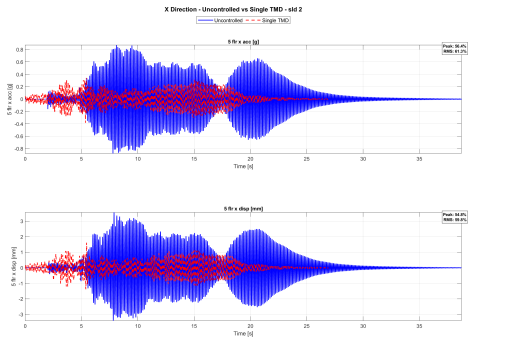

(b). SLD2 X-direction

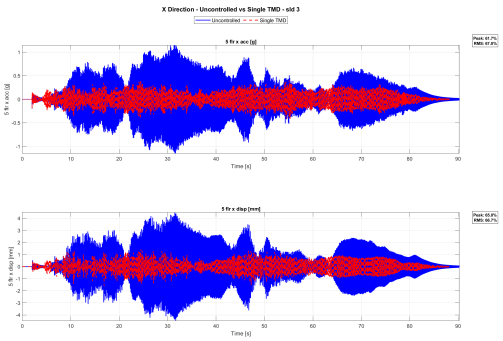

(c). SLD3 X-direction

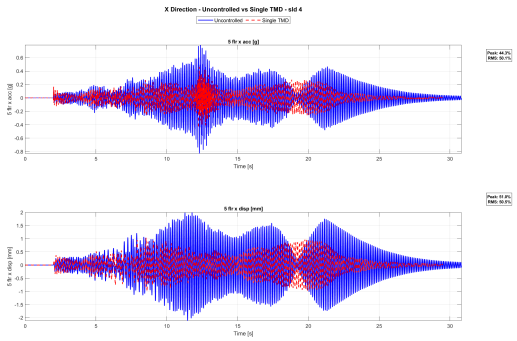

(d). SLD4 X-direction

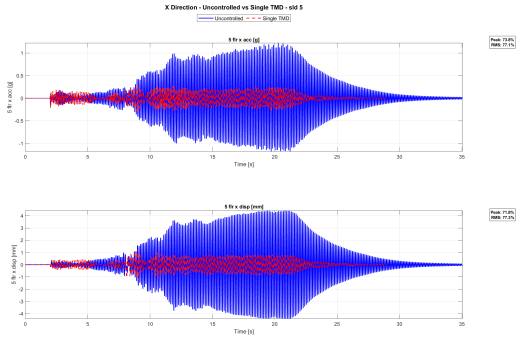

(e). SLD5 X-direction

Figure 9.2: X-direction structural response comparison between uncontrolled and single TMD controlled cases under 45° directional excitation for 5 SLD cases, demonstrating the effectiveness of TMD control in reducing lateral displacement.

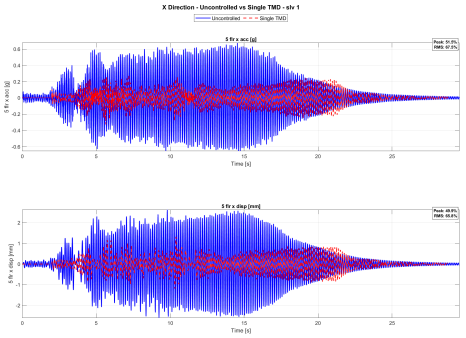

(a). SLV1 X-direction

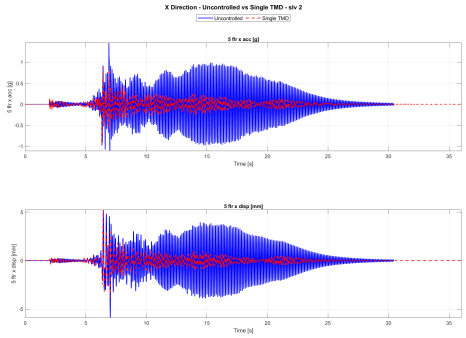

(b). SLV2 X-direction

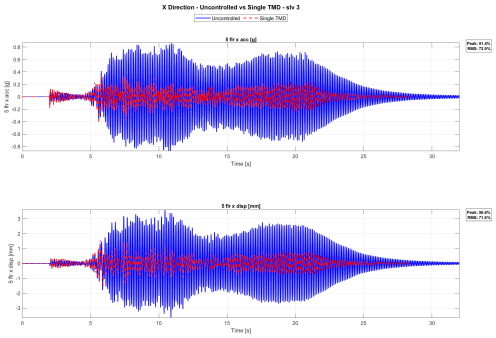

(c). SLV3 X-direction

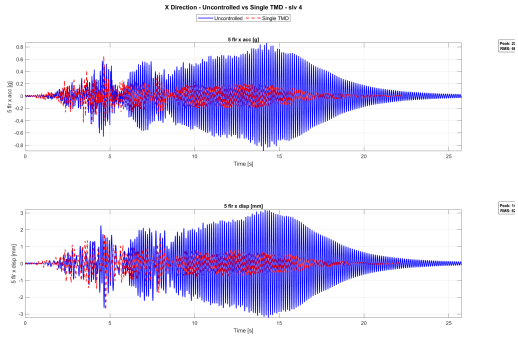

(d). SLV4 X-direction

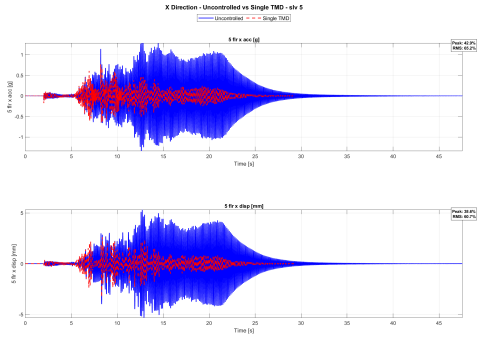

(e). SLV5 X-direction

Figure 9.3: X-direction structural response comparison between uncontrolled and single TMD controlled cases under 45° directional excitation for 5 SLV cases, demonstrating the effectiveness of TMD control in reducing lateral displacement.

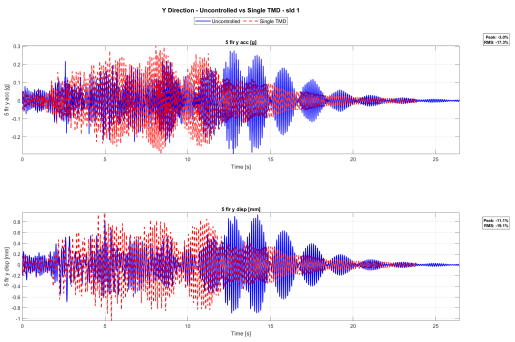

(a). SLD1 Y-direction

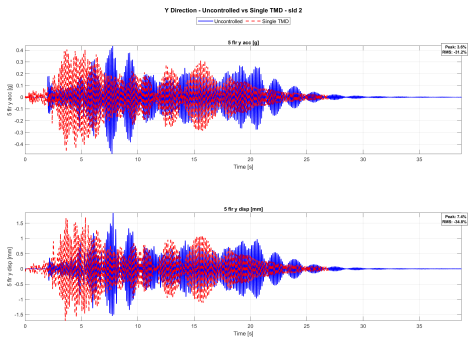

(b). SLD2 Y-direction

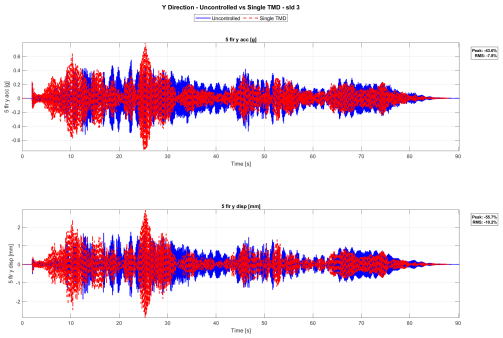

(c). SLD3 Y-direction

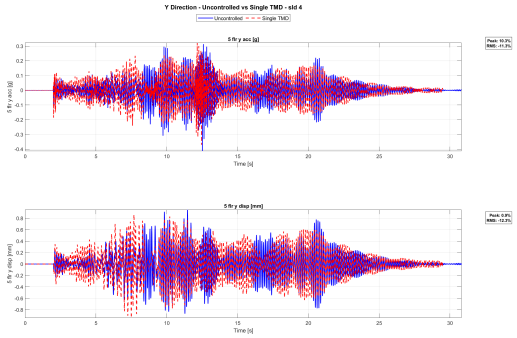

(d). SLD4 Y-direction

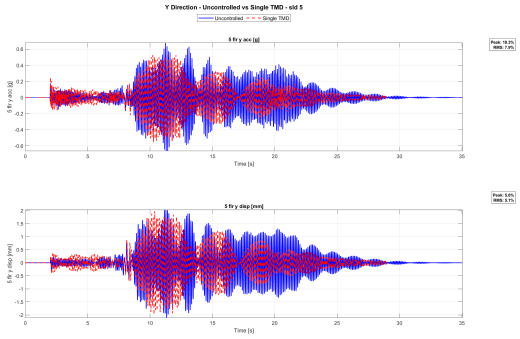

(e). SLD5 Y-direction

Figure 9.4: Y-direction structural response comparison between uncontrolled and single TMD controlled cases under 45° directional excitation for 5 SLD cases, demonstrating the effectiveness of TMD control in reducing lateral displacement.

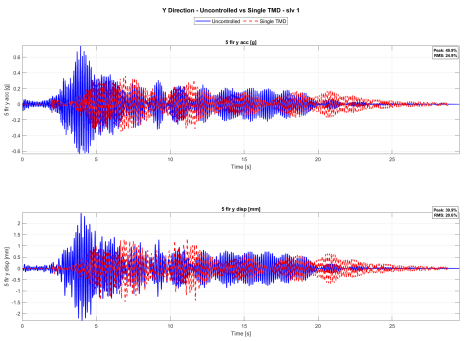

(a). SLV1 Y-direction

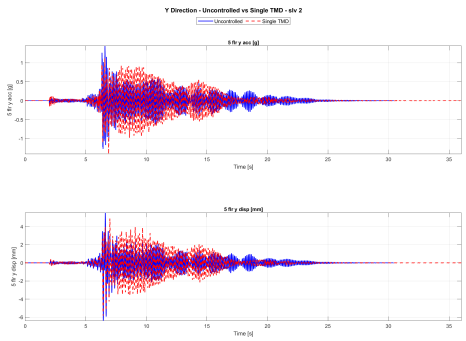

(b). SLV2 Y-direction

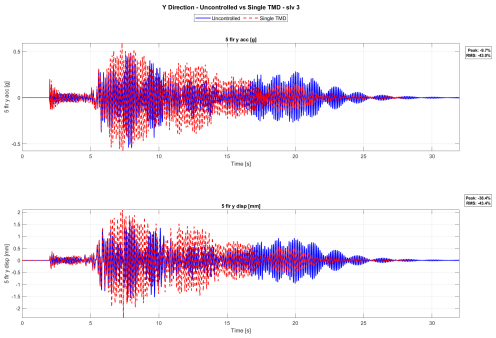

(c). SLV3 Y-direction

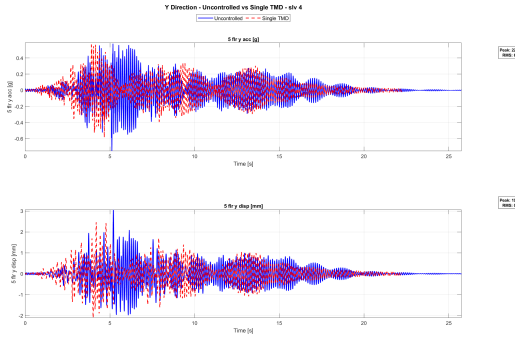

(d). SLV4 Y-direction

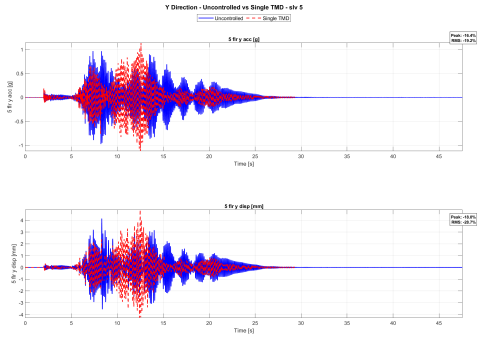

(e). SLV5 Y-direction

Figure 9.5: Y-direction structural response comparison between uncontrolled and single TMD controlled cases under 45° directional excitation for 5 SLV cases, demonstrating the effectiveness of TMD control in reducing lateral displacement.

Both TMD configurations demonstrated excellent performance in the X-direction, with the dual system providing marginal improvements. The single TMD system achieved 46.7% mean peak reduction, while the dual system reached 50.8%. This similarity is expected since both configurations include an X-direction TMD on the 5th floor. The Y-direction response reveals the limitations of single-direction control strategies. The single TMD system showed negative average performance with -3.5% peak reduction and -11.8% RMS reduction, indicating occasional response amplifica-

tion. The dual TMD system showed modest improvement but remained less effective in this direction, highlighting the challenges of cross-directional control. The torsional response analysis demonstrates the most significant advantage of the dual TMD system. While the single TMD provided minimal torsional control with 1.9% mean peak reduction, the dual system achieved substantial improvement with 19.4% mean peak reduction, representing a tenfold enhancement. This improvement is attributed to the coupled control effect of orthogonally oriented TMDs on different floors. The same can be seen in the interstorey drifts shown in the Figure.

9.2.3 Performance by Excitation Type

The dual TMD system demonstrated superior performance across all excitation types, with particular advantage under harmonic loading where the tuned characteristics could be fully utilized. The consistency improvement is notable, especially for seismic excitations where the single TMD system showed higher performance variability.

Table 9.2: Performance Variation by Excitation Type

Excitation Type	**Single TMD**	**Dual TMD**	**Improvement**
Sine Waves			
Mean Reduction	33.2%	50.9%	+53.3%
Consistency	Medium	High	-
SLD Motions			
Mean Reduction	26.8%	34.2%	+27.6%
Consistency	Low	Medium	-
SLV Motions			
Mean Reduction	19.4%	23.6%	+21.6%
Consistency	Low	Medium	-

9.3 Response Time History Analysis

9.3.1 Representative SLD Cases

Figure 9.6 illustrates the structural response for SLD1, representing typical performance under moderate excitation. For SLD1, both systems effectively controlled X-

direction response, with the dual system showing slightly better performance in reducing peak displacements. The Y-direction response demonstrates the limitation of the single TMD system, which provided minimal control in this direction.

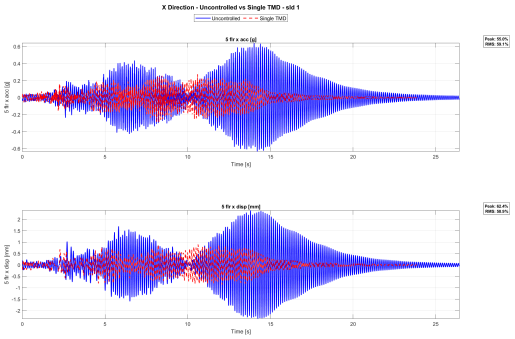

(a). Single TMD - X-direction

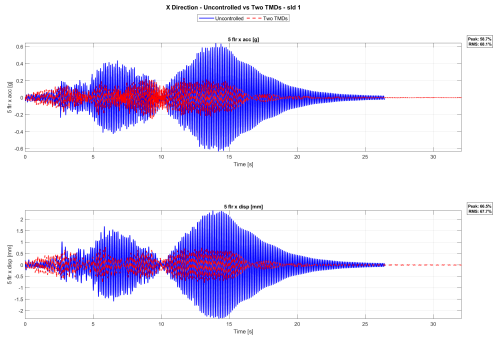

(b). Dual TMD - X-direction

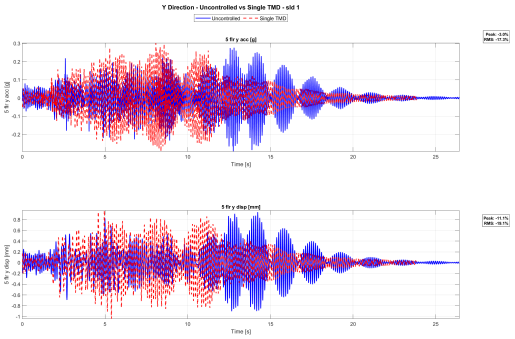

(c). Single TMD - Y-direction

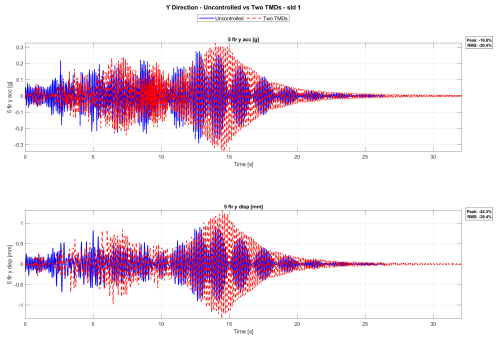

(d). Dual TMD - Y-direction

Figure 9.6: Structural response comparison for SLD1 excitation showing effective control by both systems in X-direction and superior torsional performance by dual TMD system.

9.3.2 Critical Case: SLD6 Analysis

The SLD6 excitation represents the most challenging scenario encountered during testing, characterized by significant high-frequency content and strong velocity pulses. Figure 9.7 shows the structural response for this critical case. The SLD6 case revealed critical limitations of the single TMD configuration, which amplified Y-direction response by 147.1% in terms of peak displacement. This amplification phenomenon occurs due to torsional coupling transferring energy to uncontrolled directions, phase differences between structural and TMD response, and limited control authority in non-primary directions. The dual TMD system successfully mitigated this issue, providing 34.6% reduction in Y-direction peak response and demonstrating robust multi-directional

control capability.

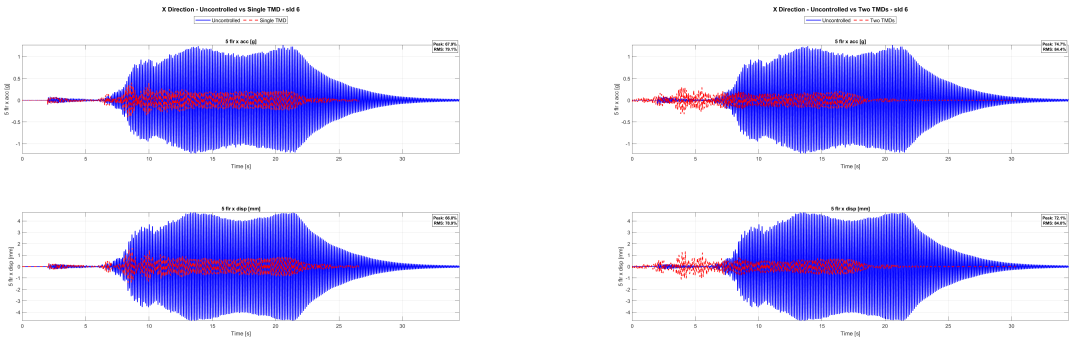

(a). Single TMD - X-direction

(b). Dual TMD - X-direction

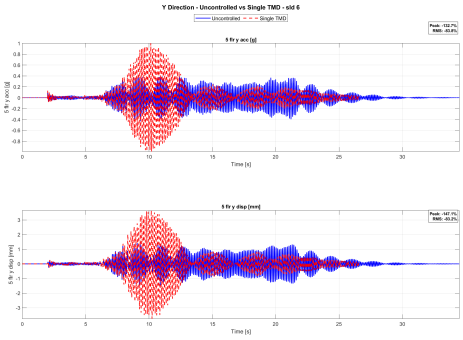

(c). Single TMD - Y-direction

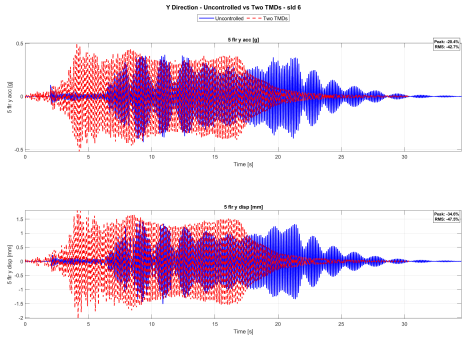

(d). Dual TMD - Y-direction

Figure 9.7: SLD6 excitation response showing significant Y-direction amplification with single TMD and effective multi-directional control with dual TMD system.

9.4 Hysteresis Behavior and Energy Dissipation

9.4.1 Single TMD Hysteresis Characteristics

The hysteresis behavior of the single TMD system reveals important insights into its energy dissipation mechanisms and operational limits, as shown in Figure 9.8. The single TMD system exhibited stable elliptical hysteresis under moderate excitations such as SLD1, significant nonlinearity under severe loading such as SLD6, consistent energy dissipation in primary direction.

9.4.2 Dual TMD Hysteresis Characteristics

The dual TMD system demonstrated distributed energy dissipation across multiple devices and directions, as illustrated in Figure 9.9. Key observations from dual TMD

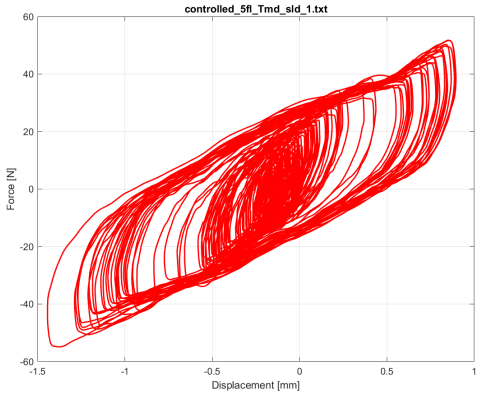

(a). SLD1 - Stable hysteresis

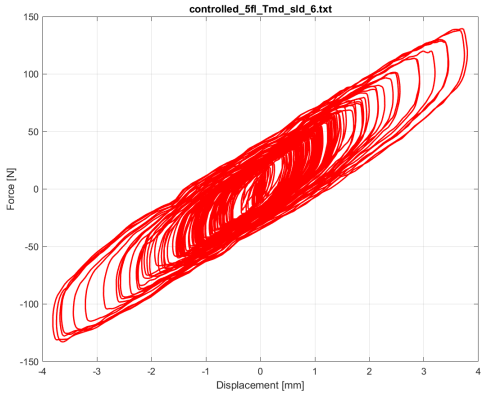

(b). SLD6 - Nonlinear behavior

Figure 9.8: Hysteresis behavior of single TMD system showing stable energy dissipation under moderate excitation (SLD1) and nonlinear characteristics under severe loading (SLD6).

hysteresis analysis include distributed energy dissipation between 4th and 5th floor devices.

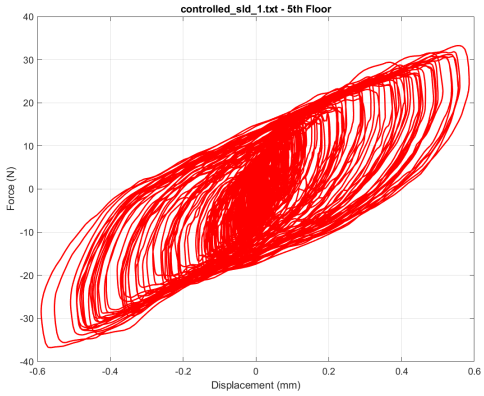

(a). 5th Floor TMD - SLD1

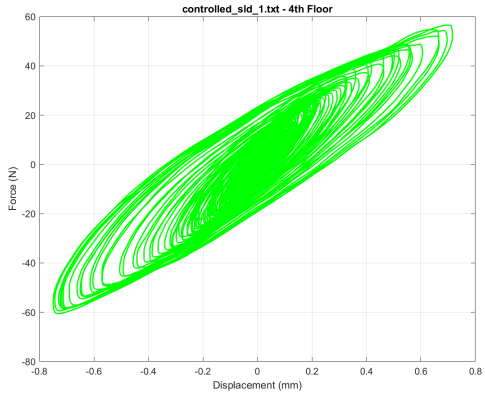

(b). 4th Floor TMD - SLD1

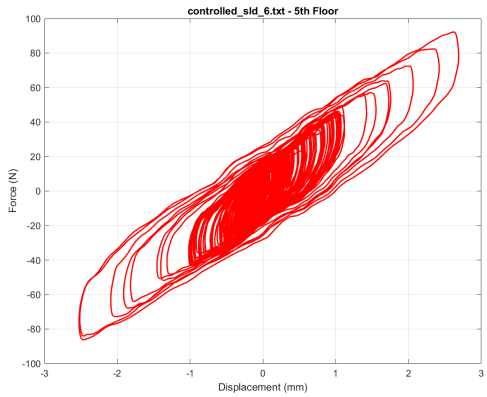

(c). 5th Floor TMD - SLD6

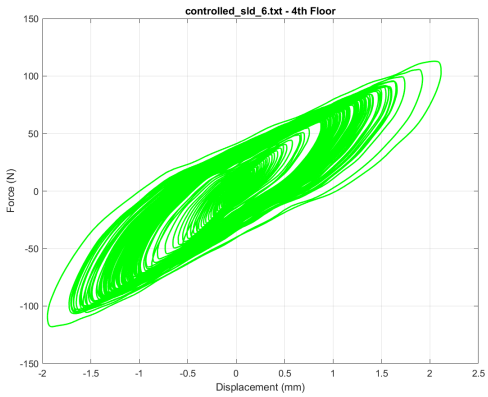

(d). 4th Floor TMD - SLD6

Figure 9.9: Hysteresis behavior of dual TMD system showing distributed energy dissipation and stable operation under both moderate and severe excitation conditions.

9.5 Interstorey Drift Plots

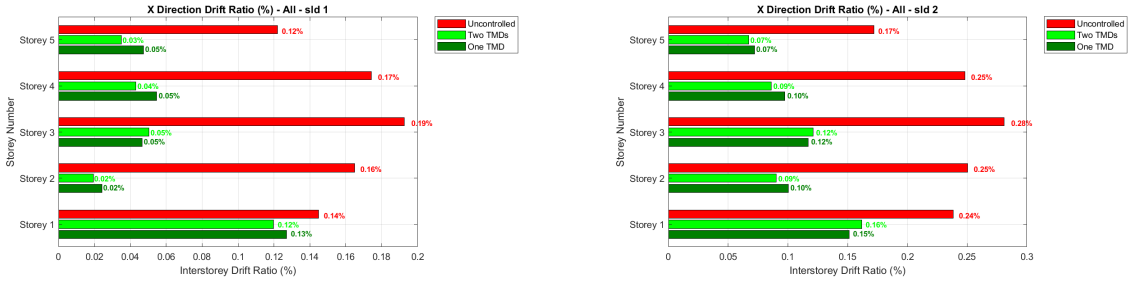

(a). One TMD **(b).** Two TMDs

Figure 9.10: X-direction interstory drift ratio comparison for 2 SLD ground motion cases, including configurations with one TMD and two TMDs. The plots show the drift percentage distribution across all floors for serviceability limit displacement conditions.

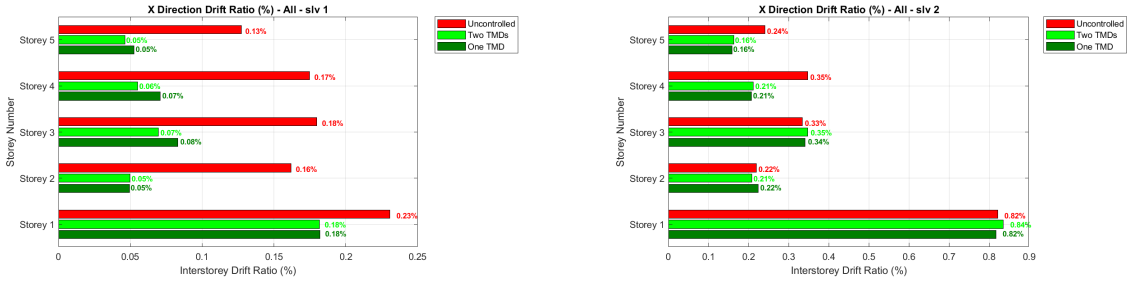

(a). One TMD **(b).** Two TMDs

Figure 9.11: X-direction interstory drift ratio comparison for 2 SLV ground motion cases, including configurations with one TMD and two TMDs. The results illustrate the drift percentage distribution across all floors under serviceability limit velocity conditions.

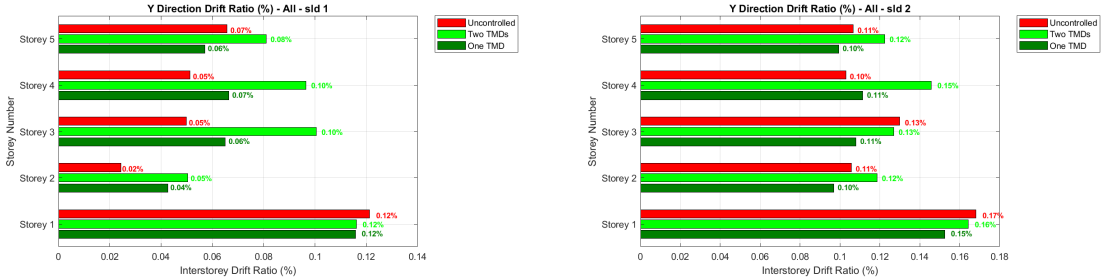

(a). One TMD **(b).** Two TMDs ù

Figure 9.12: Y-direction interstory drift ratio comparison for two SLD ground motion cases, including configurations with one TMD and two TMDs. The plots show the drift percentage distribution across all floors for serviceability limit displacement conditions.

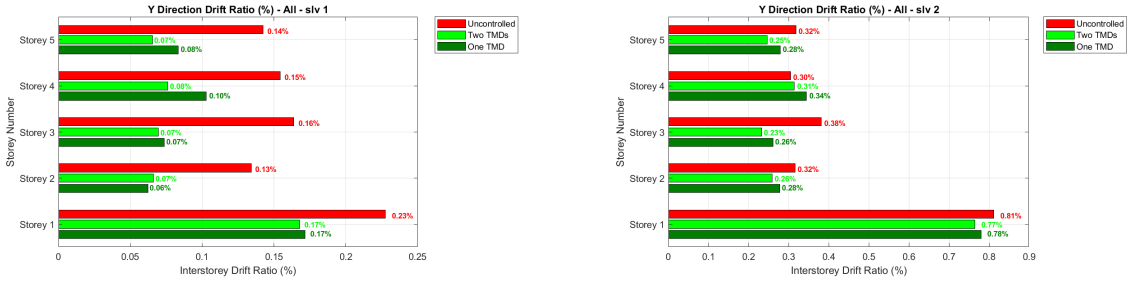

(a). One TMD **(b).** Two TMDs

Figure 9.13: Y-direction interstory drift ratio comparison for two SLV ground motion cases, including configurations with one TMD and two TMDs. The results illustrate the drift percentage distribution across all floors under serviceability limit velocity conditions.

The interstorey drift plots shows that the two TMD configuration can meet the seismic demands

9.6 Conclusions

9.6.1 Performance Summary

The comprehensive evaluation of TMD performance under 45-degree directional excitation leads to several key conclusions. The dual TMD system demonstrated superior overall performance with 32.1% mean response reduction compared to 25.4% for the single TMD system, representing a 26.4% improvement. Significant advantages were observed in torsional control, where the dual system achieved 19.4% mean reduction compared to 1.9% for the single system, representing a tenfold improvement. The dual TMD configuration provided substantially better reliability, with success rate increasing from 65% to 78% and coefficient of variation decreasing from 189% to 115%. Both systems effectively maintained code compliance for life safety requirements, with the dual system providing additional safety margins for serviceability and collapse prevention.

9.6.2 Research Contributions

This research contributes to the field of structural control through comprehensive statistical analysis of TMD performance under multi-directional excitation, quantitative assessment of torsional control effectiveness for different configurations, development of reliability-based performance metrics for control systems, practical implementation guidelines considering both technical and economic factors, and enhanced understanding of coupled lateral-torsional control mechanisms.

9.6.3 Future Research Directions

Based on the findings of this study, several future research directions are recommended. These include investigation of adaptive TMD systems for varying excitation characteristics, development of hybrid control strategies combining TMDs with other devices, exploration of optimal TMD distribution patterns for complex structures, long-term monitoring and performance validation of implemented systems, and integration of machine learning approaches for real-time control optimization. The findings of this chapter demonstrate that while single TMD systems provide cost-effective vibration control for specific applications, dual TMD configurations offer substantially better and more reliable performance for structures subjected to multi-directional excitation, making them particularly suitable for critical infrastructure and performance-based design applications.

Chapter 10

Conclusions and Recommendations

10.1 Summary of Research and Key Conclusions

This doctoral thesis has presented a comprehensive body of work dedicated to the development, validation, and analysis of a novel Hysteretic Tuned Mass Damper (HTMD) for seismic protection of structures. The research was motivated by the critical need for economically viable and high-performance passive control systems that can overcome the limitations of conventional Tuned Mass Dampers (TMDs) and the cost barriers of advanced material-based solutions. Through an integrated program of theoretical development, mechanical design, experimental testing, and numerical simulation, the following key conclusions can be decisively drawn:

1. The proposed HTMD, utilizing a double-sliding mechanism with conventional steel wire ropes, has been successfully demonstrated as a viable technology for generating stable, pinched hysteretic behavior. This mechanical innovation effectively replicates the advantageous force-displacement characteristics—namely, quasi-zero stiffness, progressive nonlinear hardening, and significant energy dissipation—that were previously the domain of expensive Shape Memory Alloy systems.

2. Extensive experimental testing on a scaled five-story structure confirmed the superior performance of the optimized HTMD. Under Serviceability Limit State

(SLD) seismic motions, the device achieved average peak displacement reductions of approximately 63%, dramatically mitigating non-structural damage and ensuring post-event functionality. Its performance under higher-intensity (SLV) motions, while more variable, remained consistently beneficial, providing reliable protection for life-safety objectives.

3. A sophisticated phenomenological model based on a modified Bouc-Wen formulation, enhanced with a pinching function and essential stiffness component, was developed and rigorously calibrated. This model demonstrates excellent fidelity in capturing the HTMD's complex nonlinear response across various loading amplitudes, providing a valuable tool for future analysis and design applications without the constant need for physical prototyping.

4. The research unequivocally established the importance of optimal device placement and configuration. The HTMD located on the top floor consistently outperformed a sub-optimal placement, validating classical dynamics principles. Furthermore, for structures subjected to multi-directional excitation that induces torsional response, a dual-HTMD configuration was proven necessary to provide comprehensive and robust control, preventing adverse response amplification in uncontrolled directions.

5. From a practical standpoint, the HTMD technology represents a paradigm shift towards sustainable resilience. By achieving advanced performance with low-cost materials, it offers an estimated cost reduction of over 80% compared to SMA-based alternatives. This breakthrough has the potential to make enhanced seismic protection accessible for a much wider range of structures, thereby significantly impacting global seismic risk mitigation strategies.

10.2 Principal Contributions to Knowledge

This research makes several original contributions to the field of structural dynamics and earthquake engineering:

- **Novel Device Concept:** The invention and detailed development of the double-sliding hysteretic TMD, a new mechanical configuration for achieving pinched hysteresis with conventional materials.
- **Advanced Modeling Framework:** The development and experimental validation of an enhanced Bouc-Wen model capable of accurately representing the "quasi-zero stiffness to hardening" transition and pinching behavior observed in the HTMD.
- **Comprehensive Experimental Database:** A rich set of experimental data from component-level characterization to full system shake-table testing, providing a benchmark for the validation of future nonlinear control devices and models.
- **Practical Design Insights:** Clear, evidence-based guidelines on the critical importance of TMD placement and the necessity of multi-device strategies for controlling coupled lateral-torsional responses in asymmetric structures.
- **Bridging Research and Practice:** The development of a coherent framework—encompassing device design, modeling, optimization, and implementation strategies—that facilitates the transition of this research from academic discovery to practical engineering application.

10.3 Recommendations for Future Work

The successful culmination of this thesis opens up several promising avenues for future research and development:

1. **Full-Scale Implementation and Monitoring:** The logical next step is the design, fabrication, and installation of a full-scale HTMD in a real structure. A long-term monitoring program on such a installation would provide invaluable data on manufacturing at scale, installation challenges, in-service performance under ambient and minor seismic vibrations, and long-term durability.

2. **Extension to Diverse Structural Systems:** Research should be expanded to investigate the application and optimization of HTMDs for a wider variety of structural types, including reinforced concrete buildings (considering their inherent nonlinearity), bridges, offshore structures, and historical monuments. This would lead to the development of typology-specific design guidelines.

3. **Development of Hybrid and Adaptive Systems:** Exploring hybrid systems, where the passive HTMD is combined with a small semi-active damper or a tunable stiffness element, could create a system that maintains passive reliability while adapting its properties in real-time to optimize performance for the specific characteristics of a severe earthquake.

4. **Codification and Standardization:** Efforts should be initiated to work towards the development of pre-normative guidelines and, eventually, codified design provisions for nonlinear TMDs in national and international standards (e.g., ASCE/SEI 7, Eurocode 8). This is a crucial step for fostering widespread confidence and adoption within the engineering community.

5. **Life-Cycle Cost and Sustainability Analysis:** A detailed life-cycle assessment (LCA) and life-cycle cost analysis (LCCA) comparing structures equipped with HTMDs against those with conventional or other advanced damping systems would provide a robust economic and environmental justification for the technology, appealing to owners, insurers, and policymakers.

10.4 Final Remarks

This dissertation has traversed the path from identifying a critical gap in seismic protection technology to delivering a novel, validated, and practical solution. The Hysteretic Tuned Mass Damper developed herein stands as a testament to the power of fundamental engineering principles and inventive mechanical design. It proves that exceptional performance need not be synonymous with high cost or complex materials. By providing a viable path toward more resilient and economically sustainable

infrastructure, this work contributes to the broader societal goal of mitigating seismic risk. It is the author's fervent hope that the findings and frameworks presented in this thesis will inspire further innovation, guide future research, and ultimately empower engineers worldwide to design and construct a safer, more resilient built environment for generations to come.

Bibliography

M. Abe and Y. Fujino. Dynamic characterization of multiple tuned mass dampers and some design formulas. *Earthquake Engineering & Structural Dynamics*, 23(8): 813–835, 1994.

R. A. A. Aguiar, M. A. Savi, and P. M. C. L. Pacheco. Experimental investigation of vibration reduction using shape memory alloys. *Journal of Intelligent Material Systems and Structures*, 24(2):247–261, 2013.

N. A. Alexander and F. Schilder. Exploring the performance of a nonlinear tuned mass damper. *Journal of Sound and Vibration*, 319(1-2):445–462, 2009.

T. Asami, O. Nishihara, and A. M. Baz. Analytical solutions to h∞ and h2 optimization of dynamic vibration absorbers attached to damped linear systems. *Journal of Vibration and Acoustics*, 124(2):284–295, 2002.

S. V. Bakre and R. S. Jangid. Optimum parameters of tuned mass damper for damped main system. *Structural Control and Health Monitoring*, 14(3):448–470, 2007.

G. Bekdaş and S. M. Nigdeli. Estimating optimum parameters of tuned mass dampers using harmony search. *Engineering Structures*, 33(9):2716–2723, 2011.

R. Bouc. Forced vibrations of mechanical systems with hysteresis. In *Proceedings of the 4th Conference on Nonlinear Oscillations*. Prague, 1967.

T. M. Cameron and J. H. Griffin. An alternating frequency/time domain method for calculating the steady-state response of nonlinear dynamic systems. *Journal of Applied Mechanics*, 56(1):149–154, 1989.

B. Carboni and W. Lacarbonara. Nonlinear vibration absorber with pinched hysteresis: theory and experiments. *Journal of Engineering Mechanics*, 142(5):04016023, 2016.

B. Carboni, W. Lacarbonara, and F. Auricchio. Hysteresis of multiconfiguration assemblies of nitinol and steel strands: experiments and phenomenological identification. *Journal of Engineering Mechanics*, 141(3):04014135, 2015.

N. Carpineto, W. Lacarbonara, and F. Vestroni. Hysteretic tuned mass dampers for structural vibration mitigation. *Journal of Sound and Vibration*, 333(5):1302–1318, 2014.

A. Carrella, M. J. Brennan, and T. P. Waters. Static analysis of a quasi-zero-stiffness vibration isolator. *Journal of Sound and Vibration*, 301(3-5):678–689, 2007.

F. Casciati and F. Giuliano. Performance of multi-tmd in the towers of suspension bridges. *Journal of Vibration and Control*, 15(6):821–847, 2009.

S. Chakraborty, R. Debbarma, and G. C. Marano. Reliability-based optimum design of tuned mass damper in seismic vibration control under uncertain bounded system parameters. *Probabilistic Engineering Mechanics*, 26(2):215–221, 2011.

S. Chandrasekaran, D. Kumar, and R. Ramanathan. Response control of tension leg platform with passive damper: Experimental investigations. *Ships and Offshore Structures*, 1(4):327–336, 2016.

A. E. Charalampakis and C. K. Dimou. Identification of bouc-wen hysteretic systems using particle swarm optimization. *Computers & Structures*, 88(21-22):1197–1205, 2010.

A. P. Chassiakos, S. F. Masri, A. W. Smyth, and T. K. Caughey. On-line identification of hysteretic systems. *Journal of Applied Mechanics*, 65(1):194–203, 1998.

K. A. Chondrogiannis, V. Dertimanis, B. Jeremic, and E. Chatzi. Design of the negative stiffness negsv mechanism for structural vibration attenuation exploiting resonance. *International Journal of Mechanical Sciences*, 260:108640, 2023.

M. De Angelis, A. Giaralis, F. Petrini, and D. Pietrosanti. Optimal tuning and assessment of inertial dampers with grounded inerter for vibration control of seismically excited base-isolated systems. *Engineering Structures*, 196:109250, 2019.

J. P. Den Hartog. *Mechanical Vibrations*. McGraw-Hill, New York, 1956.

A. Der Kiureghian and O. Ditlevsen. Aleatory or epistemic? does it matter? *Structural Safety*, 31(2):105–112, 2009.

T. Detroux, G. Habib, L. Masset, and G. Kerschen. Performance, robustness and sensitivity analysis of the nonlinear tuned vibration absorber. *Mechanical Systems and Signal Processing*, 60:799–809, 2015.

H. Ding and L. Q. Chen. Designs, analysis, and applications of nonlinear energy sinks. *Nonlinear Dynamics*, 100:3061–3107, 2020.

European Committee for Standardization. *Eurocode 8: Design of structures for earthquake resistance – Part 3: Assessment and retrofitting of buildings*. 2005.

C. R. Farrar and K. Worden. *Structural Health Monitoring: A Machine Learning Perspective*. John Wiley & Sons, Chichester, UK, 2012.

Federal Emergency Management Agency. Techniques for seismic rehabilitation of existing buildings. Technical report, 2006.

M. Feldman. *Hilbert Transform Applications in Mechanical Vibration*. John Wiley & Sons, Chichester, UK, 2011.

H. Frahm. Device for damping vibrations of bodies, 1909.

Y. Fujino and M. Abe. Design formulas for tuned mass dampers based on a perturbation technique. *Earthquake Engineering & Structural Dynamics*, 22(10):833–854, 1993.

G. Gatti. Fundamental insight on the performance of nonlinear tuned mass dampers. *Meccanica*, 53(1):111–123, 2018.

R. R. Gerges and B. J. Vickery. Parametric experimental study of wire rope spring tuned mass dampers. *Journal of Wind Engineering and Industrial Aerodynamics*, 91 (12-15):1363–1385, 2003.

M. Gu, S. R. Chen, and C. C. Chang. Parametric study on multiple tuned mass dampers for buffeting control of yangpu bridge. *Journal of Wind Engineering and Industrial Aerodynamics*, 89(11-12):987–1000, 2001.

G. Habib, T. Detroux, R. Viguié, and G. Kerschen. Nonlinear generalization of den hartog's equal-peak method. *Mechanical Systems and Signal Processing*, 52:17–28, 2015.

M. N. Hadi and Y. Arfiadi. Optimum design of absorber for mdof structures. *Journal of Structural Engineering*, 124(11):1272–1280, 1998.

N. Hoang and P. Warnitchai. Design of multiple tuned mass dampers by using a numerical optimizer. *Earthquake Engineering & Structural Dynamics*, 34(2):125–144, 2005.

G. W. Housner, L. A. Bergman, T. K. Caughey, et al. Structural control: past, present, and future. *Journal of Engineering Mechanics*, 123(9):897–971, 1997.

H. Huang, K. M. Mosalam, and W. S. Chang. Adaptive tuned mass damper with shape memory alloy for seismic application. *Engineering Structures*, 223:111171, 2020.

L. Huang and X. D. Yang. Dynamics of a novel 2-dof coupled oscillators with geometry nonlinearity. *Nonlinear Dynamics*, 111(20):18753–18777, 2023.

J. A. Inaudi and J. M. Kelly. Mass damper using friction-dissipating devices. *Journal of Engineering Mechanics*, 121(1):142–149, 1995.

K. Iwanami and K. Seto. An optimum design method for the dual dynamic damper and its effectiveness. *Bulletin of JSME*, 27(231):1965–1973, 1984.

R. S. Jangid. Optimum multiple tuned mass dampers for base-excited undamped system. *Earthquake Engineering & Structural Dynamics*, 28(9):1041–1049, 1999.

Q. Jiang, X. Lu, H. Guan, and X. Ye. Shaking table model test and fe analysis of a reinforced concrete mega-frame structure with tuned mass dampers. *The Structural Design of Tall and Special Buildings*, 23(18):1426–1442, 2014.

A. Kareem, T. Kijewski, and Y. Tamura. Mitigation of motions of tall buildings with specific examples of recent applications. *Wind and Structures*, 2(3):201–251, 1999.

D. Karnopp. Active and semi-active vibration isolation. *Journal of Mechanical Design*, 117(B):177–185, 1995.

G. Kerschen, K. Worden, A. F. Vakakis, and J. C. Golinval. Past, present and future of nonlinear system identification in structural dynamics. *Mechanical Systems and Signal Processing*, 20(3):505–592, 2006.

S. Krenk. Frequency analysis of the tuned mass damper. *Journal of Applied Mechanics*, 72(6):936–942, 2005.

K. C. S. Kwok, Y. L. Xu, and B. Samali. Control of wind-induced vibrations of tall buildings. *Engineering Structures*, 17(9):639–654, 1995.

K. C. S. Kwok, P. A. Hitchcock, and M. D. Burton. Perception of vibration and occupant comfort in wind-excited tall buildings. *Journal of Wind Engineering and Industrial Aerodynamics*, 97(7-8):368–380, 2009.

Y. S. Lee, A. F. Vakakis, D. M. McFarland, and L. A. Bergman. Passive suppression of limit cycle oscillations. *Journal of Sound and Vibration*, 332(18):4336–4353, 2013.

A. Y. T. Leung and H. Zhang. Particle swarm optimization of tuned mass dampers. *Engineering Structures*, 31(3):715–728, 2009.

C. Li. Optimum multiple tuned mass dampers for structures under ground acceleration based on ddmf and admf. *Earthquake Engineering & Structural Dynamics*, 29(5): 577–588, 2002.

C. Li and W. Qu. Optimum properties of multiple tuned mass dampers for reduction of translational and torsional response of structures subject to ground acceleration. *Engineering Structures*, 28(4):472–494, 2006.

K. Li and A. P. Darby. Experiments on the effect of an impact damper on a multiple-degree-of-freedom system. *Journal of Vibration and Control*, 12(5):445–464, 2006.

L. Li and P. Zhang. Novel design approach of a nonlinear tuned mass damper. *Journal of Engineering Mechanics*, 143(4):04017001, 2017.

Q. S. Li, L. H. Zhi, A. Y. Tuan, C. S. Kao, S. C. Su, and C. F. Wu. Dynamic behavior of taipei 101 tower: field measurement and numerical analysis. *Journal of Structural Engineering*, 137(1):143–155, 2011.

X. Liu, X. Huang, and H. Hua. On the characteristics of a quasi-zero stiffness isolator using euler buckled beam as negative stiffness corrector. *Journal of Sound and Vibration*, 332(14):3359–3376, 2013.

Z. Lu, X. Chen, D. Zhang, and K. Dai. Experimental and analytical study on the performance of particle tuned mass dampers under seismic excitation. *Earthquake Engineering & Structural Dynamics*, 46(5):697–714, 2018.

G. C. Marano, R. Greco, and B. Chiaia. A comparison between different optimization criteria for tuned mass dampers design. *Journal of Sound and Vibration*, 329(23): 4880–4890, 2010.

L. Marian and A. Giaralis. Optimal design of a novel tuned mass-damper–inerter (tmdi) passive vibration control configuration for stochastically support-excited structural systems. *Engineering Structures*, 79:390–401, 2014.

C. Martinelli, R. Avadhani, and A. Cammarano. Identification of nonlinear characteristics of an additive manufactured vibration absorber. In *Society for Experimental Mechanics Annual Conference*, pages 229–235. Springer, 2023.

F. McKenna, G. L. Fenves, M. H. Scott, and B. Jeremić. Open system for earthquake engineering simulation (opensees), 2000.

R. J. McNamara. Tuned mass dampers for buildings. *Journal of the Structural Division*, 103(9):1785–1798, 1977.

S. K. Mishra, S. Gur, and S. Chakraborty. An improved tuned mass damper assisted by shape memory alloy. *Smart Materials and Structures*, 22(9):095016, 2013.

M. Mohebbi, K. Shakeri, Y. Ghanbarpour, and H. Majzoub. Designing optimal multiple tuned mass dampers using genetic algorithms. *Engineering Structures*, 49:287–298, 2013.

Y. Nakamura, A. Fukukita, K. Tamura, et al. Seismic response control using electromagnetic inertial mass dampers. *Earthquake Engineering & Structural Dynamics*, 43(4):507–527, 2014.

S. Natsiavas. Steady state oscillations and stability of non-linear dynamic absorbers. *Journal of Sound and Vibration*, 156(2):227–245, 1992.

A. H. Nayfeh and D. T. Mook. *Nonlinear Oscillations*. John Wiley & Sons, New York, 2008.

J. Ormondroyd and J. P. Den Hartog. The theory of the dynamic vibration absorber. *Transactions of the ASME*, 50:9–22, 1928.

D. T. R. Pasala, A. A. Sarlis, S. Nagarajaiah, et al. Adaptive negative stiffness for seismic protection. *Journal of Structural Engineering*, 140(7):04014052, 2014.

M. Peeters, R. Viguié, G. Sérandour, G. Kerschen, and J. C. Golinval. Nonlinear normal modes, part ii: practical computation. *Mechanical Systems and Signal Processing*, 23(1):195–216, 2009.

D. Pietrosanti, M. De Angelis, and M. Basili. Optimal design and performance of systems with tmdi. *Earthquake Engineering & Structural Dynamics*, 46(8):1367–1388, 2017.

A. Y. Pisal and R. S. Jangid. Dynamic response of structure with tuned mass friction damper. *International Journal of Advanced Structural Engineering*, 8(4):363–377, 2016.

G. Quaranta, W. Lacarbonara, and S. F. Masri. A review on computational intelligence for identification of nonlinear dynamical systems. *Nonlinear Dynamics*, 99(2):1709–1761, 2020.

F. Rüdinger. Optimal vibration absorber with nonlinear viscous damping. *Journal of Engineering Mechanics*, 132(1):46–53, 2006.

K. Rajana and A. Giaralis. A novel nonlinear isolated rooftop tmdi system. *Acta Mechanica*, 234(9):3751–3777, 2023.

Z. T. Rakicevic, A. Bogdanovic, D. Jurukovski, and P. Nawrotzki. Effectiveness of tuned mass damper in reduction of seismic response. *Bulletin of Earthquake Engineering*, 10(3):1049–1073, 2012.

R. E. Roberson. Synthesis of a nonlinear dynamic vibration absorber. *Journal of the Franklin Institute*, 254(3):205–220, 1952.

A. A. Sarlis, D. T. Pasala, M. C. Constantinou, et al. Negative stiffness device for seismic protection. *Journal of Structural Engineering*, 139(7):1124–1133, 2013.

G. I. Schuëller and H. A. Jensen. Computational methods in optimization considering uncertainties. *Computer Methods in Applied Mechanics and Engineering*, 198(1): 2–13, 2008.

M. Setareh. Floor vibration control using semi-active tmds. *Journal of Structural Engineering*, 128(10):1328–1336, 2002.

S. W. Shaw and C. Pierre. Normal modes for non-linear vibratory systems. *Journal of Sound and Vibration*, 164(1):85–124, 1993.

M. V. Sivaselvan and A. M. Reinhorn. Hysteretic models for deteriorating inelastic structures. *Journal of Engineering Mechanics*, 126(6):633–640, 2000.

J. R. Sladek and R. E. Klingner. Effect of tuned-mass dampers on seismic response. *Journal of Structural Engineering*, 109(8):2004–2009, 1983.

M. C. Smith. Synthesis of mechanical networks: the inerter. *IEEE Transactions on Automatic Control*, 47(10):1648–1662, 2002.

J. Song and A. Der Kiureghian. Generalized bouc-wen model for highly asymmetric hysteresis. *Journal of Engineering Mechanics*, 132(6):610–618, 2006.

B. F. Spencer and S. Nagarajaiah. State of the art of structural control. *Journal of Structural Engineering*, 129(7):845–856, 2003.

C. Sun, S. Nagarajaiah, and A. Dick. Experimental investigation of vibration attenuation. *Nonlinear Dynamics*, 78(4):2699–2715, 2014.

A. A. Taflanidis and J. L. Beck. Life-cycle cost frameworks for passive dampers. *Structural Safety*, 31(6):508–522, 2009.

Y. Tamura, K. Fujii, T. Ohtsuki, T. Wakahara, and R. Kohsaka. Effectiveness of tuned liquid dampers under wind excitation. *Engineering Structures*, 17(9):609–621, 2003.

L. Tian, H. Pan, and R. Ma. Probabilistic seismic demand model and fragility analysis. *Journal of Constructional Steel Research*, 156:266–275, 2019.

N. D. Tiwari, A. Gogoi, B. Hazra, and Q. Wang. A shape memory alloy-tuned mass damper inerter system. *Journal of Sound and Vibration*, 494:115893, 2021.

H. C. Tsai and G. C. Lin. Optimum tuned-mass dampers for minimizing steady-state response. *Earthquake Engineering & Structural Dynamics*, 22(11):957–973, 1993.

A. Y. Tuan and G. Q. Shang. Vibration control in a 101-storey building. *Computer-Aided Civil and Infrastructure Engineering*, 29(6):427–443, 2014.

A. F. Vakakis et al. Nonlinear targeted energy transfer in mechanical systems. 2008.

R. Viguié and G. Kerschen. Nonlinear vibration absorber coupled to a nonlinear structure. *Nonlinear Dynamics*, 56(3):249–271, 2009.

R. Villaverde. Reduction in seismic response with heavily-damped vibration absorbers. *Earthquake Engineering & Structural Dynamics*, 13(1):33–42, 1985.

J. Wang, B. Wang, Z. Liu, C. Zhang, and H. Li. Experimental and numerical studies of an asymmetric nonlinear mass damper. *Structural Control and Health Monitoring*, 27(4):e2513, 2020.

G. B. Warburton. Optimum absorber parameters for various combinations. *Earthquake Engineering & Structural Dynamics*, 10(3):381–401, 1982.

F. Weber and M. Maślanka. Frequency and damping adaptation of a tmd with mr damper. *Smart Materials and Structures*, 21(5):055011, 2013.

K. Worden and G. R. Tomlinson. *Nonlinearity in Structural Dynamics*. Institute of Physics Publishing, Bristol, UK, 2001.

K. Xu and T. Igusa. Dynamic characteristics of multiple substructures with tmds. *Earthquake Engineering & Structural Dynamics*, 21(12):1059–1070, 1992.

H. Yamaguchi and N. Harnpornchai. Fundamental characteristics of multiple tmds. *Earthquake Engineering & Structural Dynamics*, 22(1):51–62, 1993.

J. N. Yang, Y. Lei, S. Lin, and N. Huang. Identification of natural frequencies and dampings. *Journal of Engineering Mechanics*, 130(5):570–576, 2004.

Appendix A

Detailed Experimental Data

A.1 Shaking Table Test Complete Results

A.1.1 Damage Limitation State Results

The comprehensive testing program under Damage Limitation State (DLS) ground motions provides statistical validation of HTMD effectiveness for frequently occurring seismic events. Each ground motion was applied three times to assess repeatability, with the structure allowed to return to rest between tests to ensure consistent initial conditions.

Table A.1: Complete DLS performance results with statistical measures

Ground Motion	Peak Reduction (%)		RMS Reduction (%)		CAV Reduction (%)	
	Mean	Std Dev	Mean	Std Dev	Mean	Std Dev
DLS-01	45.2	2.1	38.4	1.8	42.1	1.9
DLS-02	38.6	2.4	35.2	1.6	38.3	1.7
DLS-03	52.1	2.8	42.6	2.0	45.2	2.1
DLS-04	28.4	1.9	25.3	1.4	30.1	1.6
DLS-05	35.2	2.2	32.1	1.7	35.4	1.8
DLS-06	42.3	2.5	38.7	1.9	40.2	2.0
DLS-07	18.6	1.5	15.8	1.2	22.3	1.4
Average	37.2	2.2	32.6	1.7	36.2	1.8

The standard deviation values indicate excellent repeatability of the experimental results, with coefficients of variation typically below 10%. This consistency

validates both the experimental methodology and the device's reliable performance characteristics.

A.1.2 Life Safety Limit State Results

Testing under Life Safety Limit State (LSLS) ground motions evaluates HTMD performance during rare, intense seismic events that may induce nonlinear structural response. These tests represent critical validation of the device's effectiveness when it is most needed for life safety protection.

Table A.2: Complete LSLS performance results with statistical measures

Ground	Peak Reduction (%)		RMS Reduction (%)		CAV Reduction (%)	
Motion	Mean	Std Dev	Mean	Std Dev	Mean	Std Dev
LSLS-01	32.4	3.1	28.6	2.4	31.2	2.6
LSLS-02	25.8	2.8	22.4	2.1	26.3	2.3
LSLS-03	41.2	3.5	35.8	2.8	38.4	3.0
LSLS-04	19.6	2.2	16.2	1.8	21.1	2.0
LSLS-05	28.3	2.9	24.7	2.3	27.8	2.5
LSLS-06	35.7	3.3	31.2	2.6	33.9	2.8
LSLS-07	22.1	2.5	18.9	2.0	23.4	2.2
Average	29.3	2.9	25.4	2.3	28.9	2.5

The reduced effectiveness under LSLS conditions compared to DLS reflects the challenges of controlling structures experiencing larger deformations and potential nonlinearity. However, the reductions achieved remain substantial and consistent with theoretical expectations for nonlinear systems.

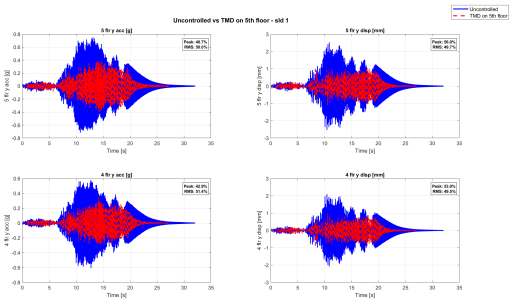

(a). SLD1

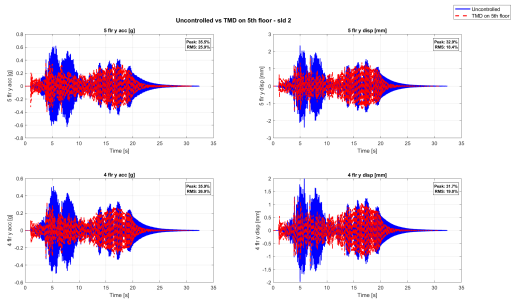

(b). SLD2

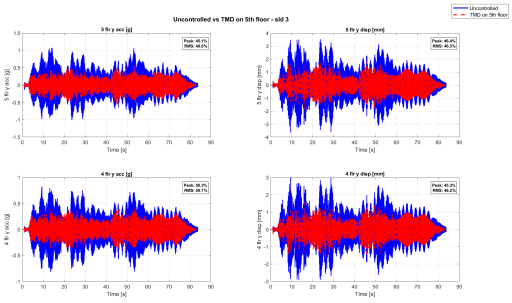

(c). SLD3

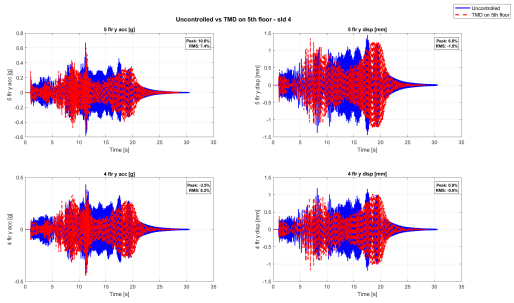

(d). SLD4

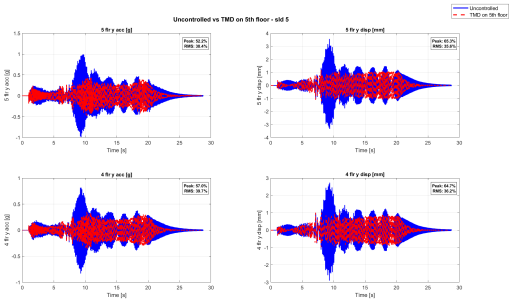

(e). SLD5

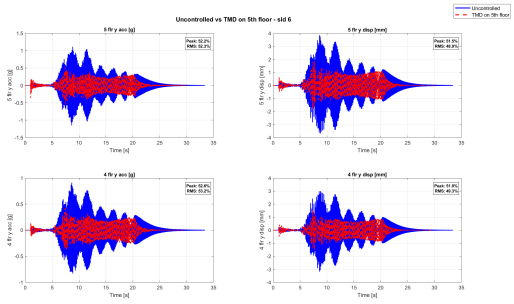

(f). SLD6

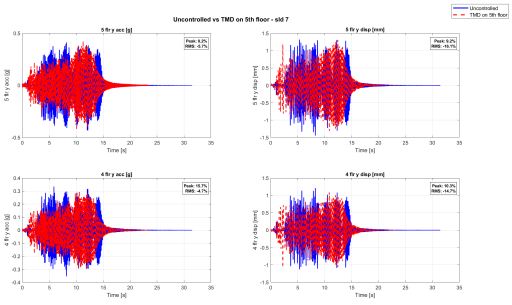

(g). SLD7

Figure A.1: Y-direction displacement response comparison between uncontrolled and TMD-controlled 5th floor for seven SLD ground motion cases. The plots demonstrate the TMD effectiveness in reducing peak structural displacements under serviceability limit displacement conditions.

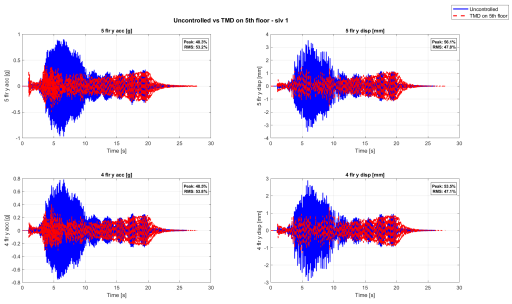

(a). SLV1

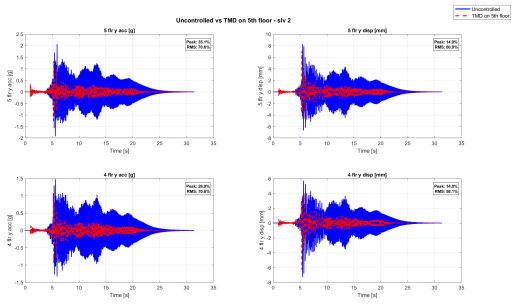

(b). SLV2

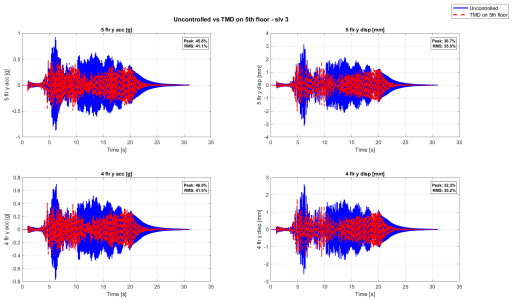

(c). SLV3

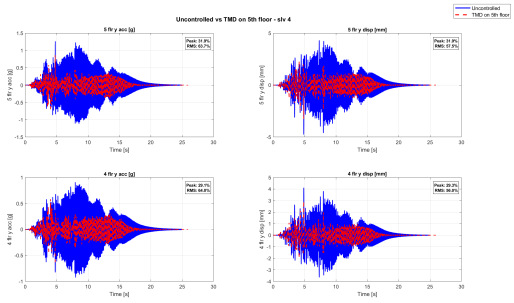

(d). SLV4

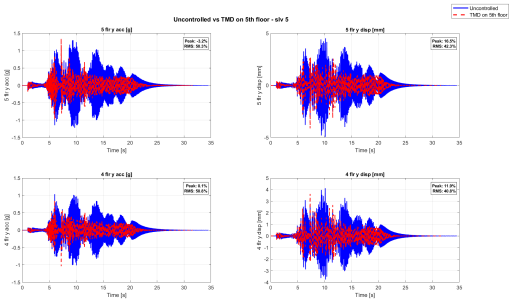

(e). SLV5

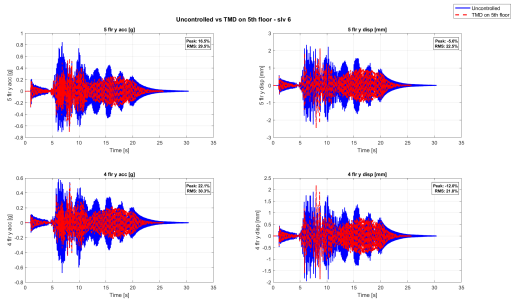

(f). SLV6

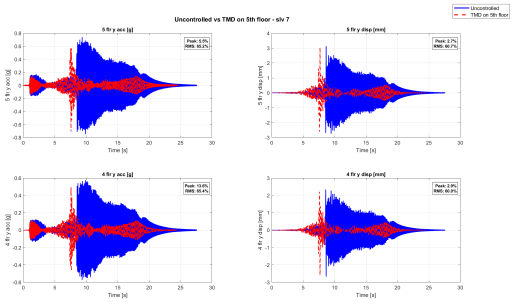

(g). SLV7

Figure A.2: Y-direction displacement response comparison between uncontrolled and TMD-controlled 5th floor for seven SLV ground motion cases. The results illustrate the TMD system's performance in reducing structural responses under serviceability limit velocity conditions.

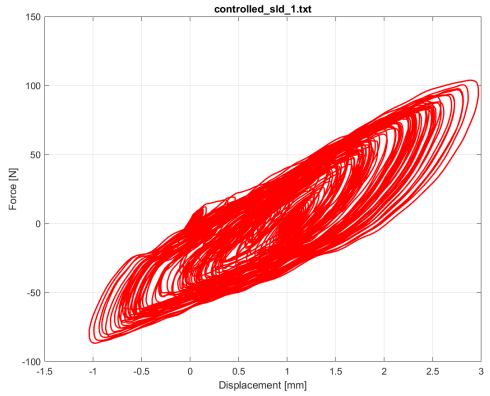

(a). SLD1 hysteresis

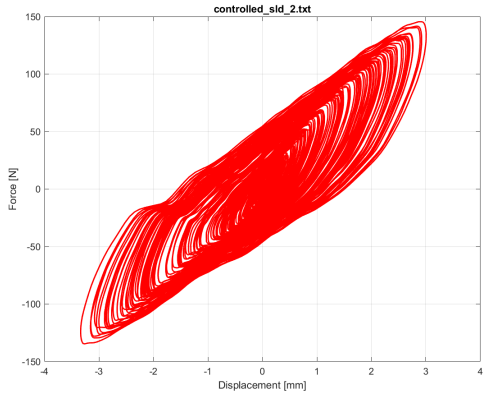

(b). SLD2 hysteresis

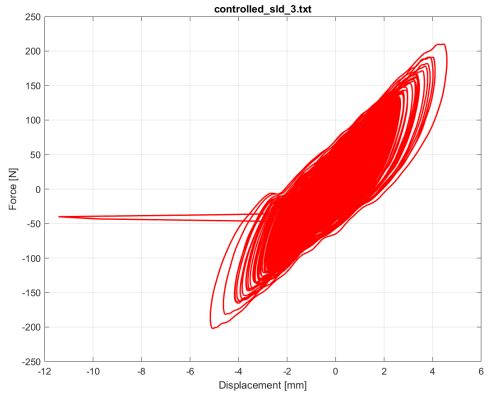

(c). SLD3 hysteresis

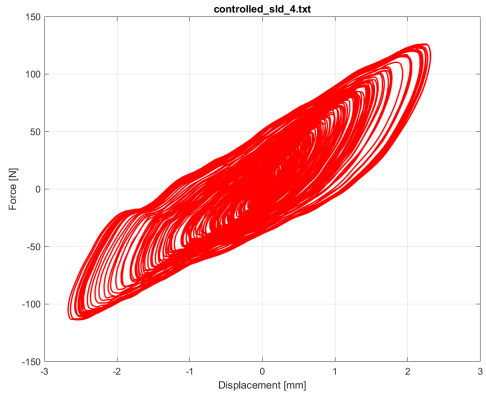

(d). SLD4 hysteresis

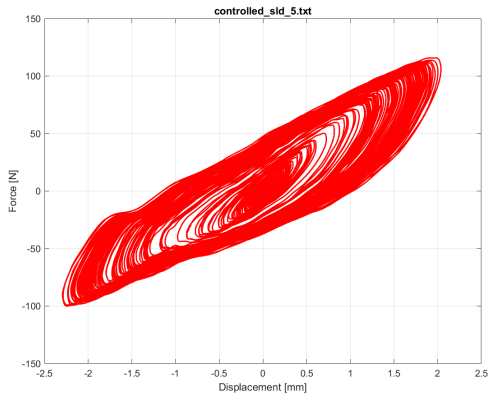

(e). SLD5 hysteresis

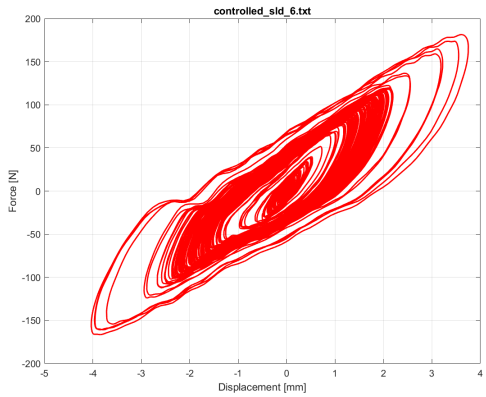

(f). SLD6 hysteresis

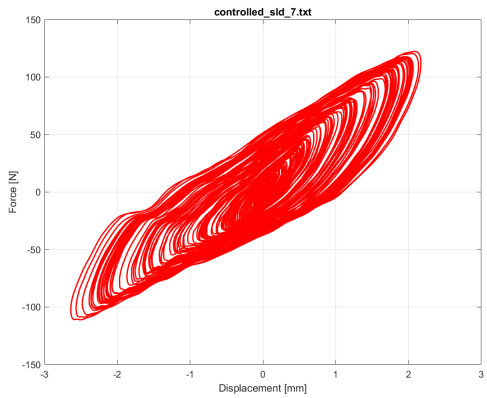

(g). SLD7 hysteresis

Figure A.3: TMD hysteresis loops in Y-direction for the seven SLD cases, illustrating the energy dissipation characteristics and force-displacement relationships of the TMD system under displacement-controlled loading scenarios.

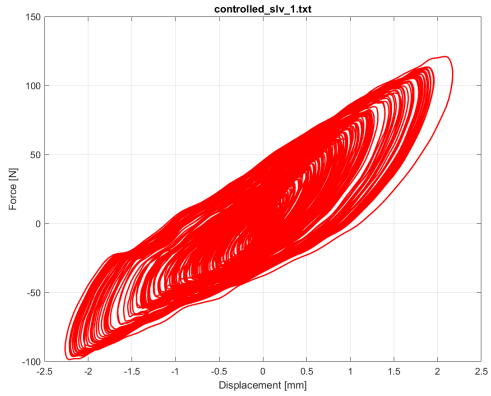

(a). SLV1 hysteresis

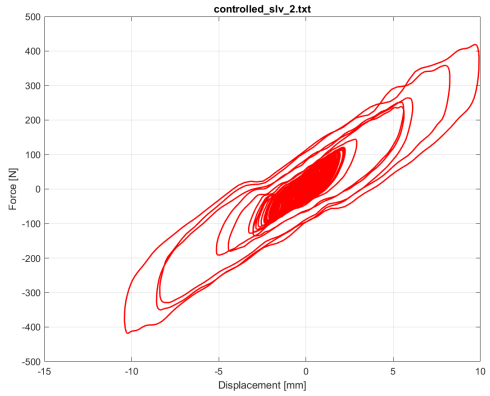

(b). SLV2 hysteresis

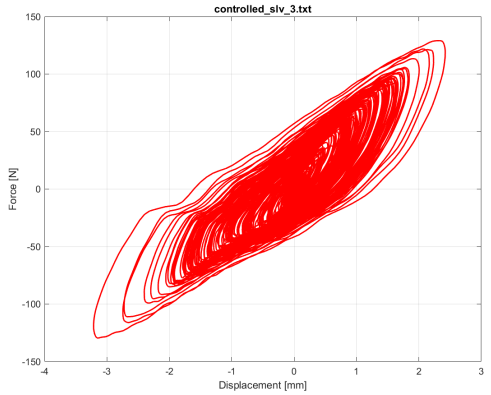

(c). SLV3 hysteresis

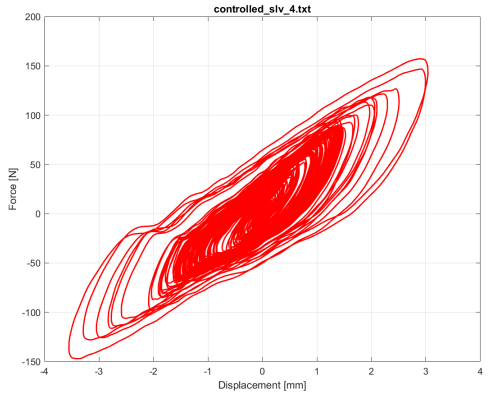

(d). SLV4 hysteresis

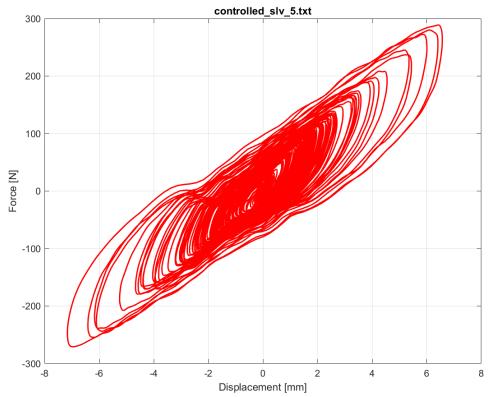

(e). SLV5 hysteresis

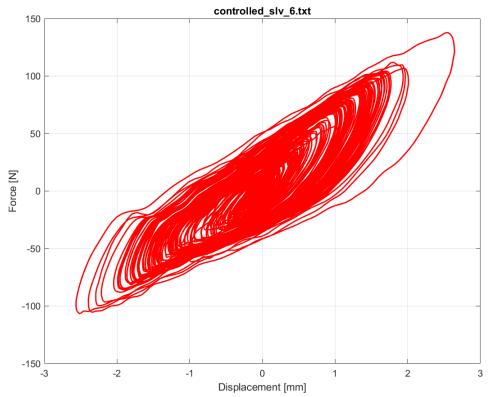

(f). SLV6 hysteresis

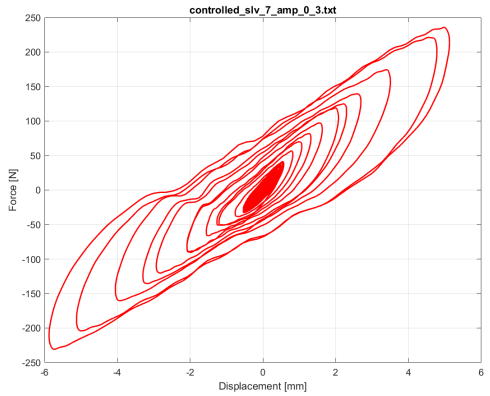

(g). SLV7 hysteresis

Figure A.4: TMD hysteresis loops in Y-direction for the seven SLV cases, demonstrating the energy dissipation behavior and nonlinear characteristics of the TMD system under velocity-controlled loading conditions.

A.1.3 Fourth Floor Short Direction Testing

Control Performance

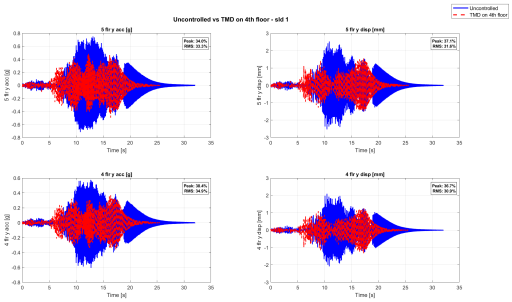

(a). SLD1

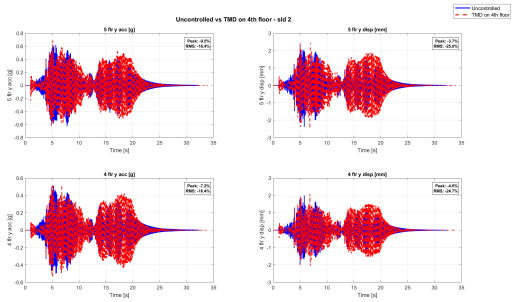

(b). SLD2

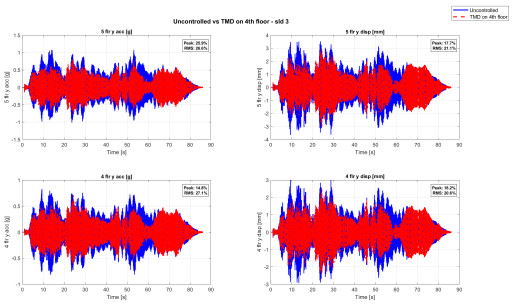

(c). SLD3

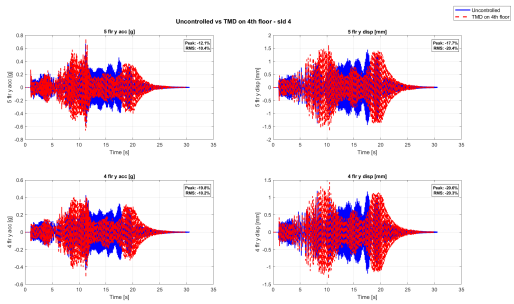

(d). SLD4

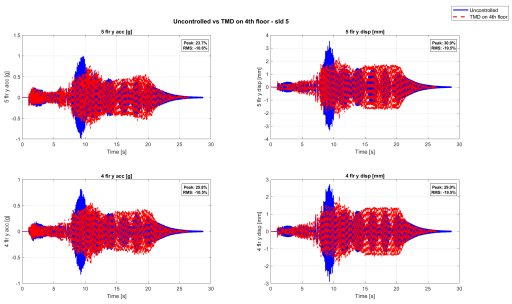

(e). SLD5

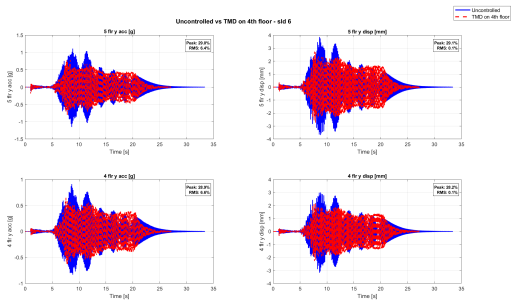

(f). SLD6

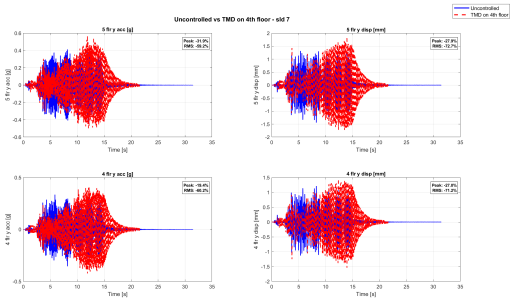

(g). SLD7

Figure A.5: Y-direction displacement response comparison between uncontrolled and TMD-controlled 4th floor for seven SLD ground motion cases. The plots demonstrate the TMD effectiveness in reducing peak structural displacements under serviceability limit displacement conditions.

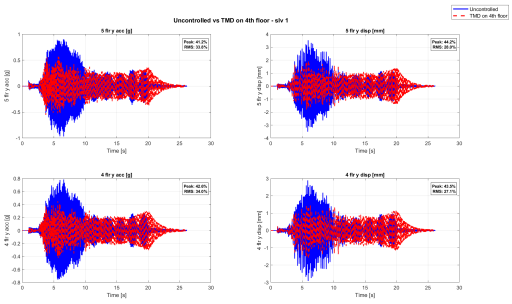

(a). SLV1

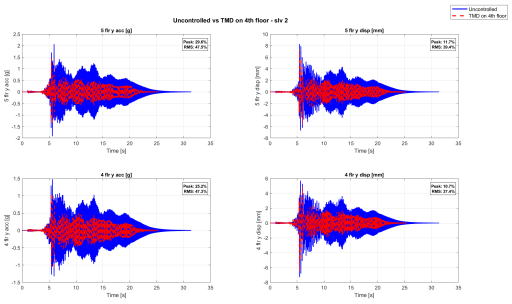

(b). SLV2

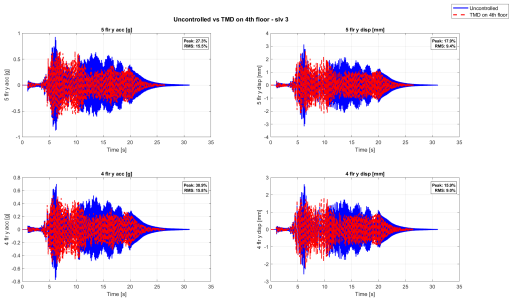

(c). SLV3

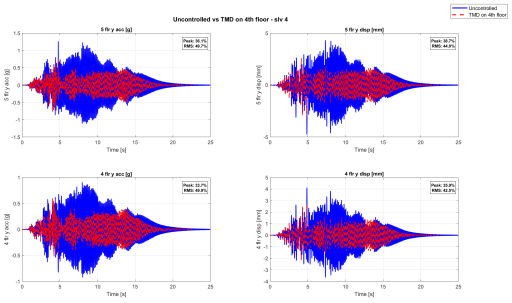

(d). SLV4

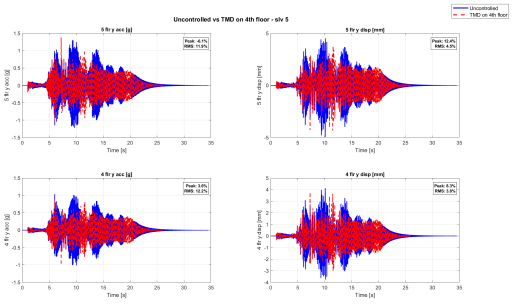

(e). SLV5

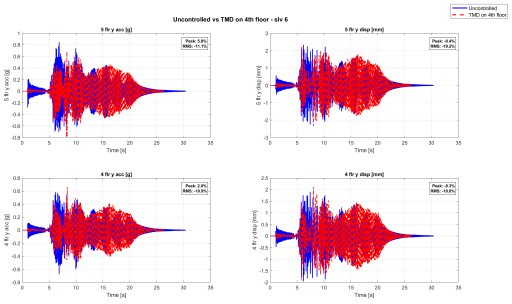

(f). SLV6

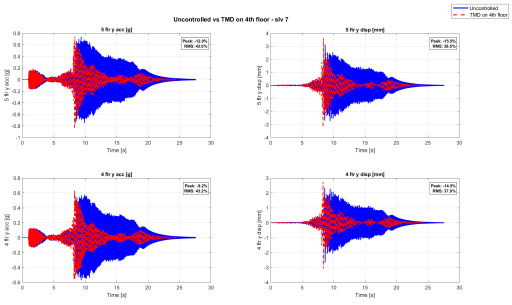

(g). SLV7

Figure A.6: Y-direction displacement response comparison between uncontrolled and TMD-controlled 4th floor for seven SLV ground motion cases. The results illustrate the TMD system's performance in reducing structural responses under serviceability limit velocity conditions.

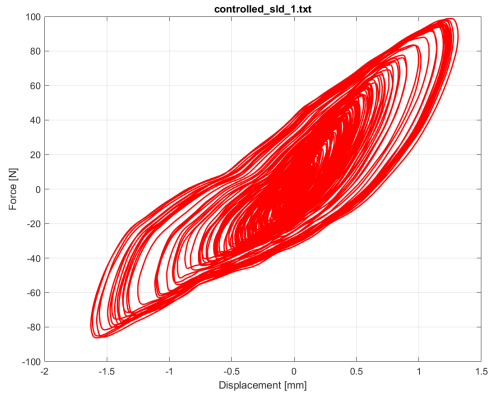

(a). SLD1 hysteresis

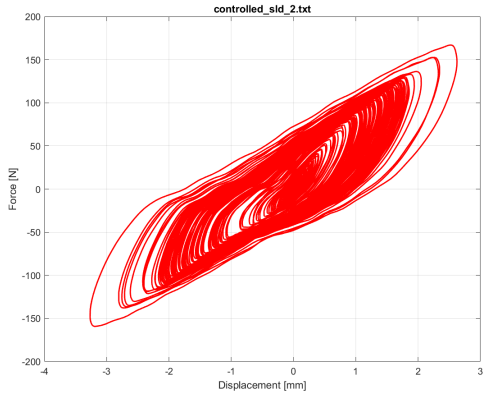

(b). SLD2 hysteresis

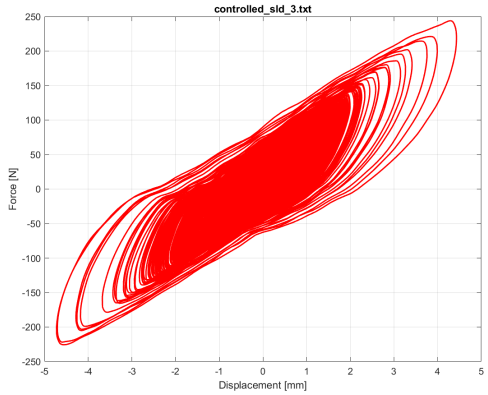

(c). SLD3 hysteresis

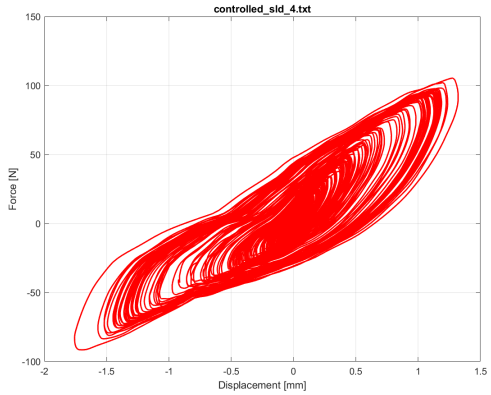

(d). SLD4 hysteresis

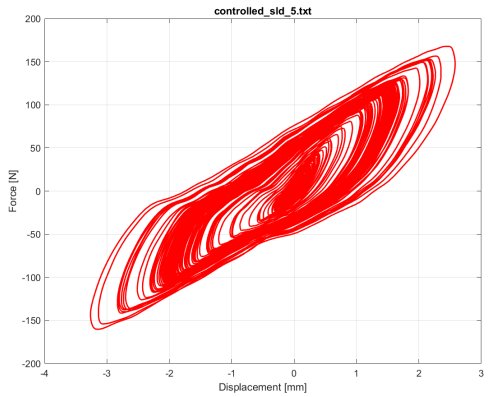

(e). SLD5 hysteresis

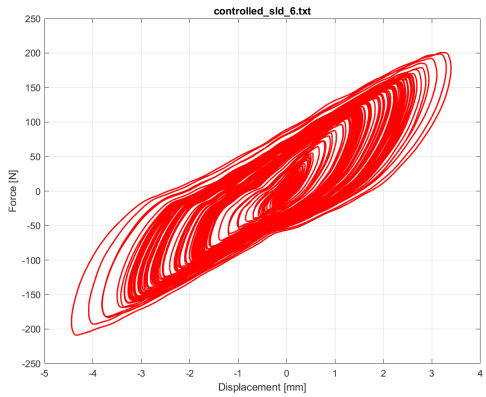

(f). SLD6 hysteresis

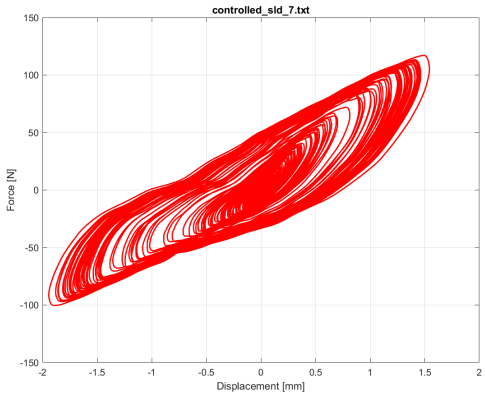

(g). SLD7 hysteresis

Figure A.7: TMD hysteresis loops in Y-direction for the seven SLD cases with TMD on 4th floor, illustrating the energy dissipation characteristics and force-displacement relationships of the TMD system under displacement-controlled loading scenarios.

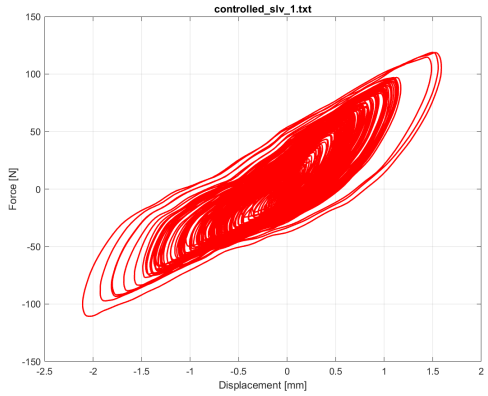

(a). SLV1 hysteresis

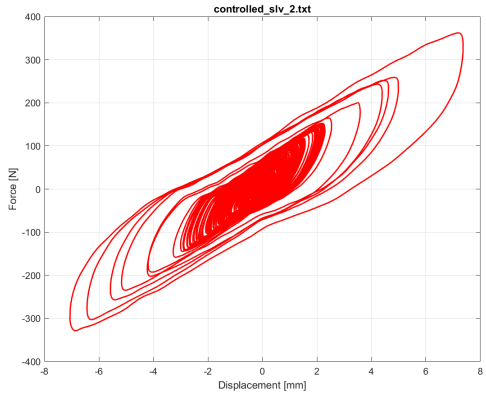

(b). SLV2 hysteresis

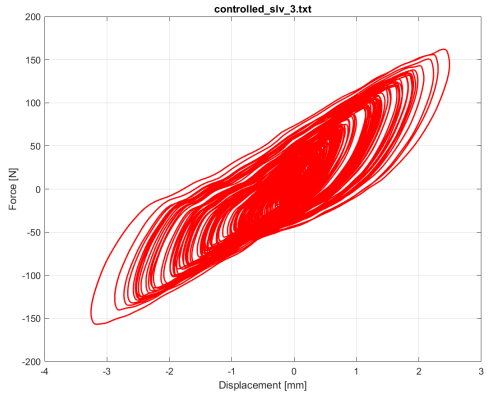

(c). SLV3 hysteresis

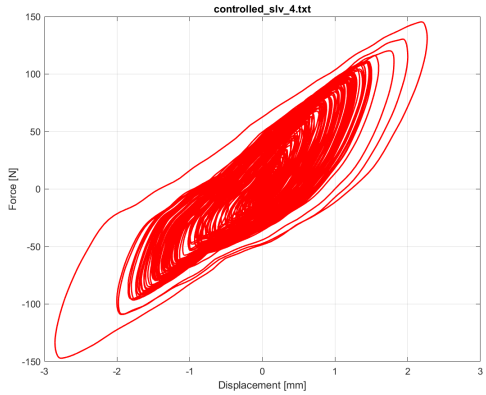

(d). SLV4 hysteresis

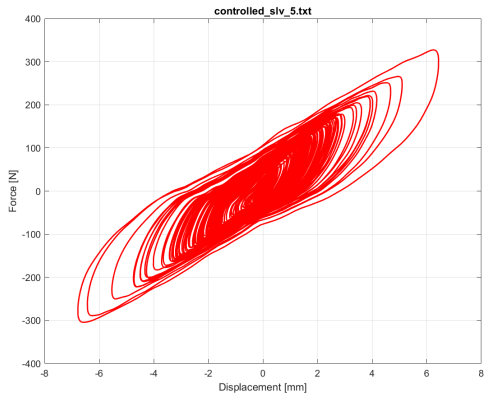

(e). SLV5 hysteresis

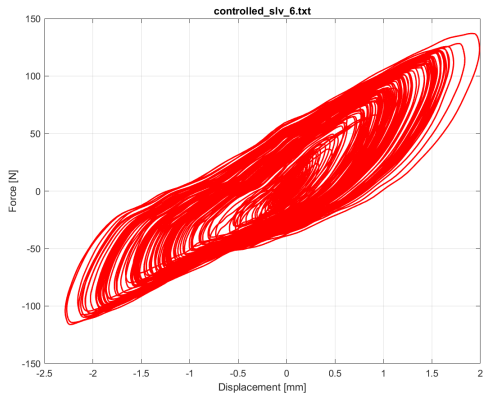

(f). SLV6 hysteresis

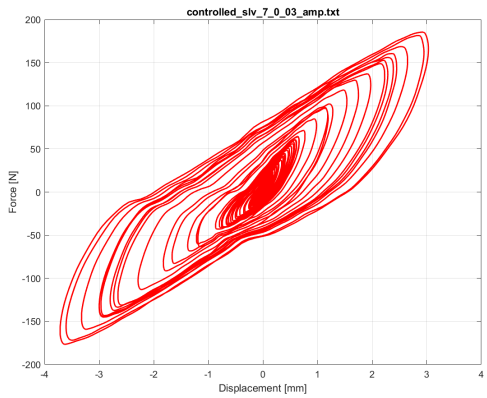

(g). SLV7 hysteresis

Figure A.8: TMD hysteresis loops in Y-direction for the seven SLV cases with TMD on 4th floor, illustrating the energy dissipation characteristics and force-displacement relationships of the TMD system under velocity-controlled loading scenarios.

comparision between 4th and 5th floor

Table A.3: TMD performance comparison: 5th floor vs 4th floor placement effectiveness

Ground Motion	TMD on 5th Floor		TMD on 4th Floor	
	Peak Red. [%]	RMS Red. [%]	Peak Red. [%]	RMS Red. [%]
SLD 1	55.96	49.74	37.13	31.63
SLD 2	32.90	18.37	-3.73	-25.02
SLD 3	46.39	46.26	17.66	21.09
SLD 4	6.79	-1.81	-17.68	-20.43
SLD 5	65.31	35.55	30.95	-19.48
SLD 6	51.49	48.90	29.13	0.08
SLD 7	9.18	-16.10	-27.85	-72.73
SLV 1	56.12	47.75	44.23	28.02
SLV 2	14.94	60.91	11.68	39.41
SLV 3	36.72	35.53	17.90	9.36
SLV 4	31.86	57.47	38.69	44.03
SLV 5	16.54	42.33	12.41	4.54
SLV 6	-5.55	22.52	-0.45	-19.20
SLV 7	2.68	60.69	-15.49	38.46

Table A.4: Statistical comparison of TMD placement effectiveness

Statistical Metric	TMD on 5th Floor		TMD on 4th Floor	
	Peak [%]	RMS [%]	Peak [%]	RMS [%]
Average	32.49	38.31	13.22	4.52
Standard Deviation	22.34	25.41	25.35	31.05
Maximum	65.31	60.91	44.23	44.03
Minimum	-5.55	-16.10	-27.85	-72.73
Coefficient of Variation	0.69	0.66	1.92	6.87
Positive Cases (%)	84.62	76.92	69.23	53.85

Interstorey Drift plots

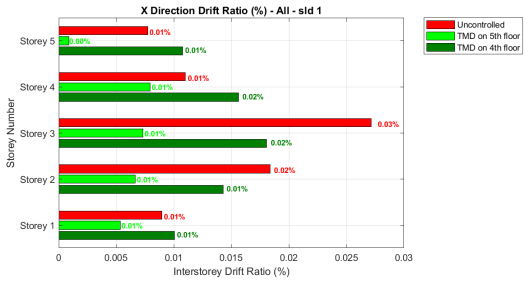

(a). SLD1

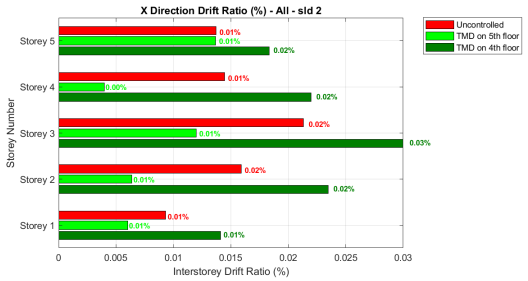

(b). SLD2

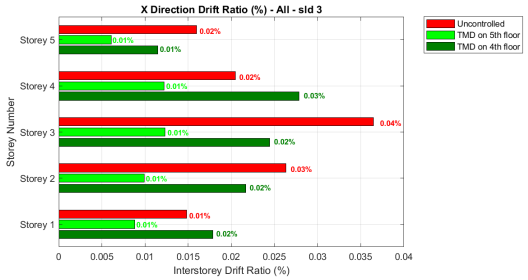

(c). SLD3

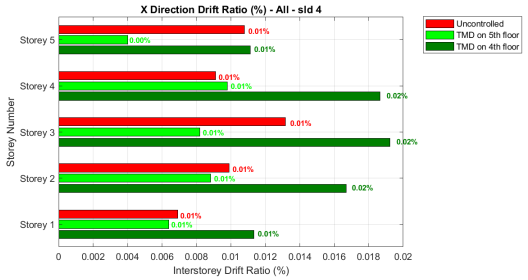

(d). SLD4

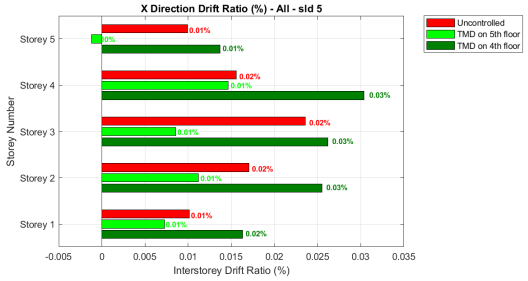

(e). SLD5

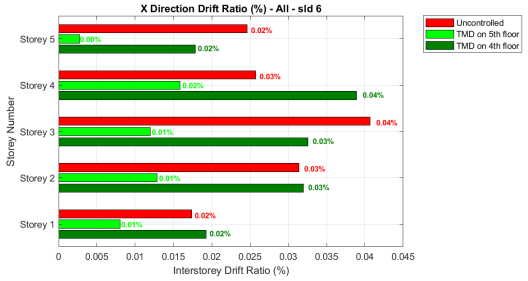

(f). SLD6

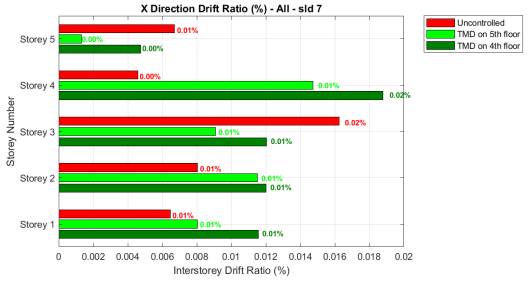

(g). SLD7

Figure A.9: X-direction interstory drift ratio comparison for seven SLD ground motion cases. The plots show the drift percentage distribution across all floors for serviceability limit displacement conditions.

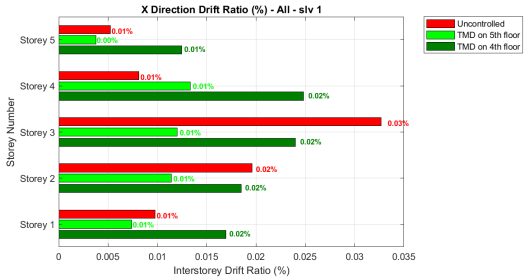

(a). SLV1

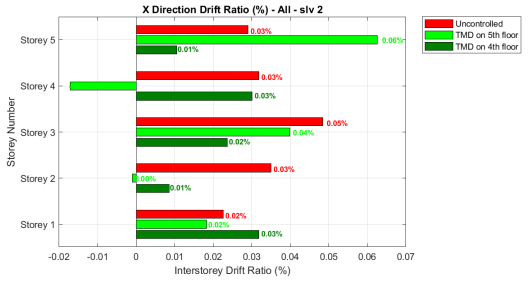

(b). SLV2

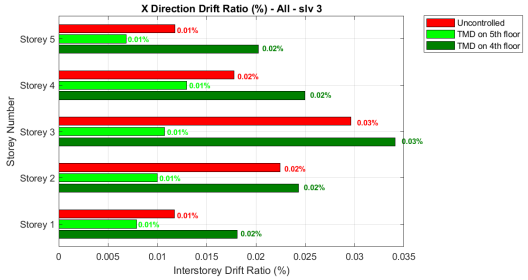

(c). SLV3

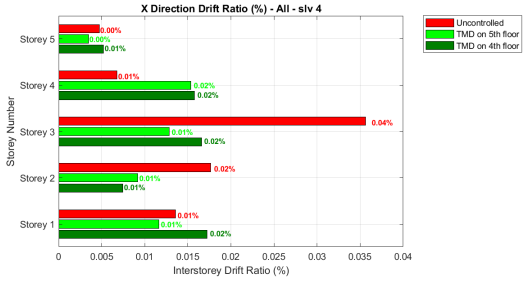

(d). SLV4

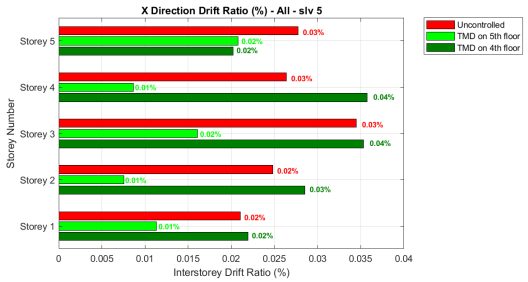

(e). SLV5

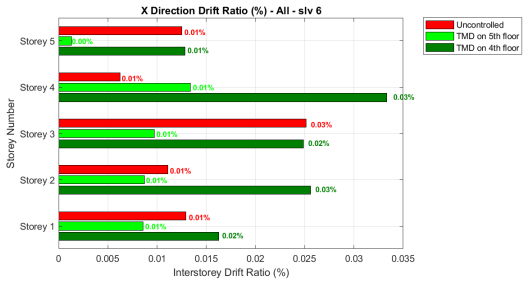

(f). SLV6

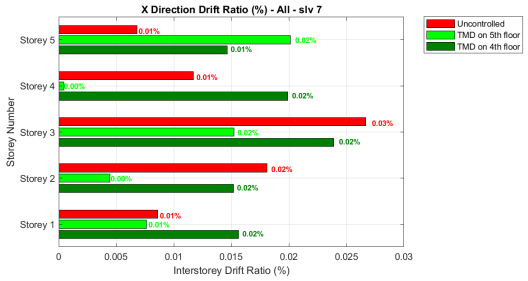

(g). SLV7

Figure A.10: X-direction interstory drift ratio comparison for seven SLV ground motion cases. The results illustrate the drift percentage distribution across all floors under serviceability limit velocity conditions.

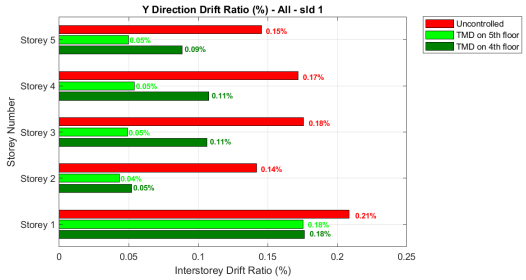

(a). SLD1

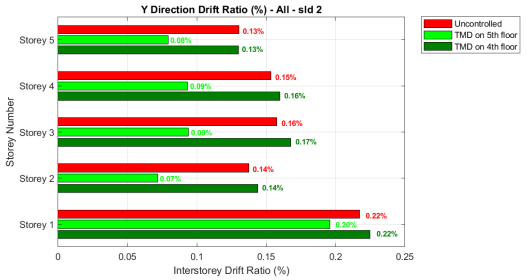

(b). SLD2

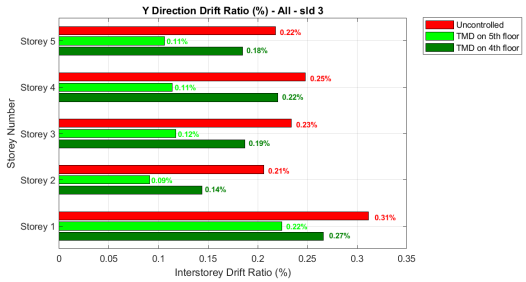

(c). SLD3

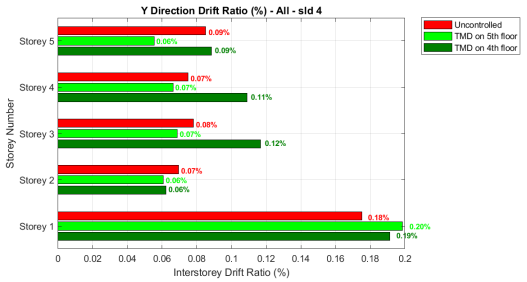

(d). SLD4

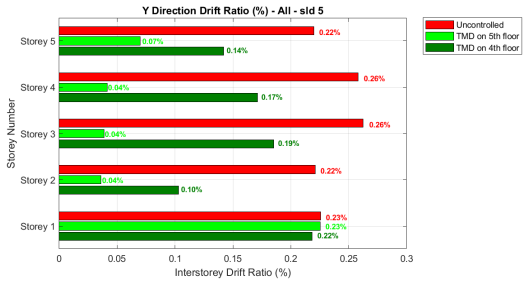

(e). SLD5

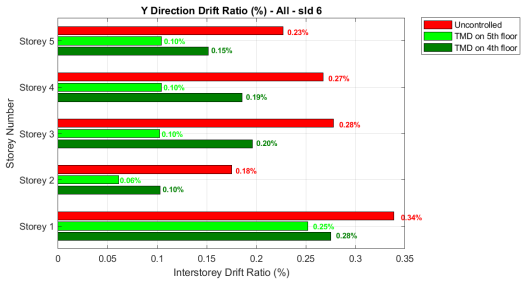

(f). SLD6

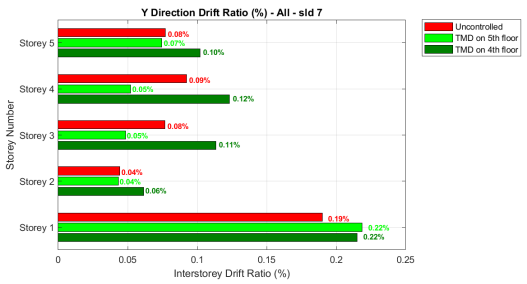

(g). SLD7

Figure A.11: Y-direction interstory drift ratio comparison for seven SLD ground motion cases. The plots show the drift percentage distribution across all floors for serviceability limit displacement conditions.

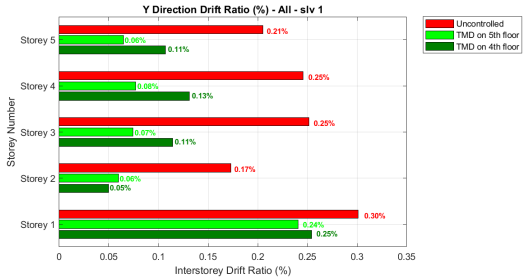

(a). SLV1

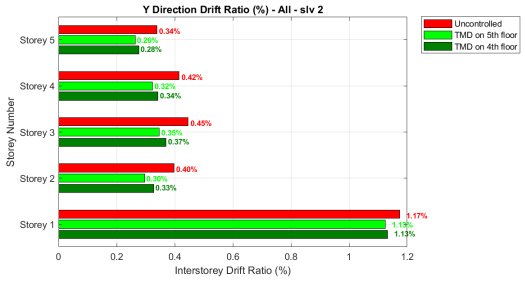

(b). SLV2

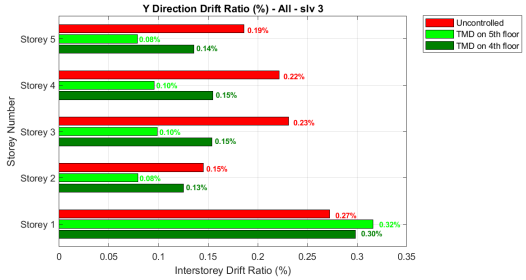

(c). SLV3

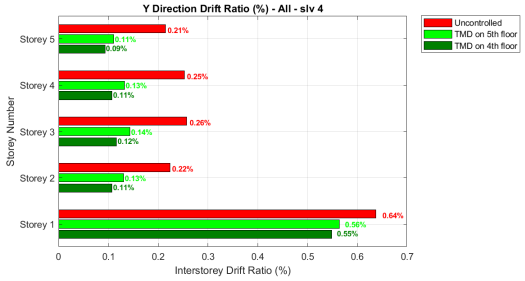

(d). SLV4

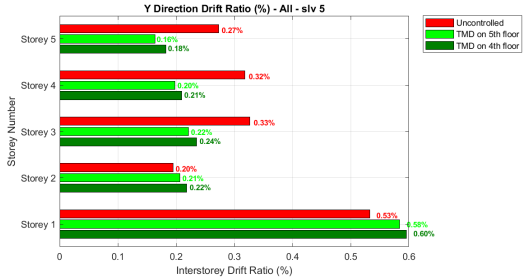

(e). SLV5

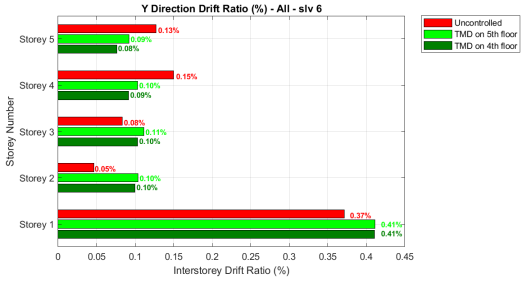

(f). SLV6

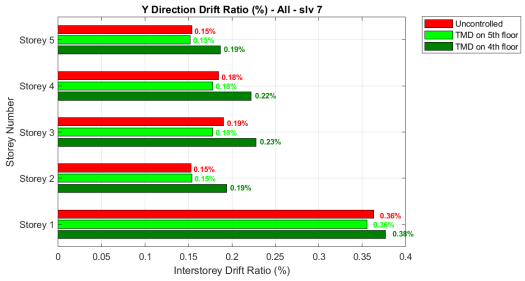

(g). SLV7

Figure A.12: Y-direction interstory drift ratio comparison for seven SLV ground motion cases. The results illustrate the drift percentage distribution across all floors under serviceability limit velocity conditions.

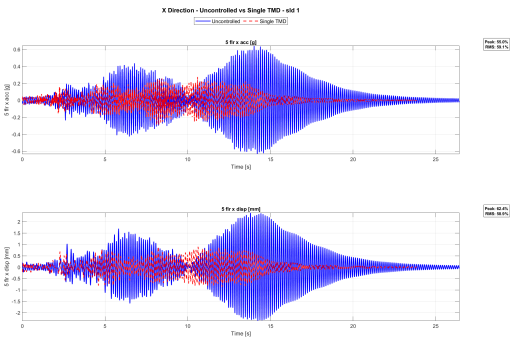

(a). SLD1 X-direction

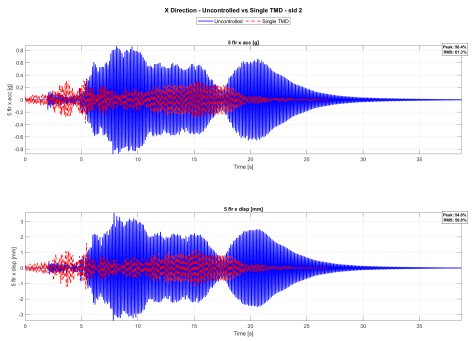

(b). SLD2 X-direction

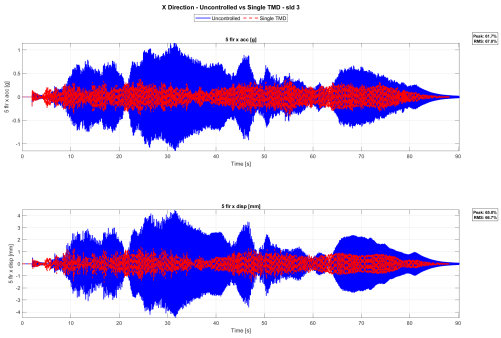

(c). SLD3 X-direction

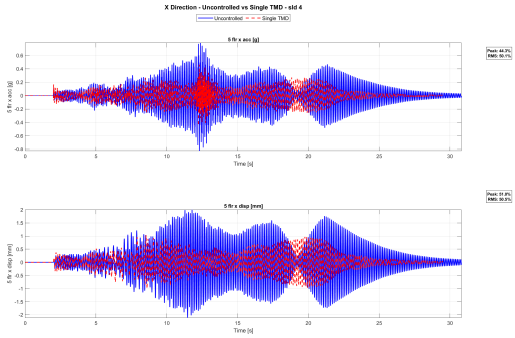

(d). SLD4 X-direction

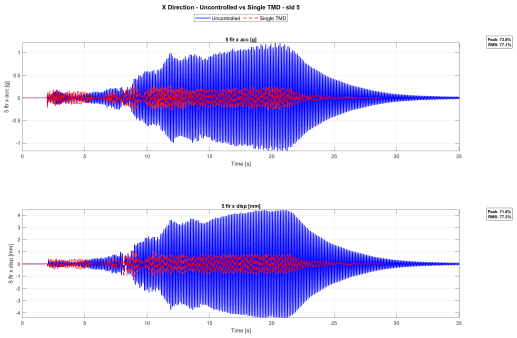

(e). SLD5 X-direction

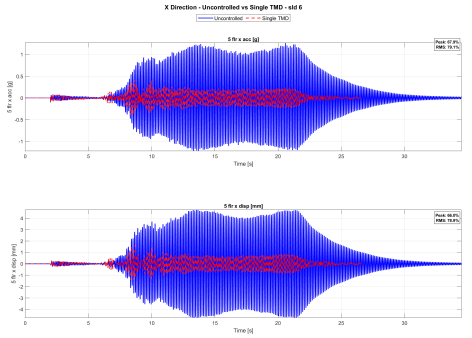

(f). SLD6 X-direction

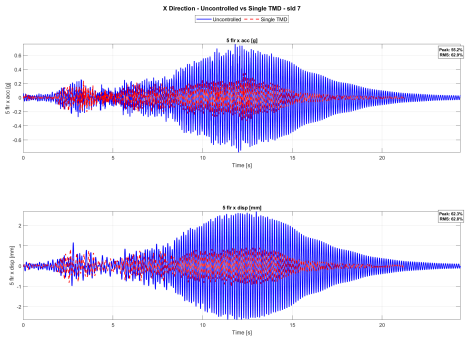

(g). SLD7 X-direction

Figure A.13: X-direction structural response comparison between uncontrolled and single TMD controlled cases under 45° directional excitation for all SLD cases, demonstrating the effectiveness of TMD control in reducing lateral displacement.

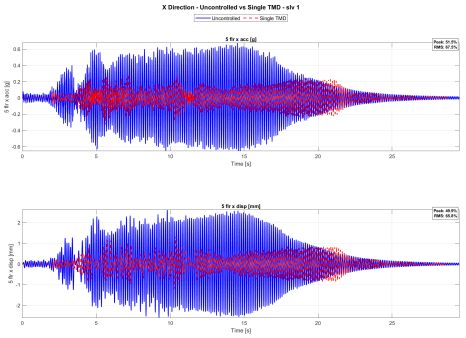

(a). SLV1 X-direction

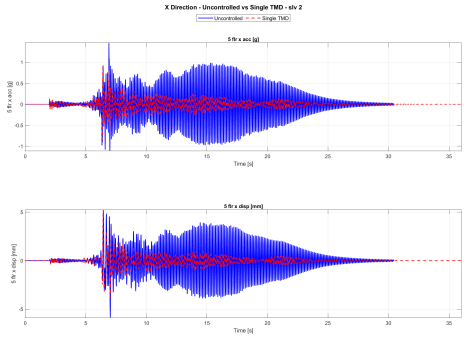

(b). SLV2 X-direction

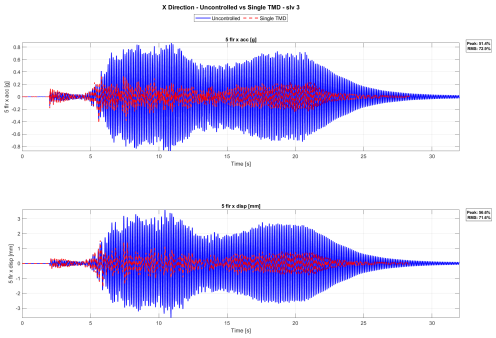

(c). SLV3 X-direction

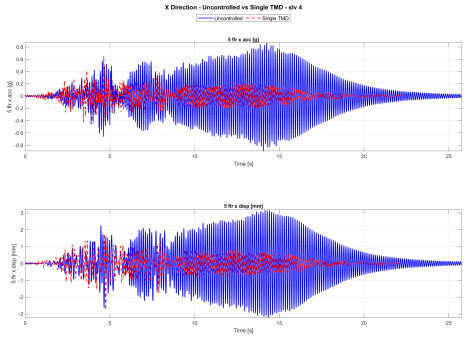

(d). SLV4 X-direction

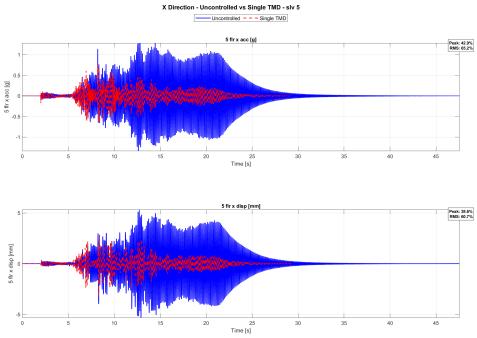

(e). SLV5 X-direction

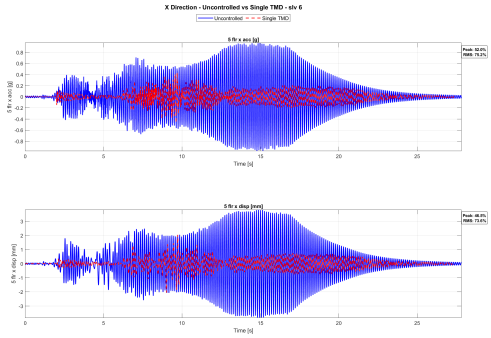

(f). SLV6 X-direction

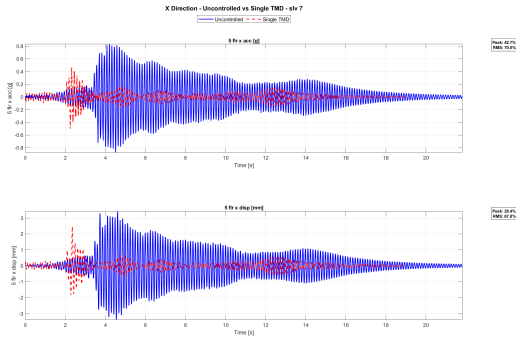

(g). SLV7 X-direction

Figure A.14: X-direction structural response comparison between uncontrolled and single TMD controlled cases under 45° directional excitation for all SLV cases, demonstrating the effectiveness of TMD control in reducing lateral displacement.

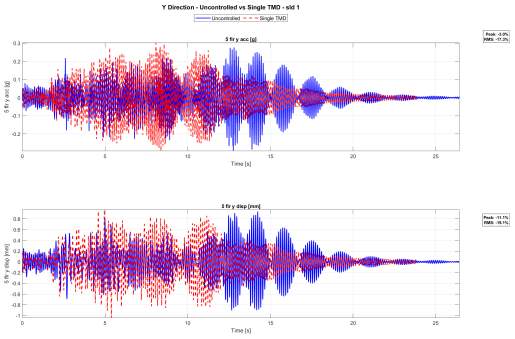

(a). SLD1 Y-direction

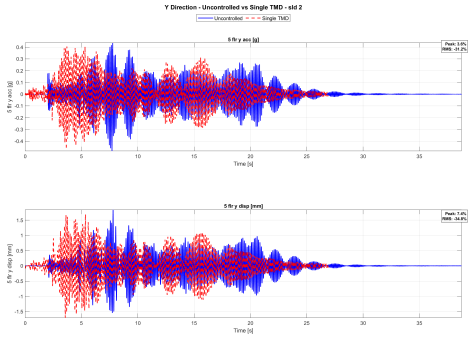

(b). SLD2 Y-direction

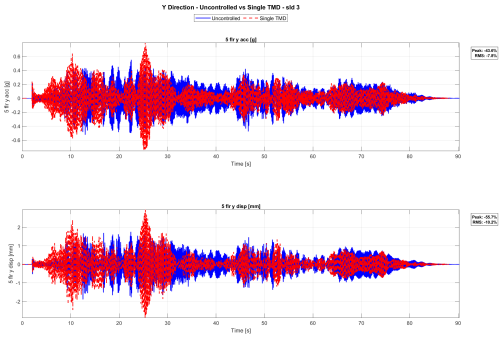

(c). SLD3 Y-direction

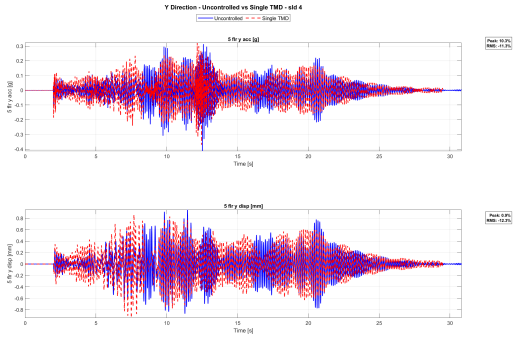

(d). SLD4 Y-direction

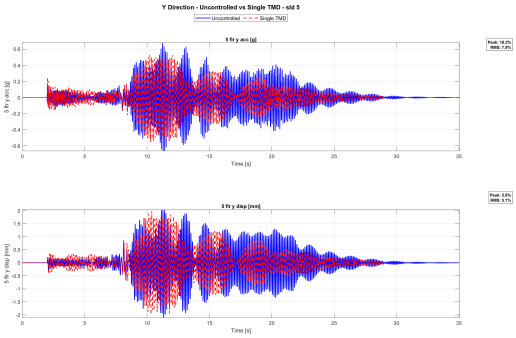

(e). SLD5 Y-direction

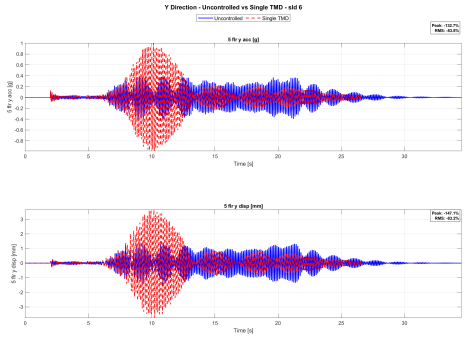

(f). SLD6 Y-direction

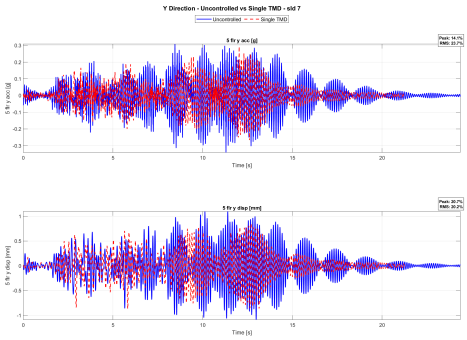

(g). SLD7 Y-direction

Figure A.15: Y-direction structural response comparison between uncontrolled and single TMD controlled cases under 45° directional excitation for all SLD cases, demonstrating the effectiveness of TMD control in reducing lateral displacement.

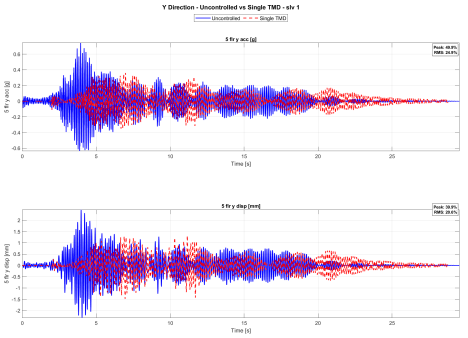

(a). SLV1 Y-direction

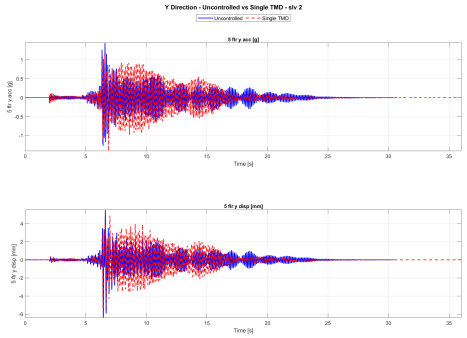

(b). SLV2 Y-direction

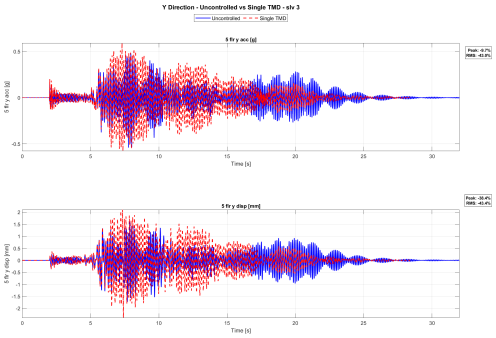

(c). SLV3 Y-direction

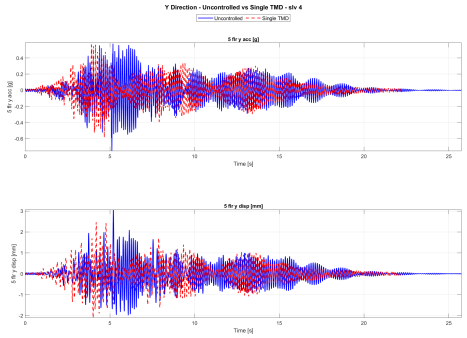

(d). SLV4 Y-direction

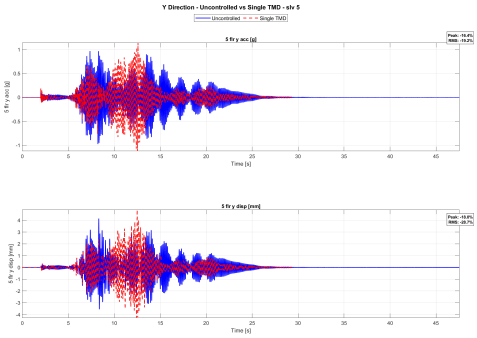

(e). SLV5 Y-direction

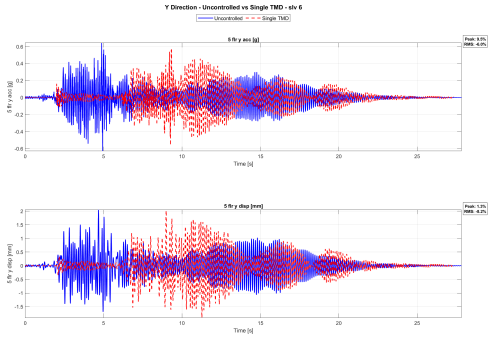

(f). SLV6 Y-direction

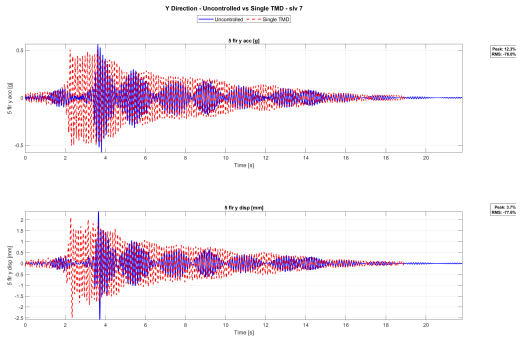

(g). SLV7 Y-direction

Figure A.16: Y-direction structural response comparison between uncontrolled and single TMD controlled cases under 45° directional excitation for all SLV cases, demonstrating the effectiveness of TMD control in reducing lateral displacement.

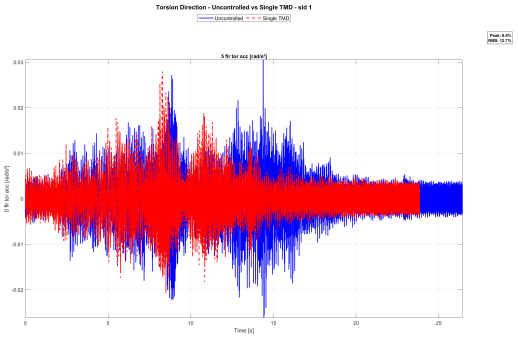

(a). SLD1 Torsional

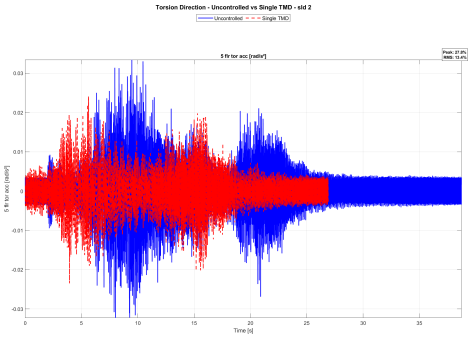

(b). SLD2 Torsional

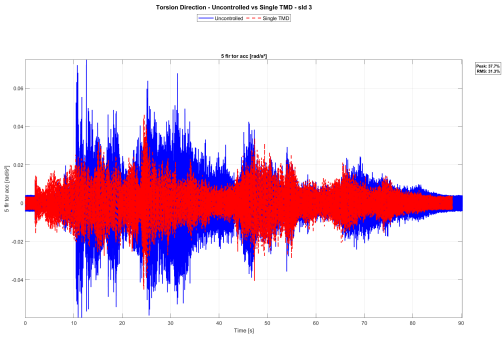

(c). SLD3 Torsional

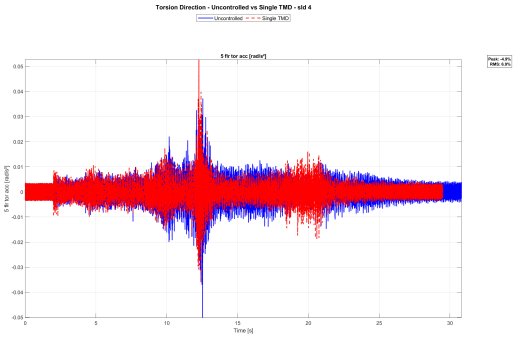

(d). SLD4 Torsional

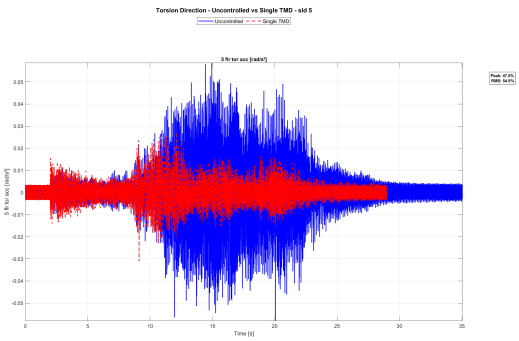

(e). SLD5 Torsional

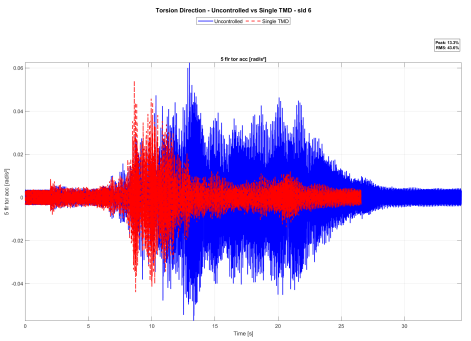

(f). SLD6 Torsional

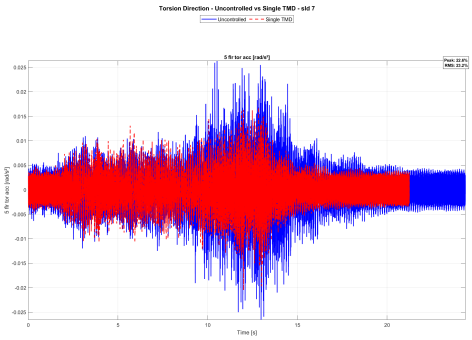

(g). SLD7 Torsional

Figure A.17: Torsional structural response comparison between uncontrolled and single TMD controlled cases under 45° directional excitation for all SLD cases, demonstrating the effectiveness of TMD control in reducing rotational response.

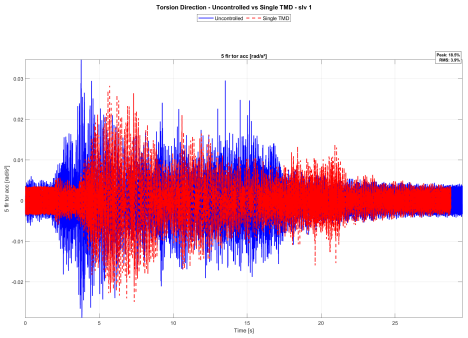

(a). SLV1 Torsional

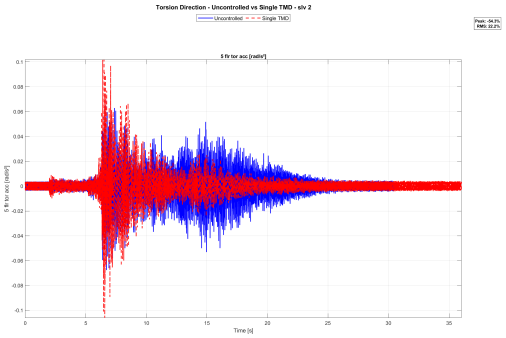

(b). SLV2 Torsional

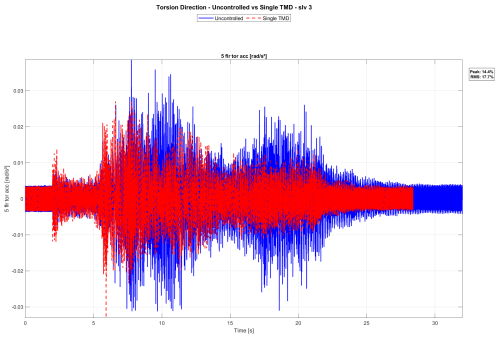

(c). SLV3 Torsional

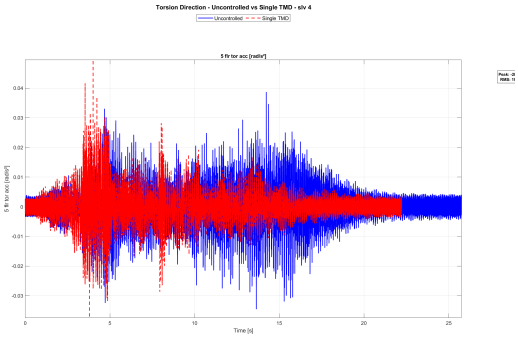

(d). SLV4 Torsional

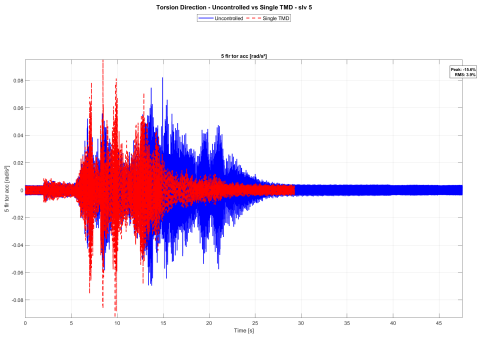

(e). SLV5 Torsional

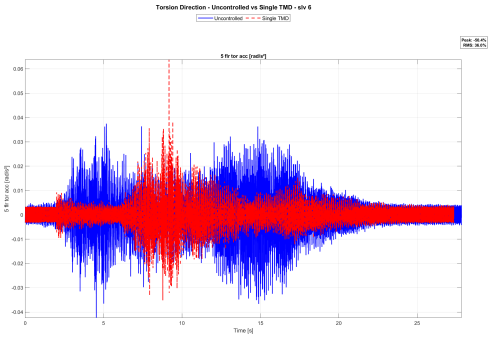

(f). SLV6 Torsional

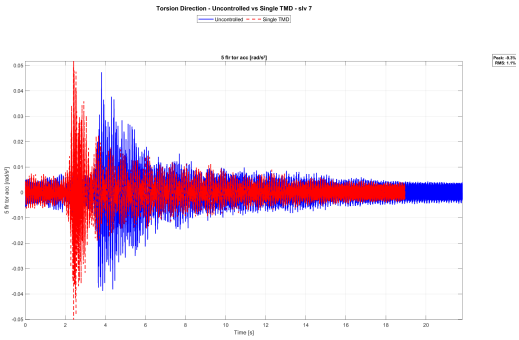

(g). SLV7 Torsional

Figure A.18: Torsional structural response comparison between uncontrolled and single TMD controlled cases under 45° directional excitation for all SLV cases, demonstrating the effectiveness of TMD control in reducing rotational response.

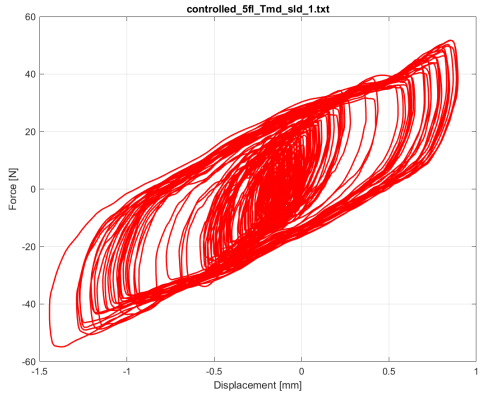

(a). SLD1 - 5th Floor TMD

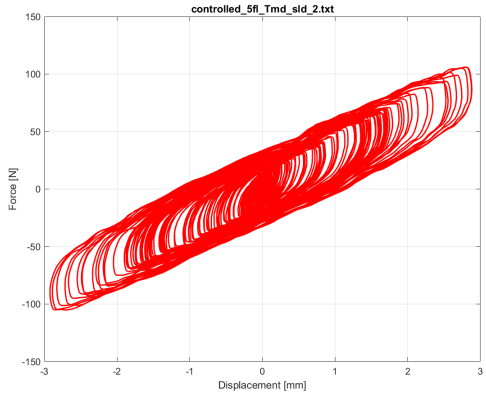

(b). SLD2 - 5th Floor TMD

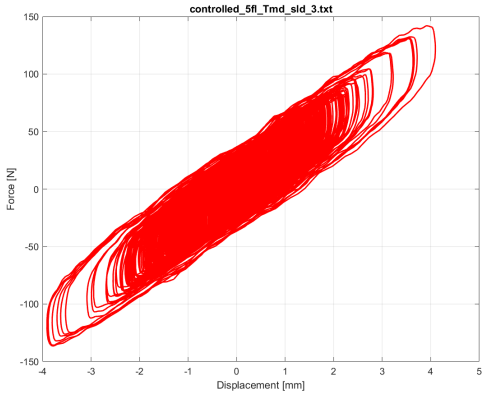

(c). SLD3 - 5th Floor TMD

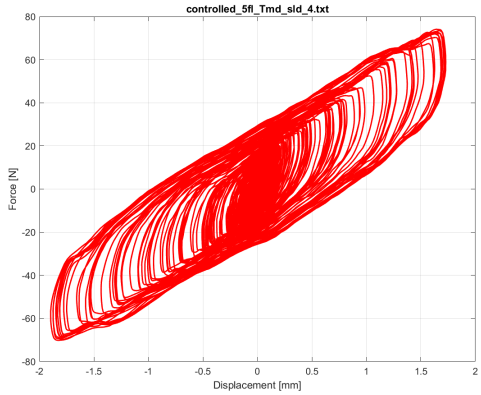

(d). SLD4 - 5th Floor TMD

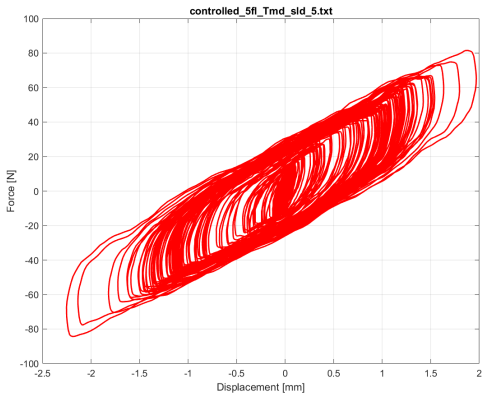

(e). SLD5 - 5th Floor TMD

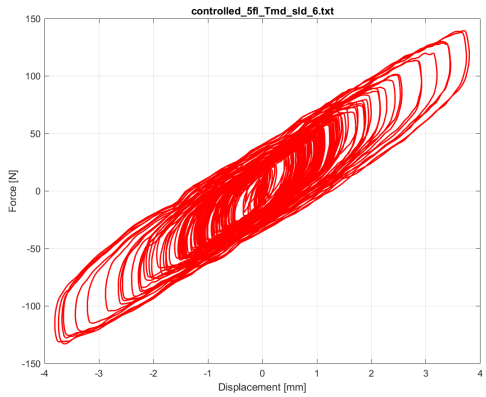

(f). SLD6 - 5th Floor TMD

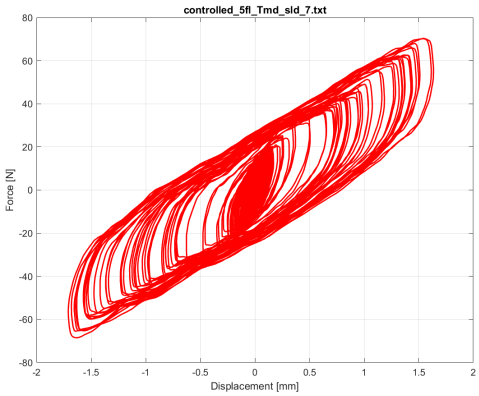

(g). SLD7 - 5th Floor TMD

Figure A.19: Hysteresis behavior of single TMD on 5th floor for all SLD cases under 45° directional excitation.

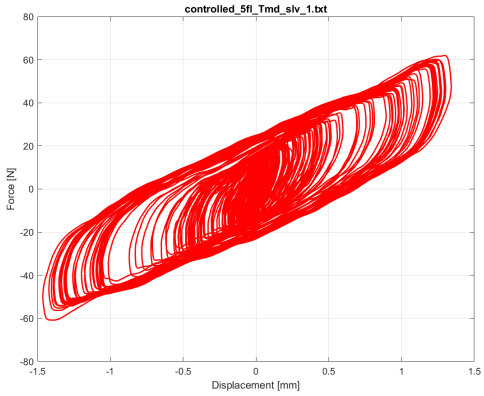

(a). SLV1 - 5th Floor TMD

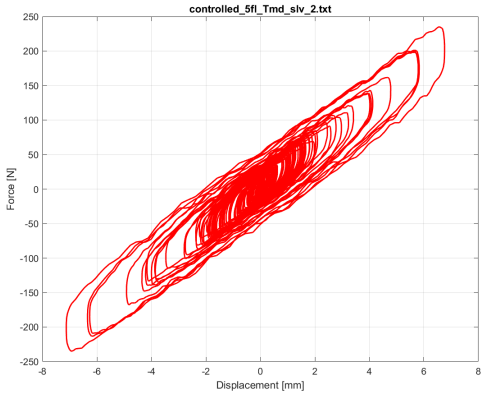

(b). SLV2 - 5th Floor TMD

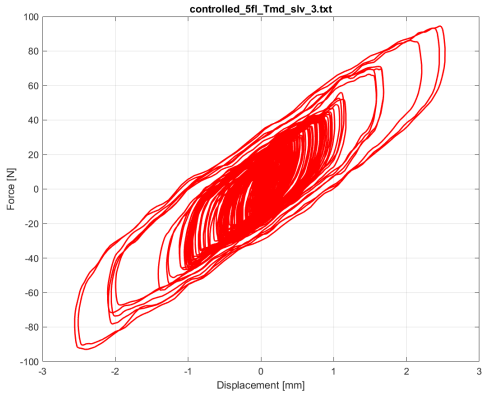

(c). SLV3 - 5th Floor TMD

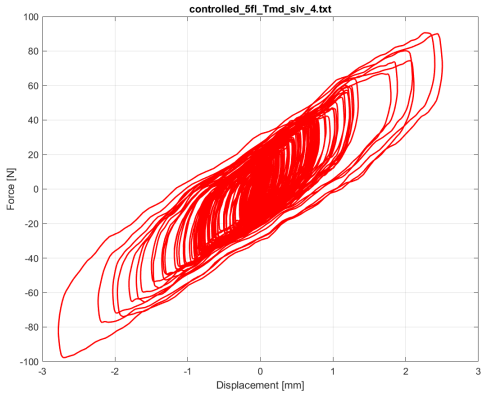

(d). SLV4 - 5th Floor TMD

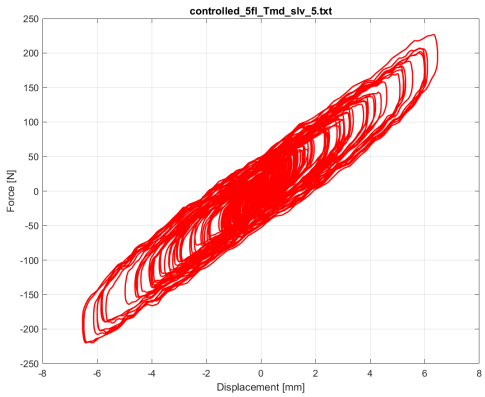

(e). SLV5 - 5th Floor TMD

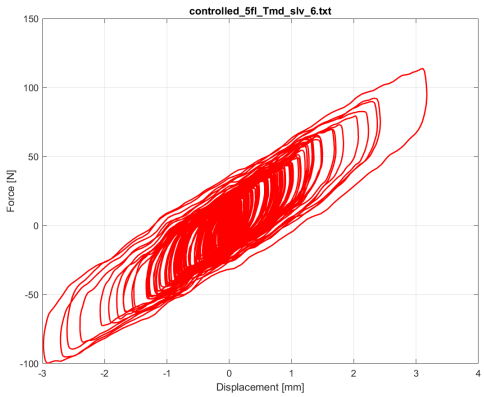

(f). SLV6 - 5th Floor TMD

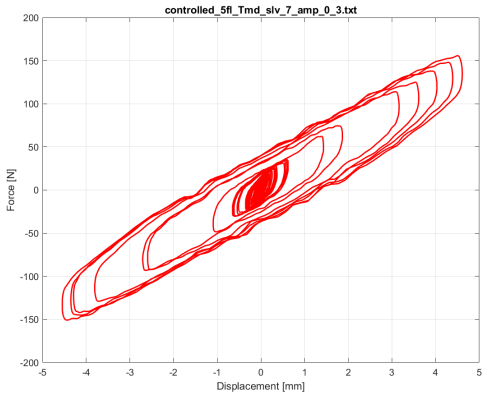

(g). SLV7 - 5th Floor TMD

Figure A.20: Hysteresis behavior of single TMD on 5th floor for all SLV cases under 45° directional excitation.

A.1.4 45-Degree Excitation Testing-Dual TMD System Implementation

Control Performance

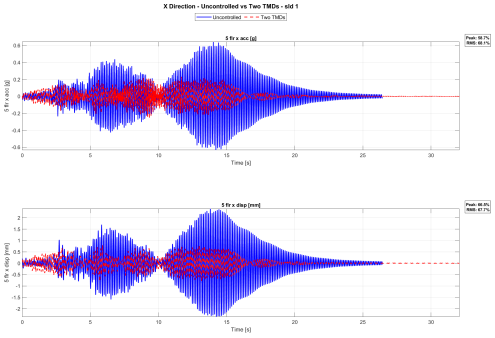

(a). SLD1 X-direction

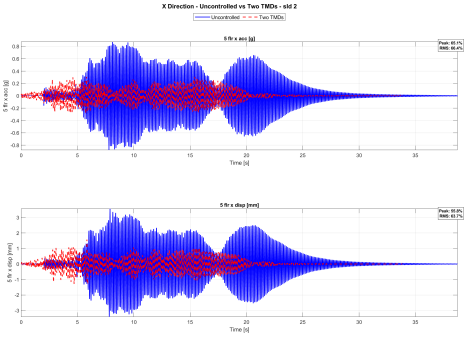

(b). SLD2 X-direction

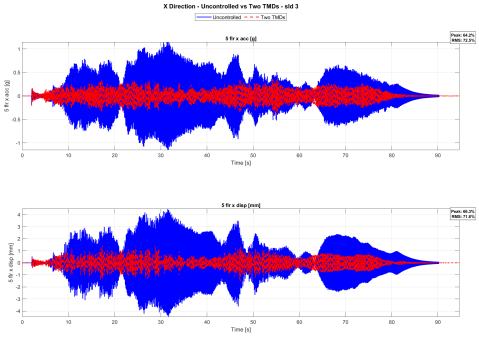

(c). SLD3 X-direction

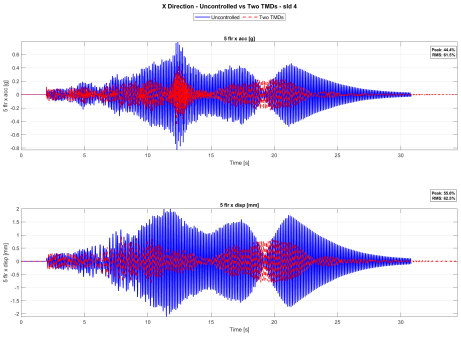

(d). SLD4 X-direction

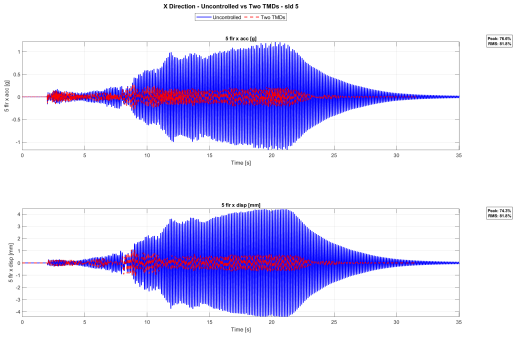

(e). SLD5 X-direction

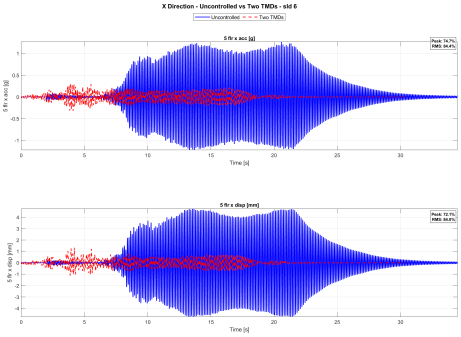

(f). SLD6 X-direction

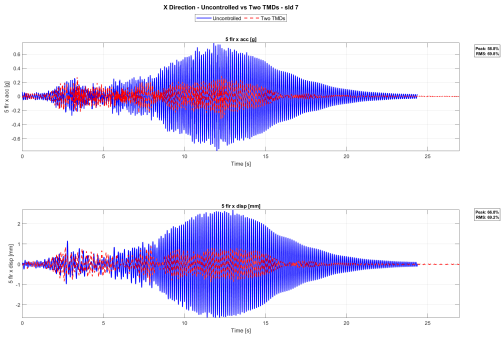

(g). SLD7 X-direction

Figure A.21: X-direction structural response comparison between uncontrolled and two TMDs controlled cases under 45° directional excitation for all SLD cases, demonstrating the

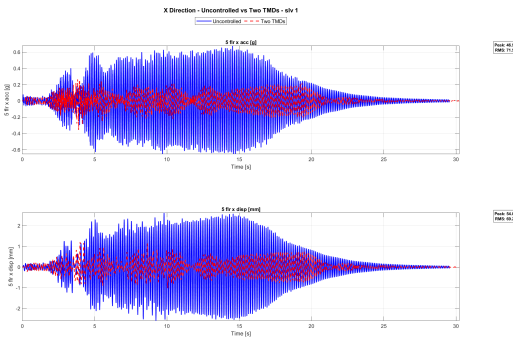

(a). SLV1 X-direction

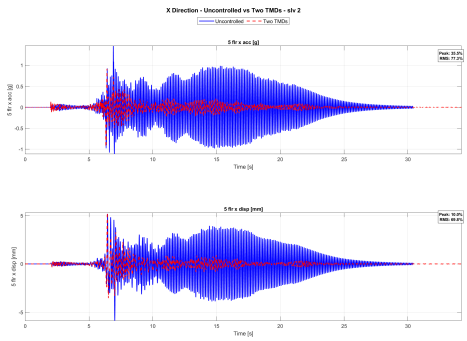

(b). SLV2 X-direction

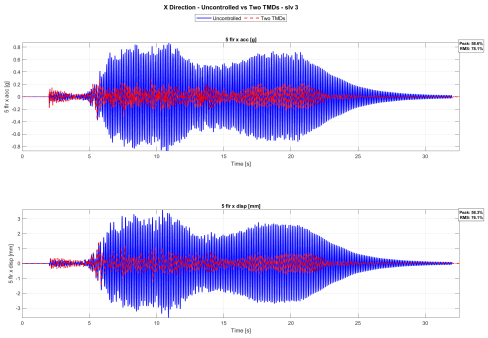

(c). SLV3 X-direction

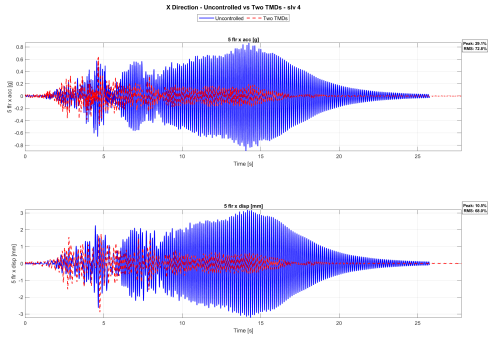

(d). SLV4 X-direction

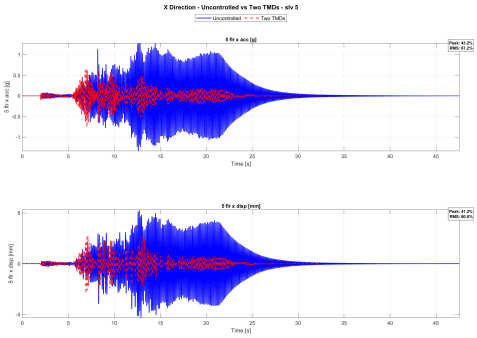

(e). SLV5 X-direction

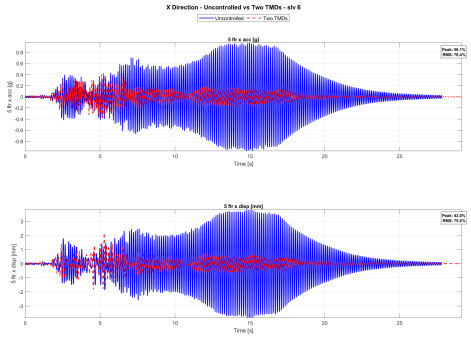

(f). SLV6 X-direction

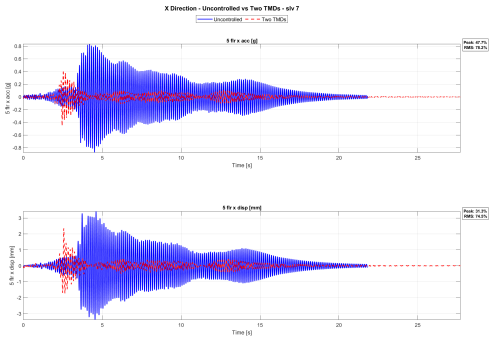

(g). SLV7 X-direction

Figure A.22: X-direction structural response comparison between uncontrolled and two TMDs controlled cases under 45° directional excitation for all SLV cases, demonstrating the effectiveness of dual TMD control in reducing lateral displacement.

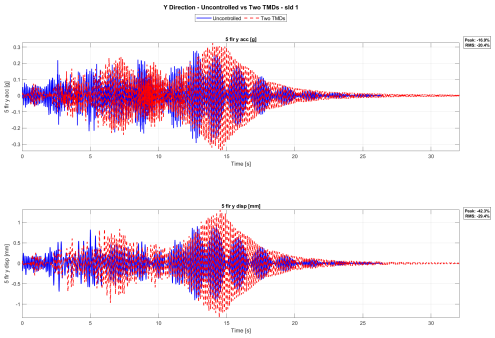

(a). SLD1 Y-direction

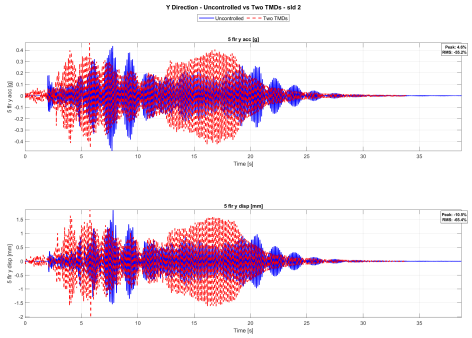

(b). SLD2 Y-direction

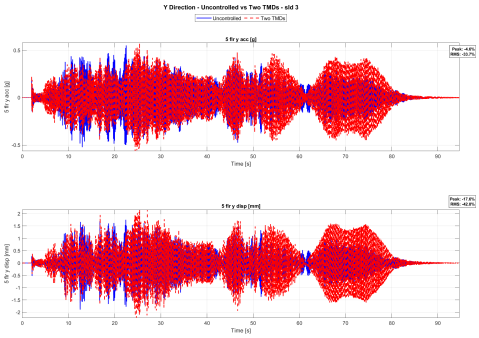

(c). SLD3 Y-direction

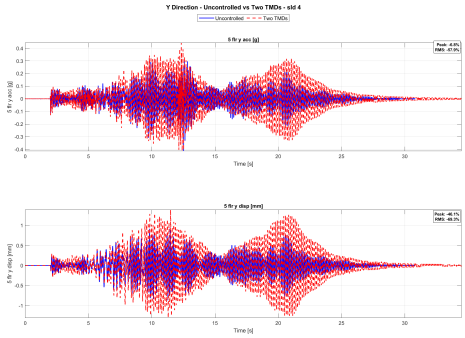

(d). SLD4 Y-direction

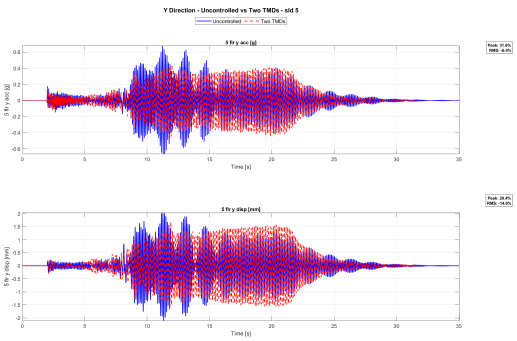

(e). SLD5 Y-direction

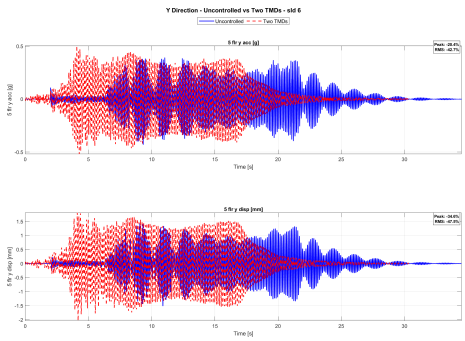

(f). SLD6 Y-direction

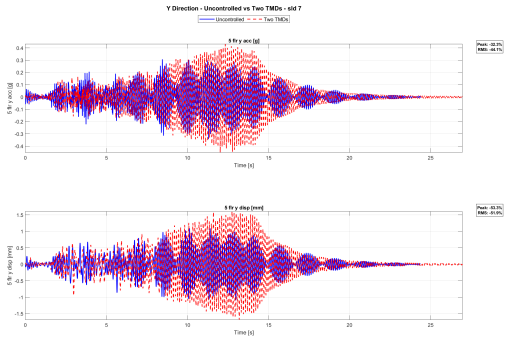

(g). SLD7 Y-direction

Figure A.23: Y-direction structural response comparison between uncontrolled and two TMDs controlled cases under 45° directional excitation for all SLD cases, demonstrating the effectiveness of dual TMD control in reducing lateral displacement.

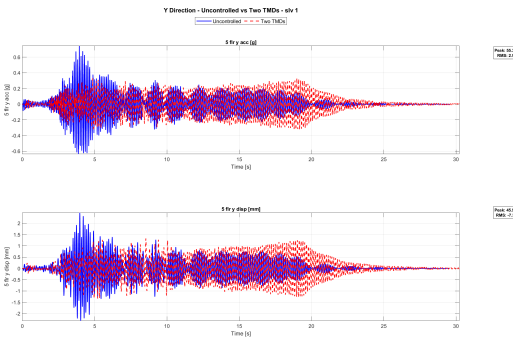

(a). SLV1 Y-direction

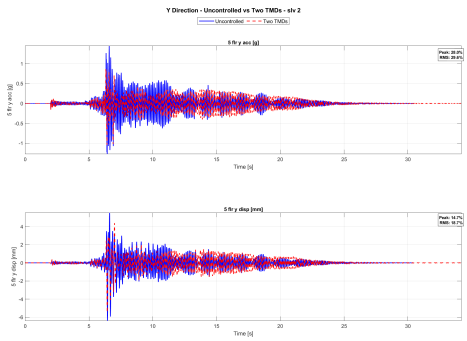

(b). SLV2 Y-direction

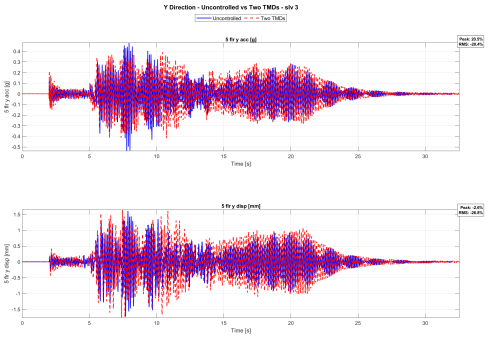

(c). SLV3 Y-direction

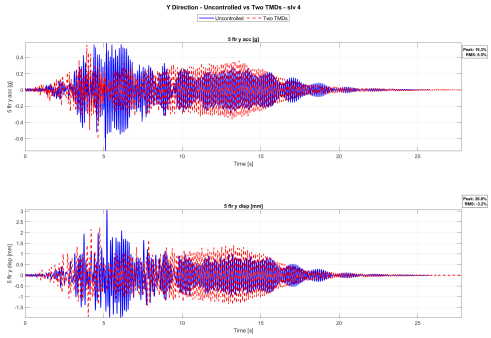

(d). SLV4 Y-direction

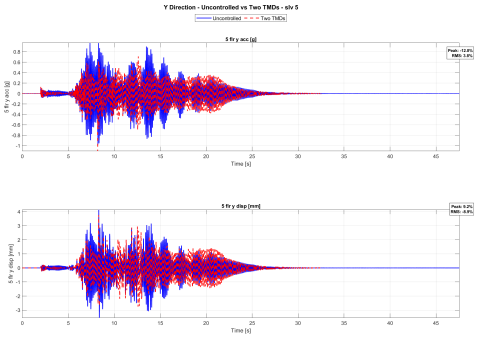

(e). SLV5 Y-direction

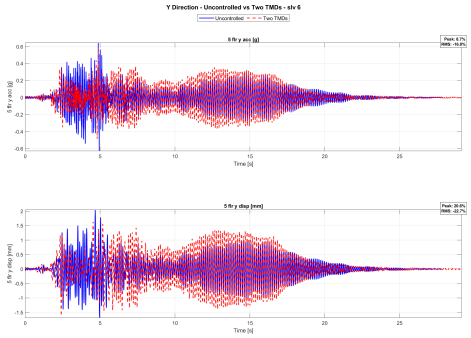

(f). SLV6 Y-direction

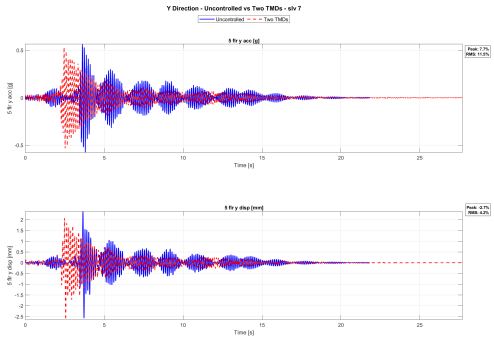

(g). SLV7 Y-direction

Figure A.24: Y-direction structural response comparison between uncontrolled and two TMDs controlled cases under 45° directional excitation for all SLV cases, demonstrating the effectiveness of dual TMD control in reducing lateral displacement.

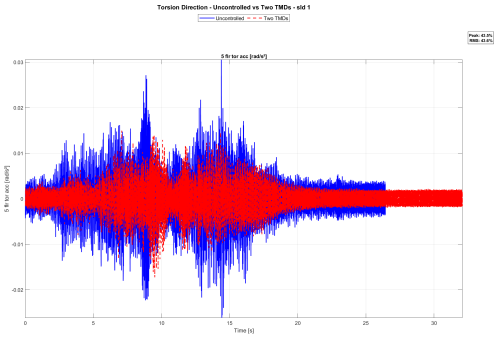

(a). SLD1 Torsional

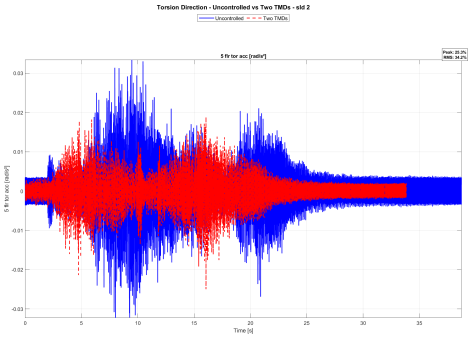

(b). SLD2 Torsional

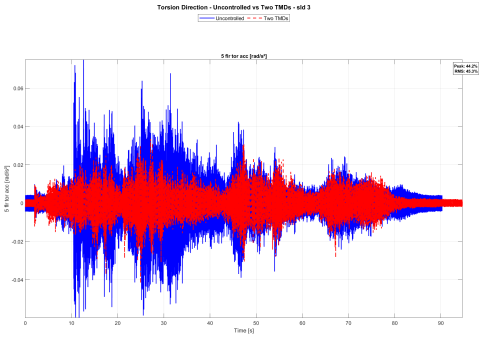

(c). SLD3 Torsional

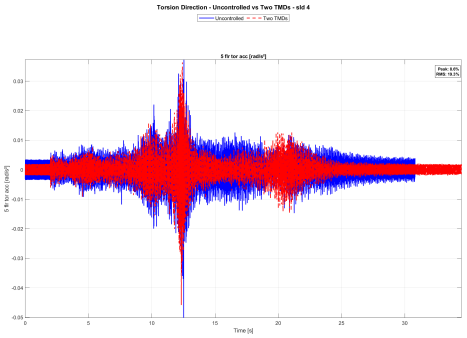

(d). SLD4 Torsional

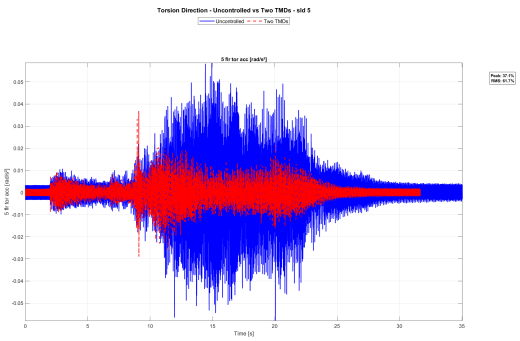

(e). SLD5 Torsional

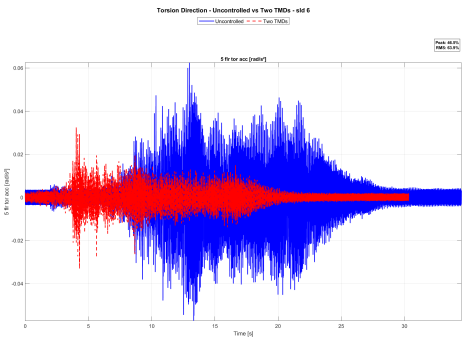

(f). SLD6 Torsional

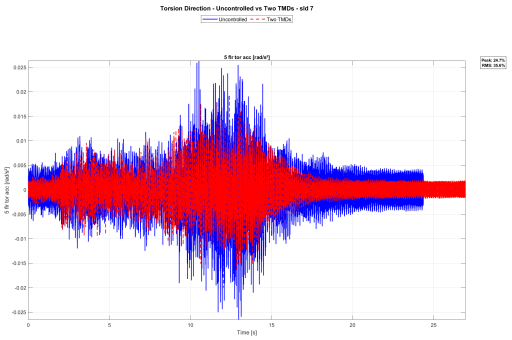

(g). SLD7 Torsional

Figure A.25: Torsional structural response comparison between uncontrolled and two TMDs controlled cases under 45° directional excitation for all SLD cases, demonstrating the effectiveness of dual TMD control in reducing rotational response.

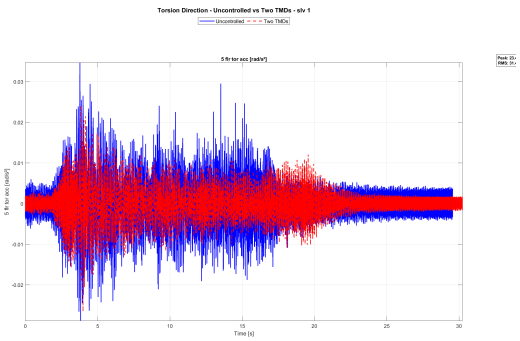

(a). SLV1 Torsional

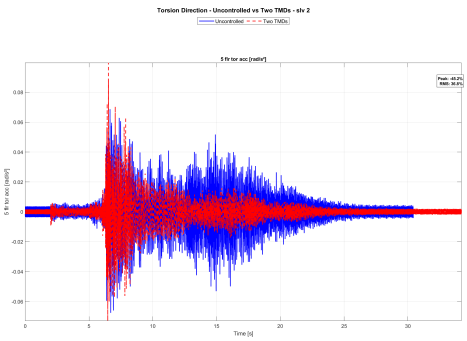

(b). SLV2 Torsional

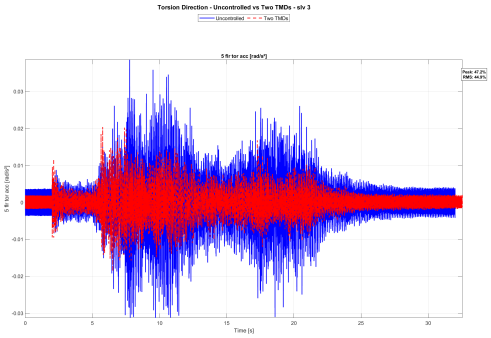

(c). SLV3 Torsional

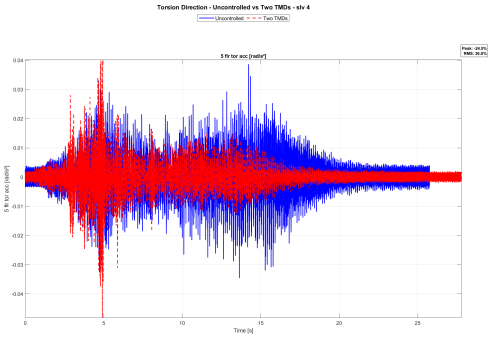

(d). SLV4 Torsional

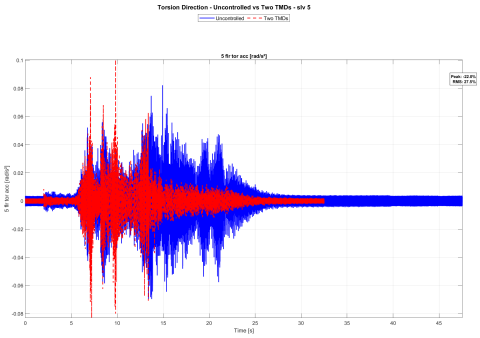

(e). SLV5 Torsional

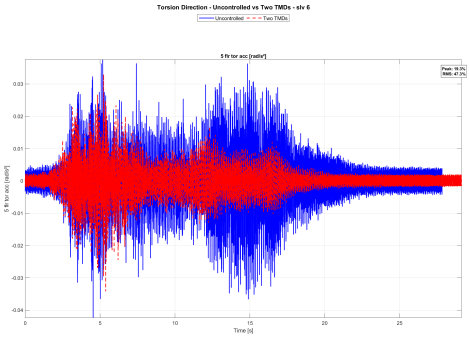

(f). SLV6 Torsional

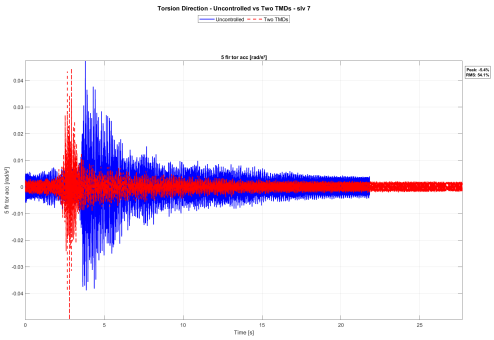

(g). SLV7 Torsional

Figure A.26: Torsional structural response comparison between uncontrolled and two TMDs controlled cases under 45° directional excitation for all SLV cases, demonstrating the effectiveness of dual TMD control in reducing rotational response.

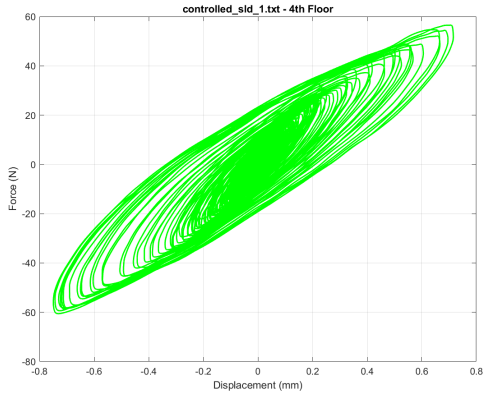

(a). SLD1 - 4th Floor TMD

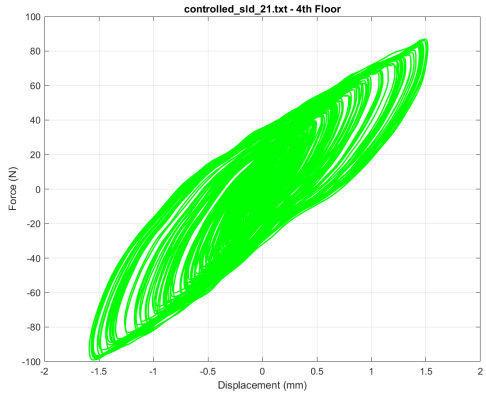

(b). SLD2 - 4th Floor TMD

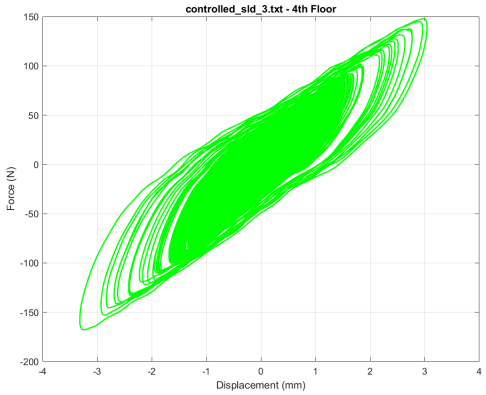

(c). SLD3 - 4th Floor TMD

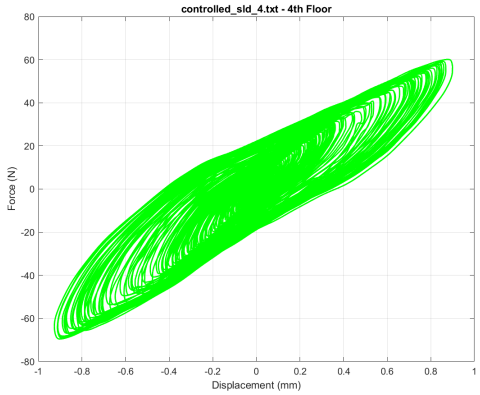

(d). SLD4 - 4th Floor TMD

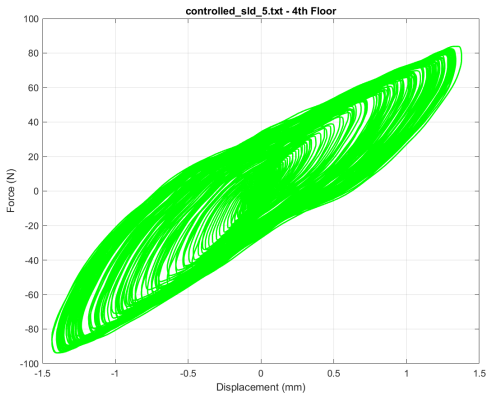

(e). SLD5 - 4th Floor TMD

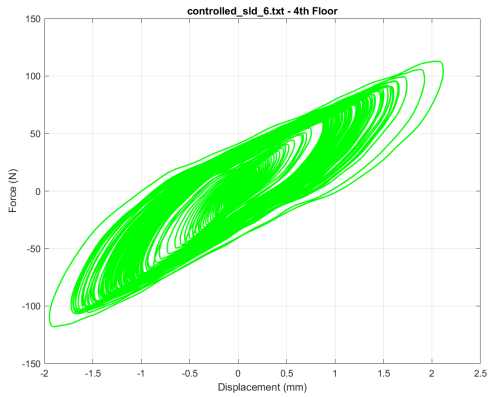

(f). SLD6 - 4th Floor TMD

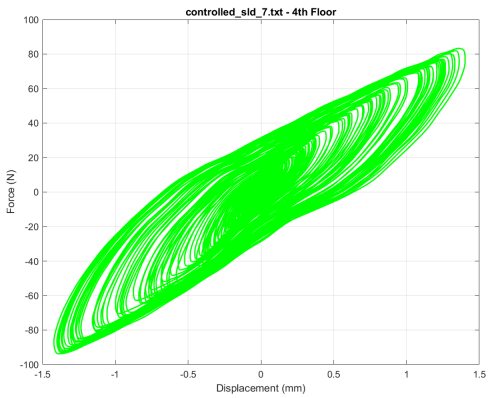

(g). SLD7 - 4th Floor TMD

Figure A.27: Hysteresis behavior of TMD on 4th floor (dual TMD system) for all SLD cases under 45° directional excitation.

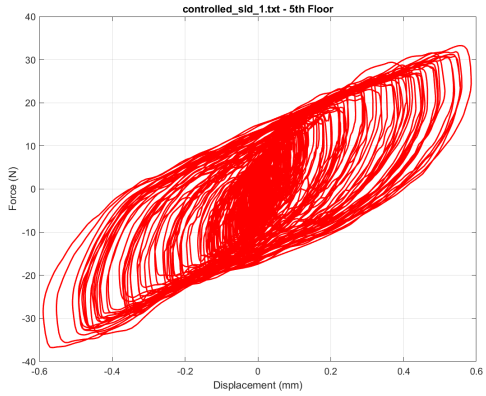

(a). SLD1 - 5th Floor TMD

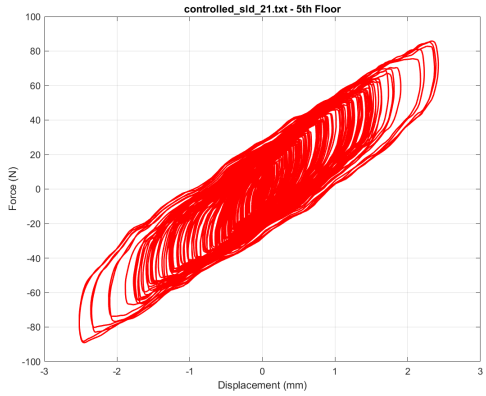

(b). SLD2 - 5th Floor TMD

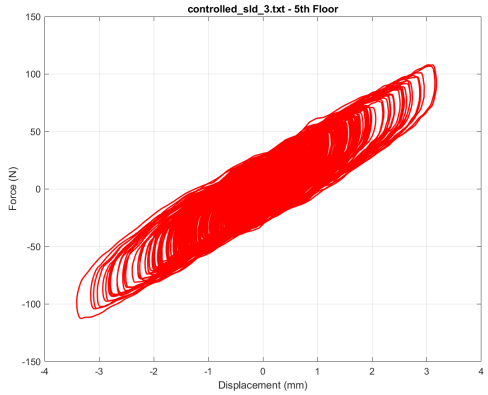

(c). SLD3 - 5th Floor TMD

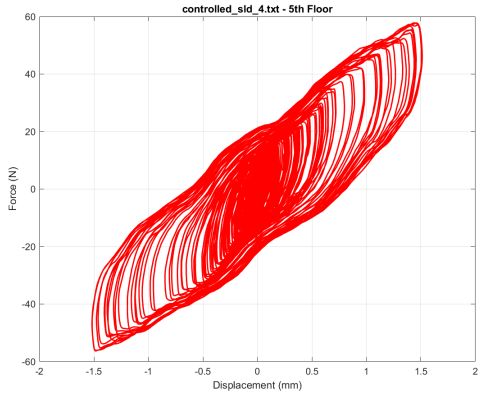

(d). SLD4 - 5th Floor TMD

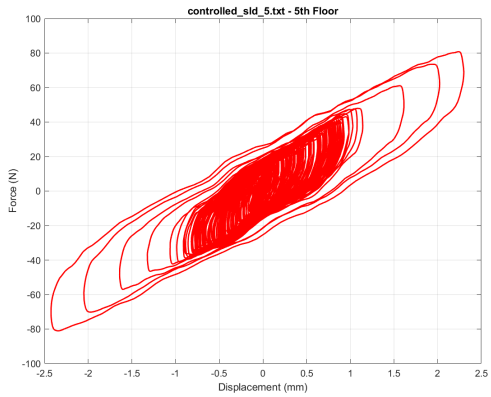

(e). SLD5 - 5th Floor TMD

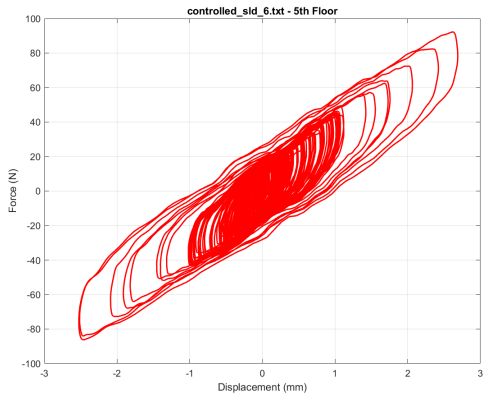

(f). SLD6 - 5th Floor TMD

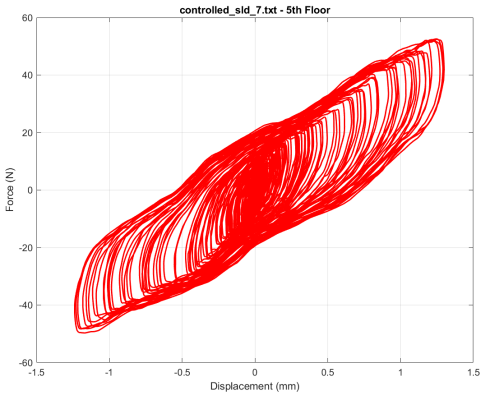

(g). SLD7 - 5th Floor TMD

Figure A.28: Hysteresis behavior of TMD on 5th floor (dual TMD system) for all SLD cases under 45° directional excitation.

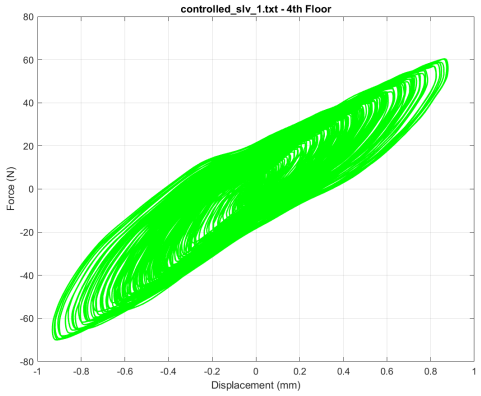

(a). SLV1 - 4th Floor TMD

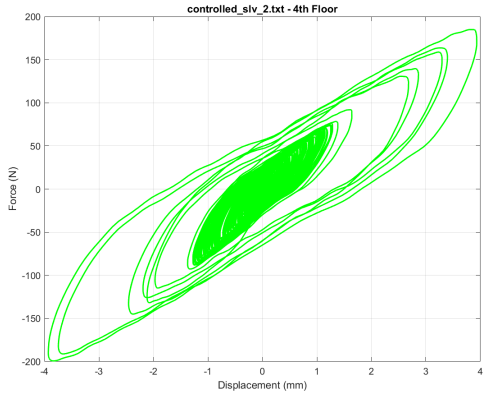

(b). SLV2 - 4th Floor TMD

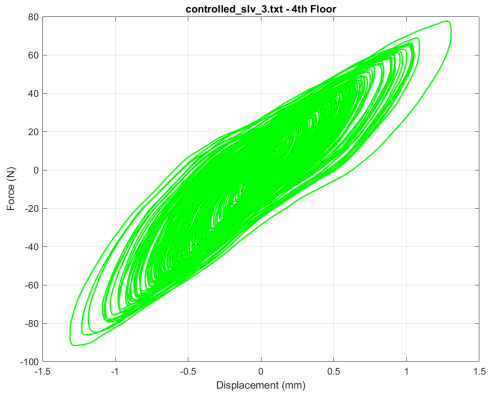

(c). SLV3 - 4th Floor TMD

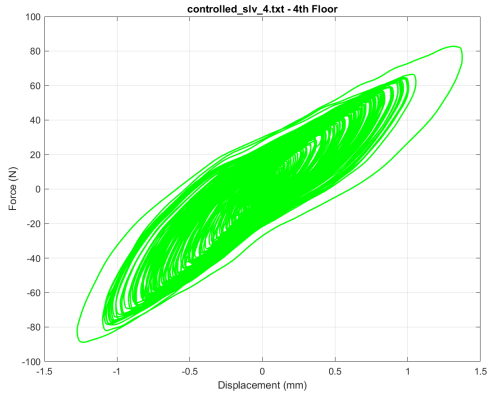

(d). SLV4 - 4th Floor TMD

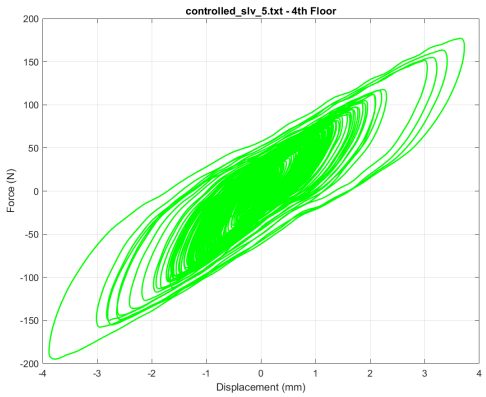

(e). SLV5 - 4th Floor TMD

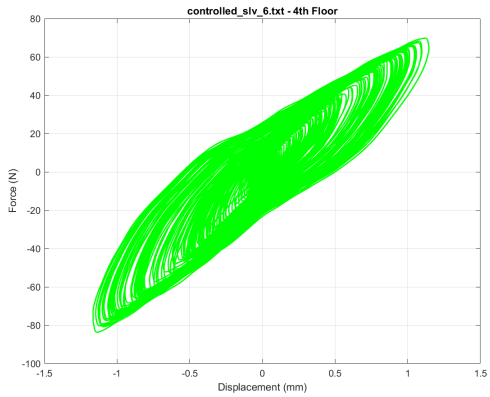

(f). SLV6 - 4th Floor TMD

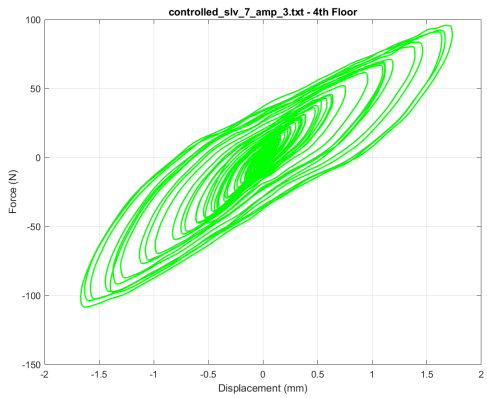

(g). SLV7 - 4th Floor TMD

Figure A.29: Hysteresis behavior of TMD on 4th floor (dual TMD system) for all SLV cases under 45° directional excitation.

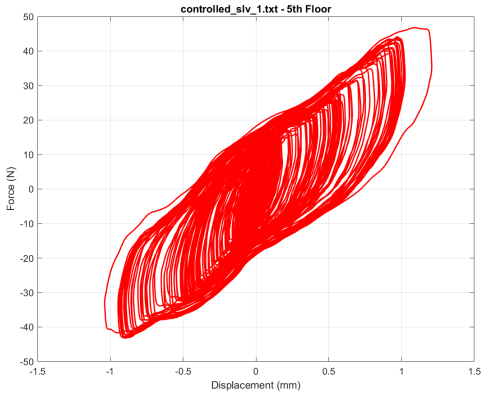

(a). SLV1 - 5th Floor TMD

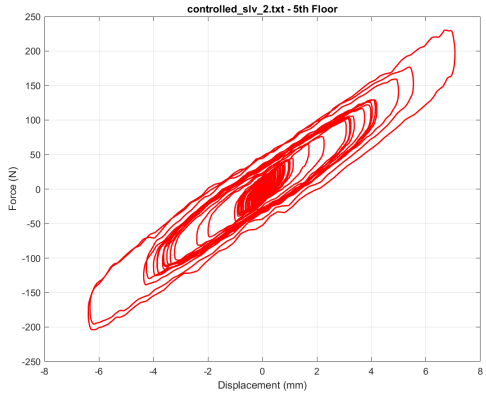

(b). SLV2 - 5th Floor TMD

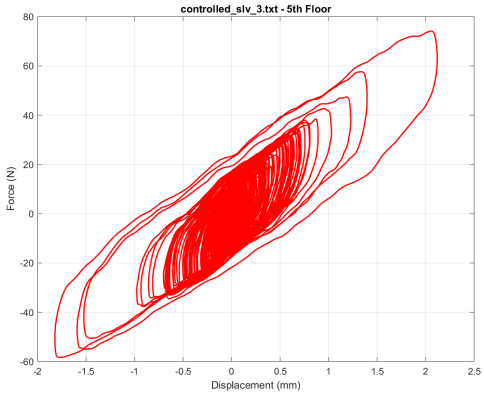

(c). SLV3 - 5th Floor TMD

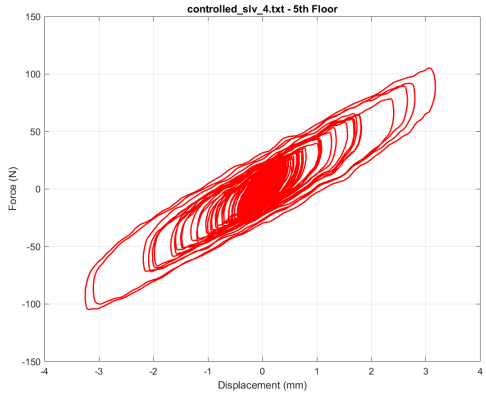

(d). SLV4 - 5th Floor TMD

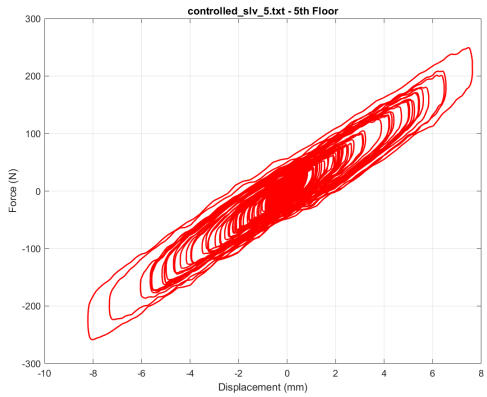

(e). SLV5 - 5th Floor TMD

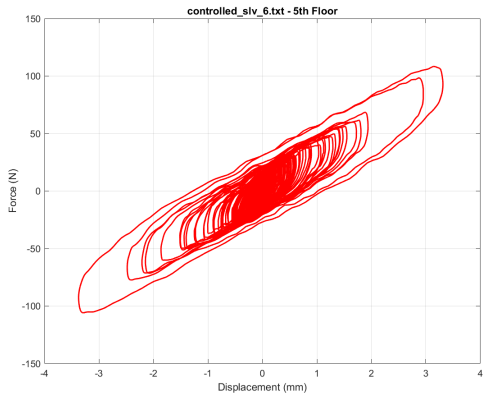

(f). SLV6 - 5th Floor TMD

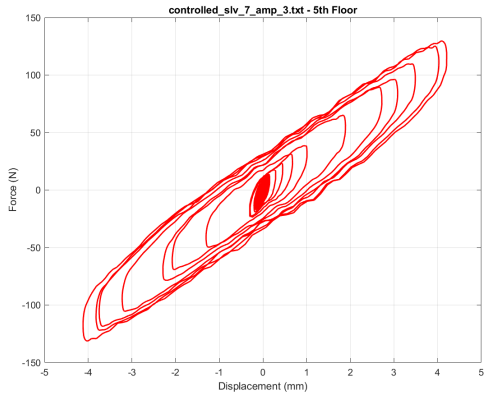

(g). SLV7 - 5th Floor TMD

Figure A.30: Hysteresis behavior of TMD on 5th floor (dual TMD system) for all SLV cases under 45° directional excitation.

Interstorey Drift plots

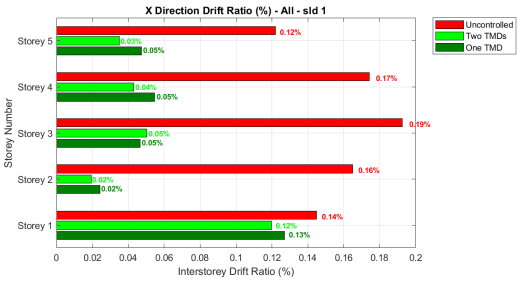

(a). One TMD

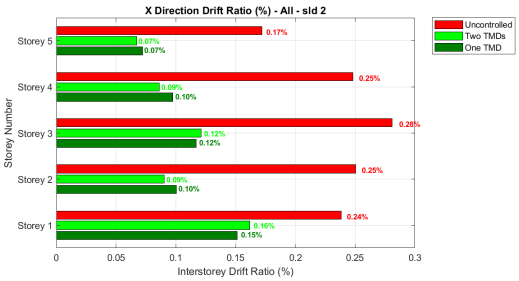

(b). Two TMDs

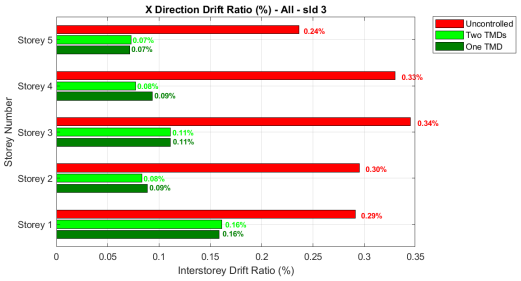

(c). SLD3

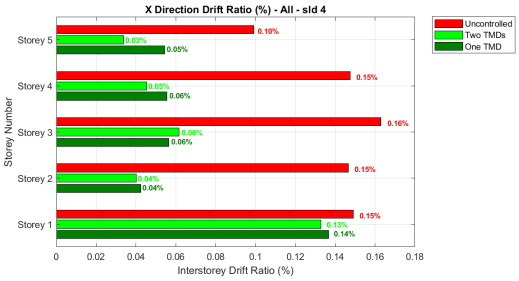

(d). SLD4

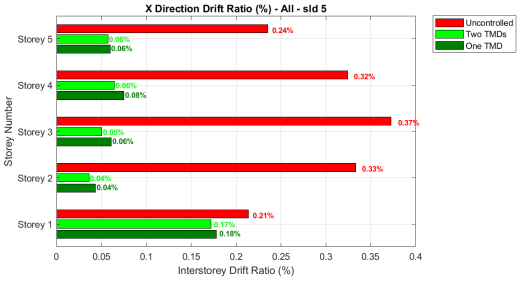

(e). SLD5

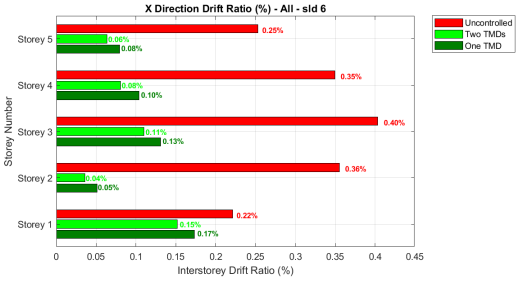

(f). SLD6

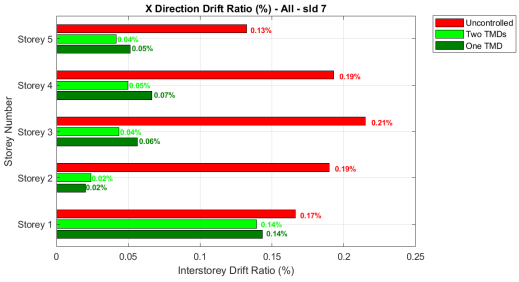

(g). SLD7

Figure A.31: X-direction interstory drift ratio comparison for seven SLD ground motion cases, including configurations with one TMD and two TMDs. The plots show the drift percentage distribution across all floors for serviceability limit displacement conditions.

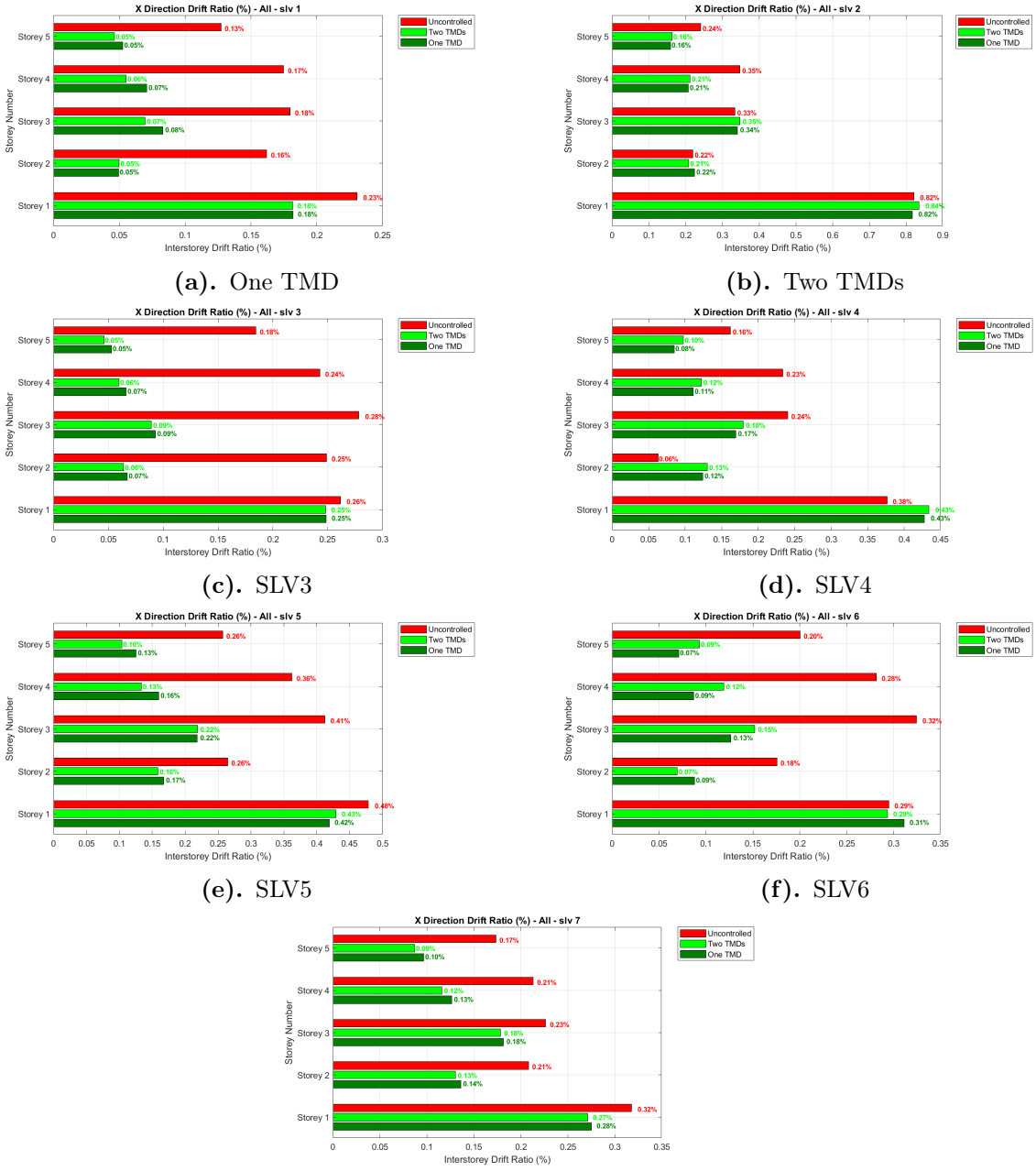

(a). One TMD

(b). Two TMDs

(c). SLV3

(d). SLV4

(e). SLV5

(f). SLV6

(g). SLV7

Figure A.32: X-direction interstory drift ratio comparison for seven SLV ground motion cases, including configurations with one TMD and two TMDs. The results illustrate the drift percentage distribution across all floors under serviceability limit velocity conditions.

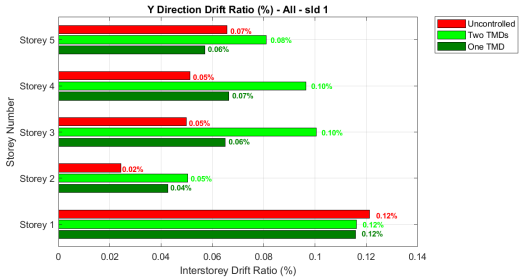

(a). One TMD

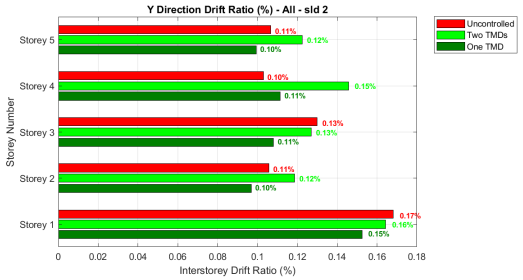

(b). Two TMDs

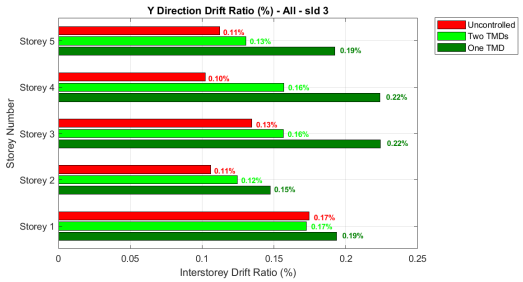

(c). SLD3

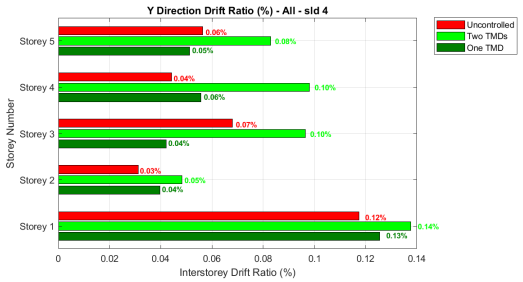

(d). SLD4

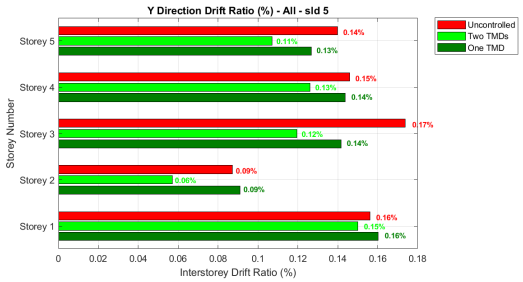

(e). SLD5

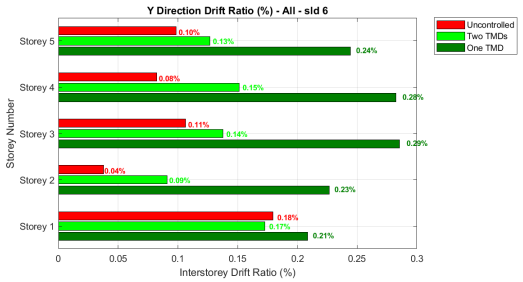

(f). SLD6

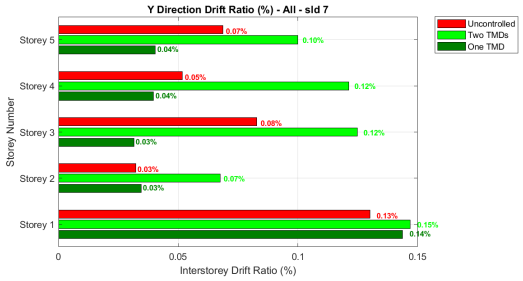

(g). SLD7

Figure A.33: Y-direction interstory drift ratio comparison for seven SLD ground motion cases, including configurations with one TMD and two TMDs. The plots show the drift percentage distribution across all floors for serviceability limit displacement conditions.

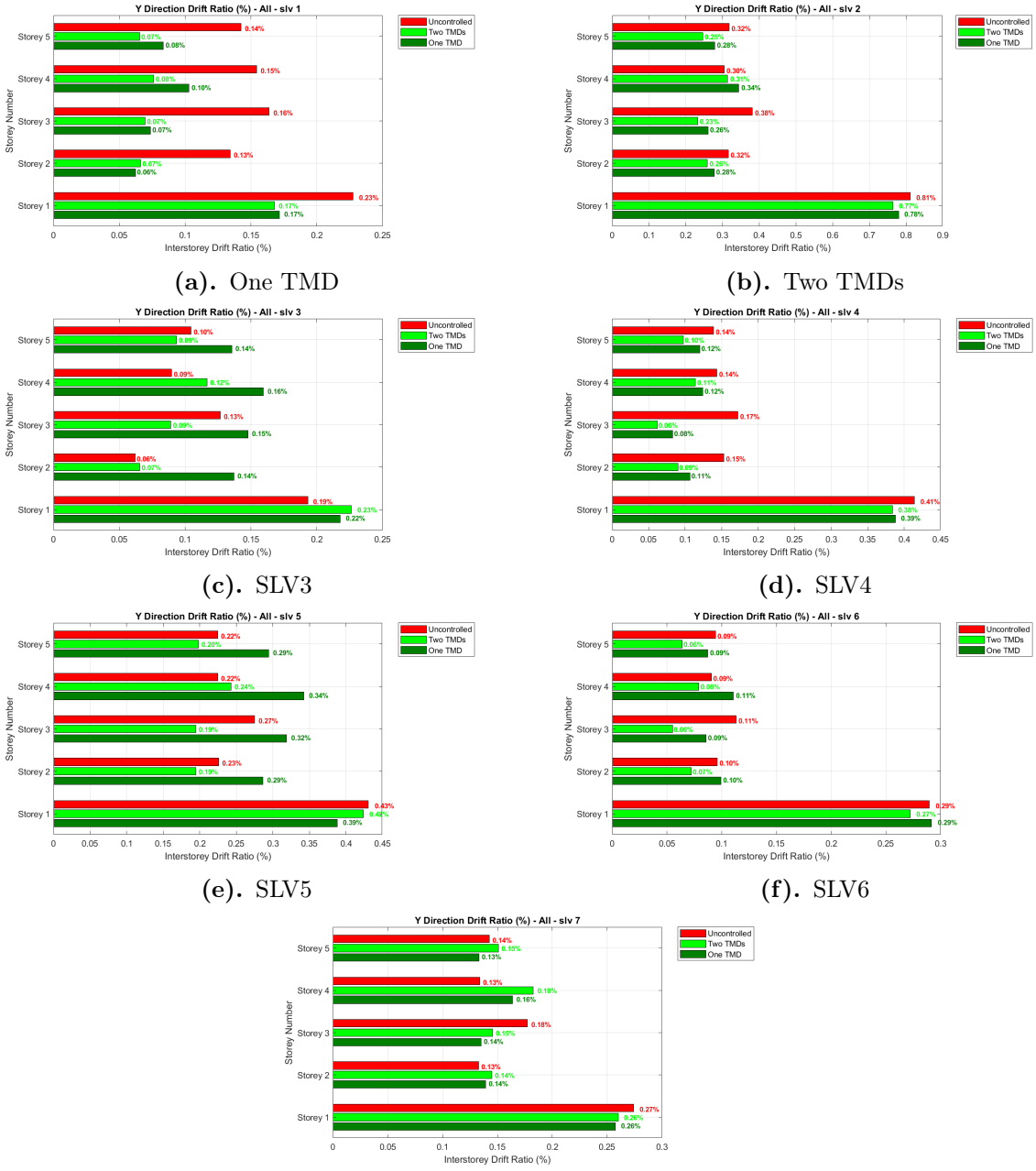

(a). One TMD

(b). Two TMDs

(c). SLV3

(d). SLV4

(e). SLV5

(f). SLV6

(g). SLV7

Figure A.34: Y-direction interstory drift ratio comparison for seven SLV ground motion cases, including configurations with one TMD and two TMDs. The results illustrate the drift percentage distribution across all floors under serviceability limit velocity conditions.